INTERCALATION KINETICS, AND NOVEL PREPARATION METHOD FOR POLYMER NANO-COMPOSITES

MARCH 2013

DOCTOR OF ENGINEERING

TOMOTAKA SAITO

TOYOHASHI UNIVERSITY OF TECHNOLOGY

INTERCALATION KINETICS AND NOVEL PREPARATION METHOD FOR POLYMER NANO-COMPOSITES

Abstract

In the last two decades, polymeric nano-composite is one of the fast-growing category of material science on a worldwide basis. Getting attention on importance of nano-technology today, some results of polymeric nano-composites have been industrialized in many countries.

Polymer nano-composite consists of polymer matrix and nano-sized filler which has at least one of the dimension is of the order of a nano-meter, and the filler is dispersed into polymer matrix in nano-scale. First report of the material was from Toyota Central Research & Development Laboratories' (TCRDL) group for polyamide 6/clay nano-composite via in-situ polymerization of ε-caprolactam, in which alkylammonium-modified montmorillonite (MMT) was thoroughly dispersed in advance. The resulting composite with loading only 4.2 wt% clay possessed a doubled modulus, a 50%-enhanced strength, and an increase in heat distortion temperature of 80 ^{o}C as compared to that of neat polyamide 6.

The main reason for these improved properties in nano-composites is interfacial interaction between matrix and OMLF as opposed to conventional composites. A few weight percent of OMLF are properly dispersed throughout the matrix thus creates a much higher surface area for polymer-filler interfacial interactions than do conventional micro-composites. In case of the nano-particle use as nano-filler, the key technnology is dispersion technique, in other words, preparation method for nano-composite materials.

Continued progresses in nano-scale controlling have contributed to the rapid development of polymer/OMLF nano-composites. Three types of main approaches for the

polymer nano-composite preparation are reported, i.e., in-situ polymerization, intercalation of polymer or pre-polymer from solution (solution cast), and melt compounding.

In case of preparation for non-polar or weak polar polymer-based nano-composites, compatibilizer was added through melt compounding process to apply shear stress to OMLF layers. In other words, non-polar polymer-based nano-composite preparation without compatibilizer is not possible through above three methods. To solve this issue, we should investigate a novel preparation method, from industrial point of view, which is able to apply to the practical industrial production system.

The main objective of this study is to bring out the factors that concerned with nano-composite formation and to feed back these factors for the preparation of the polymer nano-composite. For this purpose, we investigated fundamental study of the phase transition of the cationic surfactant located at the interlayer space in montmorillonite, and examined the intercalation behavior of the small molecules by using various types of nano-fillers, which have a strong impact on the explanation for the intercalation kinetics. We chose an optimal OMLF and conducted the Poly(*p*-phenylenesulfide) (PPS)-based nano-composites preparation with and/or without shear processing. Furthermore, we have developed more innovative compounding process, i.e., solid-state processing, to delaminate the stacked-and-layered filler in the polymer matrix. And we adopted non-polar polymer as matrix to confirm the processing ability, and to investigate the effect of polarity of the matrix polymer on solid-state processing. The present thesis consists of the following 6 chapters.

In Chapter 1, the previous reported papers are totally reviewed about the polymer nano-composite studies and preparation methods for the materials, from which the unsolved problems are picked up and the motivation of the present research will be clarified.

In Chapter 2, we investigated nonisothermal order-disorder transition behavior of alkylammonium ions in nano-confined space i.e., interlayer space of MMT, compared with crystallized dioctadecyl dimethyl ammonium bromide ($DC_{18}DM$-Br) through temperature modulated differential scanning calorimeter, wide-angle X-ray diffraction (WAXD), and Fourier transform infrared spectroscopy (FTIR).

In Chapter 3, we investigated the intercalation behavior of small molecules, as a model compound for PPS, into various OMLFs interlayer evaluated from WAXD analysis. In the first part of Chapter 3, the effect of miscibility between small guest molecules and intercalants on the basis of DSC analysis was investigated. After that, the intercalation behavior of the molecules into the various types of OMLFs was discussed. In the remaining part, we chose an optimal OMLF and conducted the PPS-based nano-composites preparation with and without shear processing.

In the first part of Chapter 4, we discussed intercalation behavior with various polymers and OMLFs prepared by melt compound. The results show same trends as small molecules investigated in Chapter 3. In latter part, novel preparation methods, solid-state processing, to improve nano-filler dispersion and to delaminate the stacked-and-layered filler in PPS matrix was conducted. From the results, effectiveness of solid-state processing is clearly showed.

In Chapter 5, we also challenged to prepare non-polar polymer based nano-composite. It is considered that preparation for non-polar polymer-based nano-composite is difficult because polarity of matrix polymer is very important for nano-filler dispersion. Fortunately, we successfully prepared polypropylene/OMLF nano-composite with solid-state processing. In this study, two thresholds during solid-state processing were found for OMLF dispersion.

Finally, we summarized the principal results and conclusions derived from this study in Chapter 6.

****

In this way the present thesis has revealed the nonisothernal odred-disorder transition in nano-confined space and intercalation behavior of the small molecules and various polymers into OMLF interlayer space. And novel preparation method for polymer nano-composites was developed. Even though, matrix is non-polar polymer, nano-composite was formed through the processing without adding compatibilizer. In this way, the present research is believed to contribute to the development of polymer nano-composite science and industry significantly.

Contents

List of abbreviations

C	
CEC	cation exchange capacity
CPS	critical particle size
C_{12}TPP	*n*-octyl *tri*-phenyl phosphonium
C_{16}TBP	*n*-hexadecyl tri-*n*-butyl phosphonium
$C_{18}Me_2Bz$	octadecyl benzyl di-methyl ammonium
C_{18}TM	octadecyl tri-methylammonium
D	
$DC_{18}DM$	dioctadecyl dimethylammonium
$DC_{18}DM$-Br	dioctadecyl dimethyl ammonium bromide
DFS	diphenyl sulfide
F	
FFT	fast Fourier transform
FTIR	Fourier transform infrared spectroscopy
FWHM	full width at half maximum
H	
HDT	heat distortion temperature
HTO	layered titanate
M	
MMT	montmorillonite
O	
ODA	octadecyl ammonium
OMLF	organically modified layered filler
P	
PBS	poly(butylenes succinate)
PEO	polyethylene oxide
PES	sulfonated poly(ethylene terephthalate) copolymers

PLA	poly(L-lactide)
PLF	polymer/layered filler
POM	polarized optical microscope
PP	polypropylene
PP-g-MA	maleic anhydrate grafted polypropylene
PPS	poly(*p*-phenylenesulfide)
PVA	polyvinyl alcohol
PVDF	poly(vinylidene fluoride)

Q

$qC_{14}(OH)$	*N*-(cocoalkyl)-*N*,*N*-[bis(2-hydroxyethyl)]-*N*-methyl ammonium

S

sc-CO_2	supercritical CO_2
SMA	poly[styrene-co-(maleic anhydride)］
SSSP	solid-state shear pulverization
syn-FH	synthetic fluorine hectorite

T

TCRDL	Toyota Central Research & Development Laboratories
TEM	transmission electron microscope
TGA	thermogravimetric analysis
TMDSC	temperature modulated differential scanning calorimeter

W

WAXD	wide angle X-ray diffraction

Chapter 1

General Introduction

1-1. Background

In the last two decades, polymeric nano-composite is one of the fast-growing category of material science on a worldwide basis. Getting attention on importance of nano-technology today, some results of polymeric nano-composites have been industrialized in many countries [1, 2].

Polymer nano-composite consists of polymer matrix and nano-sized filler which has at least one of the dimension is of the order of a nano-meter, and the filler is dispersed into polymer matrix in nano-scale. First report of the material was from Toyota Central Research & Development Laboratories' (TCRDL) group for polyamide 6/clay nano-composite via in-situ polymerization of ε-caprolactam, in which alkylammonium-modified montmorillonite (MMT) was thoroughly dispersed in advance [3-7]. The resulting composite with loading only 4.2 wt% clay possessed a doubled modulus, a 50%-enhanced strength, and an increase in heat distortion temperature (HDT) of 80 ^{o}C as compared to that of neat polyamide 6.

Of particular interest is a recently developed nano-composite technology consisting of a polymer and organically modified layered filler (OMLF) because they often exhibit remarkably improved materials properties including not only high muduli [4], increased strength and heat resistance [8], but also decreased gas permeability [4], flammability [9], and increased biodegradability of biodegradable polymers [10] as compared with those of the virgin polymers [11].

The main reason for these improved properties in nano-composites is interfacial interaction between matrix and OMLF as opposed to conventional composites. A few weight percent of

OMLF are properly dispersed throughout the matrix thus creates a much higher surface area for polymer-filler interfacial interactions than do conventional micro-composites [12].

1-2.Layered nano-filler

1-2-1.Structure and Properties

Montmorillonite (MMT), hectorite, and saponite are the most commonly used layered nano-filler for preparing polymer nano-composite, and these minerals are classified to smectite type clay. Smectite consists from tetrahedral sheet which is like hexagonal mesh by shearing three oxygen atoms on SiO_2 tetrahedron, and octahedral sheet which shear edge line of the octagon. The octagon is made from six O atoms or OH groups which are on edge of the shape, and Al or Mg takes position in the octagon. Smectite type clay is called 2:1 type clay mineral because the mineral consists from two tetrahedral sheets and one octahedral sheet (Fig.1-1a). The layer thickness is around 1 nm and the lateral dimensions of these layers may vary from 30 nm to several microns and even larger depending on the particular layered silicate. Stacking of the layers leads to a regular van der Waals gap between the layers called interlayer or gallery. Isomorphic substitution within the layers (for example, Al^{3+} replaced by Mg^{2+} or by Fe^{2+}, or Mg^{2+} replaced by Li^{+}) generates negative charges that are counterbalanced by alkali and alkaline earth cations situated inside the galleries. The type of layered silicate is characterized by a moderate surface charge (known as cation exchange capacity (CEC), and generally expressed by mequiv/100g). This charge is not locally constant as it varies from layer to layer and considered as an average value over the whole crystal. Layered silicates take two types of

structure, i.e., tetrahedral-substituted and octahedral substituted. In the case of tetrahedral substituted layered silicates the negative charge is located on the surface of the silicate layers, and hence, the polymer matrices can react with tetrahedral-substituted silicate more readily compared to octahedral-substituted. And these cations are easily exchange to other cations. Interlayer space of the tetrahedral-substituted mineral is expanded by the exchanged cations and the variations are determined by type and alignment of the ions. Chemical formula and schematic images of montmorillonite (MMT), one of the natural smectite, are shown in Table 1-1 and Figure 1-1, respectively [13, 14].

Natural mica has larger layer charge density comparison with smectite and no swellable property because interlayer cation, K^+, is captured in hexagonal hole on bottom face of the tetragonal sheet. On the other hand, some synthetic mica which is changed interlayer cation K^+ to Na^+ or Li^+ and has lower layer charge density compared to natural mica, is given swellable ability. The synthetic mica is also called swelling mica, and OH groups on layer edge are changed to fluorine. And interlayer cations in the synthetic fluorine mica are able to exchange to other cations as MMT. Crystal structure and chemical formula of synthetic fluorine hectorite (syn-FH), one of the synthetic mica, is shown in Figure 1-1a and Table 1-1, respectively.

Chemical formula of potassium titanate is represented as $K_2O \cdot nTiO_2$ and the chemical compounds takes different *n* values. 4-potassium titanate, the value of *n* is four, forms layer structure and has K^+ as interlayer cations. The K^+ cation is exchangeable to other organic/inorganic cation. [15, 16] The characteristic parameters and structure of layered titanate (HTO) used in this study are shown in Table 1-1 and Figure 1-1b, respectively.

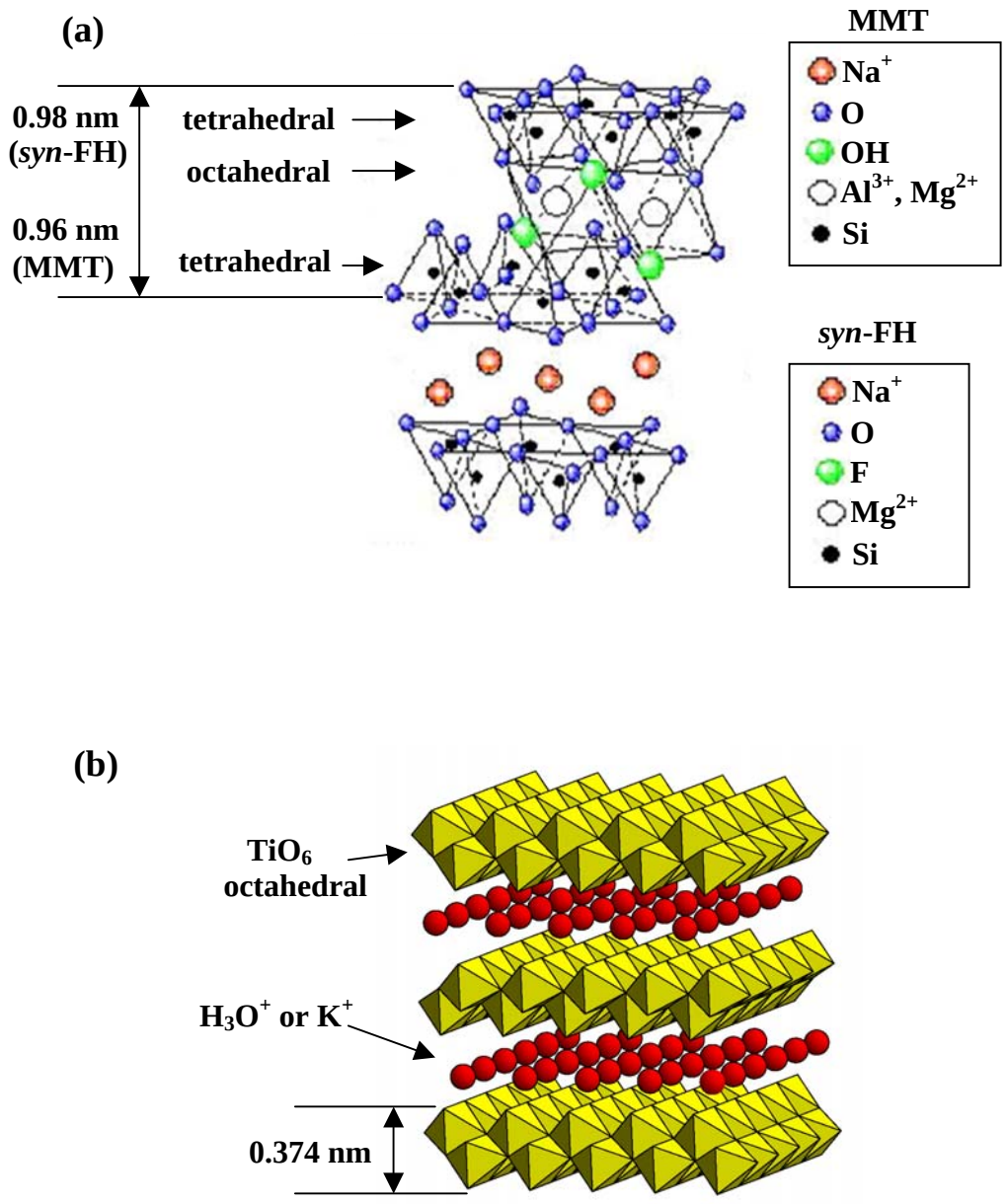

Figure 1-1. Crystal structure of (a) *syn*-FH and MMT and (b) HTO.

Table 1-1. Characteristic parameter of nano-fillers

Parameters	HTO	*syn*-FH	MMT
Chemical formula	$H_{1.07}Ti_{1.73}O_{3.95}\cdot 0.5H_2O$	$Na_{0.66}Mg_{2.6}Si_4O_{10}(F)_2$	$Na_{0.33}(Al_{1.67}Mg_{0.33})Si_4O_{10}(OH)_2$
Particle size / nm	~100-200	~100-200	~100-200
BET area / m^2/g	~2400	~800	~700
CEC[a)] / meq/100g	~200	~120	~90
Surface charge/ e^-/nm^2	1.26	0.971	0.780
Density /g/ml	2.40	2.50	2.50
Refractive index (n^{20}_D)	2.3	1.55	1.55
pH	4-6	9-11	7.5-10

[a)]Methylene blue adsorption method.

There are two particular characteristics of layered fillers that we generally consider in polymer/layered filler (PLF) nano-composites. The first is the ability of the particles to disperse into the individual layers. The second characteristic is the ability to fine-tune their surface chemistry through ion exchange reactions with organic and inorganic cations. These two characteristics of layered filler in a particular polymer matrix depend on the interlayer cation.

1-2-2. Organophilic Modification

Any simple physical mixture of a polymer and layered filler does not form a nano-composite. This situation is analogous to polymer blends, and in most cases separation into discrete phases normally takes place. In immiscible systems, which typically correspond to the more conventionally filled polymers, the poor physical interaction between the organic and the

inorganic components leads to poor mechanical and thermal properties. In contrast, the strong interactions between the polymer and the layered filler in PLF nano-composites lead to the organic and inorganic phases being dispersed at nano-meter level. As a result nano-composites exhibit unique properties not shared by their micro counterparts or conventionally filled polymers.

Pristine layered fillers usually contain hydrated Na^+ or K^+ ions [15, 17]. Obviously, in this pristine state layered silicates are only compatible with hydrophilic polymers, such as polyethylene oxide (PEO) [18-23], polyvinyl alcohol (PVA) [24, 25] etc. To render layered silicates compatible with other polymer matrices, the layers must convert the normally hydrophilic surface to organophilic, which makes the intercalation of many engineering polymers possible. Generally, this can be done by ion-exchange reactions with cationic surfactants including primary, secondary, tertiary, and quaternary alkylammonium or alkylphosphonium cations. The role of alkylammonium or alkylphosphonium cations on the layer surfaces is to lower the surface energy of the inorganic host and to improve the wetting characteristics with the polymer matrix, and results in a larger interlayer spacing. It can evaluate that about 100 alkylammonium salt molecules are localized near the individual layers ($\sim 8 \times 10^{-15}$ m^2) and active surface area is ~800 m^2/g. Additionally, the alkylammonium or alkylphosphonium cations could provide functional groups that can react with the polymer matrix or in some cases initiate the polymerization of monomers to improve the strength of the interface between the inorganic layer and the polymer matrix [26, 27].

Traditional structural characterization to determine the orientation and arrangement of the alkyl chain involves primarily by the use of wide angle X-ray diffraction (WAXD). Depending on the packing density, temperature and alkyl chain length, the chains were thought to take interdigitated layer structure, and the structure is controlled by surface charge density of the layered filler and molecular size of the organic cations [15]. Vaia and Giannelis [28] have shown that alkyl chains can vary from liquid-like to solid-like, with the liquid-like structure dominating as the interlayer density or chain length decreases (Figure 1-2), or as the temperature increases. They used Fourier transform infrared spectroscopy (FTIR), because of the relatively small energy differences between the *trans* and *gauche* conformers. The idealized models described earlier assume all *trans* conformations. In addition, for the longer chain length surfactants, the surfactants in the layered silicate can show thermal transition akin to melting or liquid-crystalline to liquid like transitions upon heating. The molecular models for some representative organic cations are shown in Figure 1-3. The molecular dimensions of the intercalants were determined by using a molecular dynamics program (MM2 in Quantum CAChe, Fujitsu Ltd.), taking van der Waals radii into consideration. Optimization of the structure is based on minimization of the total energy of the molecular system.

1-3. Preparative methods for PLF nano-composites

After TCRDL group reported the marked improvements in the mechanical and physical properties, studies on polymer/OMLF nano-composites have been extended to various other polymer systems, such as polystyrene [29-31], epoxy resin [32], polypropyrene [33, 34],

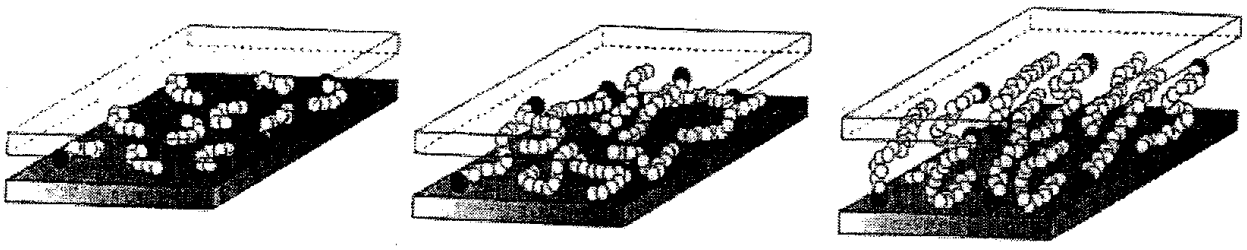

(a) **(b)** **(c)**

Figure 1-2. Alkyl chain aggregation models: (a) short chain lengths, the molecules are effectively isolated from each other, (b) medium lengths, quasi-discrete layers from with various degrees of inplane disorder and interdigitation between the layers and (c) long lengths, interlayer order increases leading to a liquid-crystalline polymer environment. Open circles represent the CH_2 segments while cationic head groups are represented by filled circles [28].

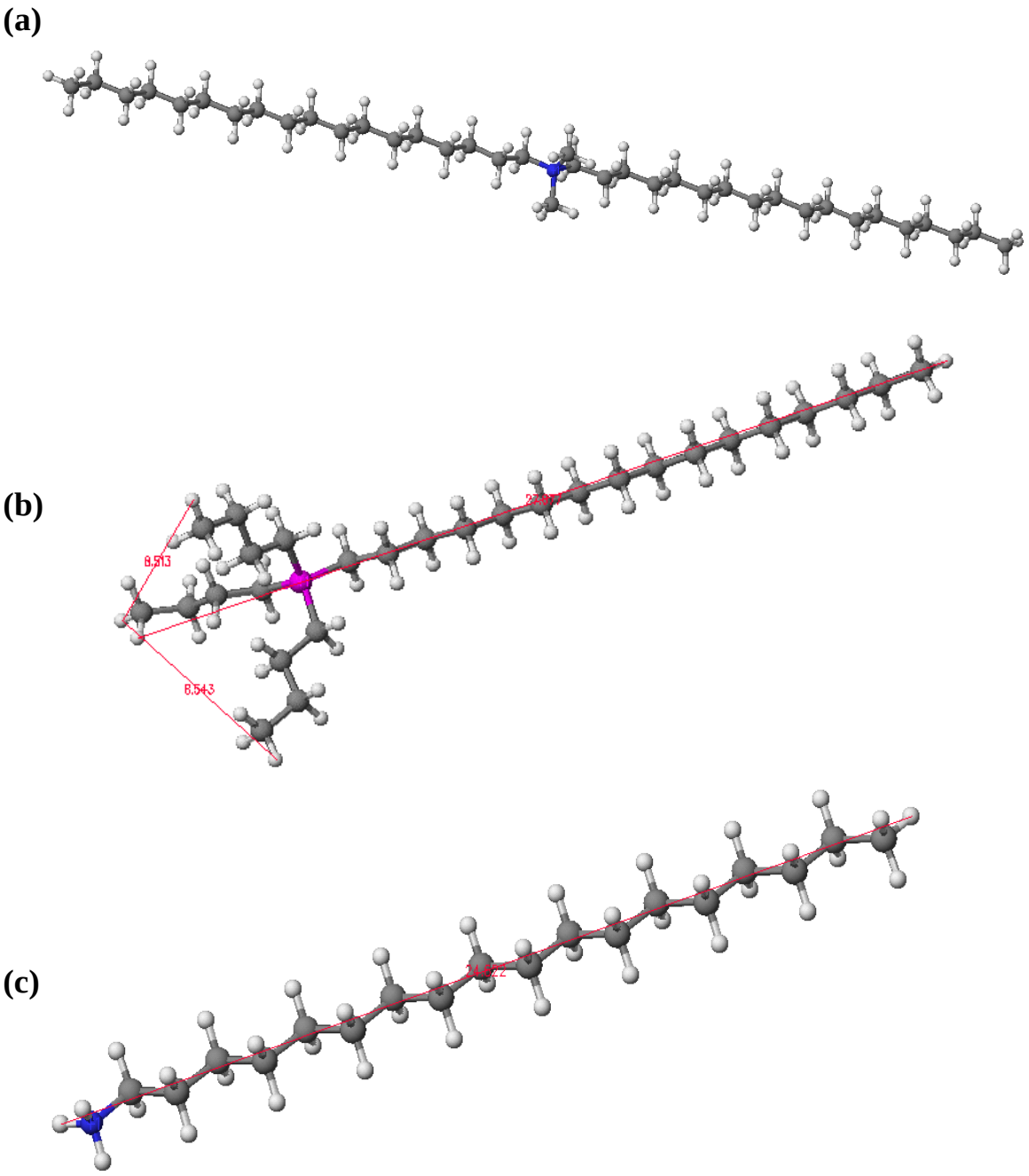

Figure 1-3. Calculated structure of (a) dioctadecyl dimethylammonium ($DC_{18}DM$), (b) hexadecyl tributylphosphonium ($C_{16}TBP$) and (c) octadecylammonium (ODA).

poly(ethyrene terephtarate) [35], poly(ε-caprolactone) [36, 37] , polyurethanes [38] , and polyimides [39] with carbon nano-tube [40-42], silica nano-particle [43-45], polyhedral oligomeric silsesquioxane: POSS [46-48] and so on. However, some of these polymers have not been achieved sufficient dispersion of the nano-fillers. It needs detail studies on the interaction between polymer and nano-filler, intercalation, and/or dispersion throughout preparation process in order that obtain well dispersed nano-composites.

Particle size of filler is very important factor. Generally, powder is changed the properties on three particle size thresholds, called critical particle size (CPS). First CPS is around 100 μm, and particle over the size has stable surface, and particle-particle interaction is almost lost. Second CPS is appeared about 1 μm, and the particle size between first and second CPS is easy for handling, mechanical pulverization and particle size control. Third CPS is around 100 nm, and the particle below 100 nm size is called nano-particle. The specific surface area of the nano-particle dramatically increases and the surface effect appears strongly. Additionally, new properties and functions are generated, and especially less than a few nm size particles, quantum effect is appeared on the nano-particles. However, strengthen particle-particle interaction on the nano-particle causes particle agglomeration which lost advantages of the nano-particle. In case of the nano-particle use as nano-filler, the key technology is dispersion technique, in other words, preparation method for nano-composite materials.

Continued progresses in nano-scale controlling have contributed to the rapid development of polymer/OMLF nano-composites [49]. Three types of main approaches for the polymer nano-

composite preparation are reported, i.e., in-situ polymerization [3-7], intercalation of polymer or pre-polymer from solution (solution cast) [24], and melt compounding [50].

1-3-1. Intercalation of polymer or pre-polymer from solution (solution cast method)

This is based on a solvent system in which polymer or pre-polymer is soluble and the filler layers are swellable. The layered filler is first swollen in a solvent, such as water, chloroform or toluene. When the polymer and layered filler solutions are mixed, the polymer chains intercalate and displace the solvent within the interlayer of the filler. Upon solvent removal, the intercalated structure remains, resulting in PLF nano-composites.

1-3-2. In-situ intercalative polymerization method

In this method, the OMLF is swollen within the liquid monomer or a monomer solution so that the polymer formation can occur in between the intercalated sheets. Polymerization can be initiated either by heat or radiation, by the diffusion of a suitable initiator, or by an organic initiator or catalyst fixed through cation exchange inside the interlayer before the swelling step by the monomer.

1-3-3. Melt intercalation method

The melt compounding method has become a main stream to prepare polymer/OMLF nano-composites, because it is compatible with the current industrial process. This method involves annealing, statically or under shear, a mixture of the polymer and OMLF above the softening

point of the polymer. This method has great advantages over either in-situ intercalative polymerization or polymer solution intercalation. Firstly, this method is environmentally benign due to the absence of organic solvents. Secondly, it is compatible with current industrial processes, such as extrusion and injection moulding. The melt intercalation method allows the use of polymers which were previously not suitable for in-situ polymerization or the solution intercalation method. This solvent-free method is much preferred for practical industrial material production because of its high efficiency and possibility of avoiding environmental hazards. During the process, the polymer chains diffuse from the bulk polymer melt into the interlayer (gallery) and then nano-fillers dispersed throughout polymer matrix. However, the penetration of the polymer chains into the nano-galleries based on OMLFs is not very well explored in literatures. The polymer matrix having simple chemical structure is probably advantageous to understand polymer penetration because it has possibilities of simplification effect of chemical structure on polymer nano-composite preparation process.

In case of preparation for non-polar or weak polar polymer-based nano-composites, compatibilizer was added through melt compounding process to apply shear stress to OMLF layers [51, 52]. In other words, non-polar polymer-based nano-composite preparation without compatibilizer is not possible through above three methods. To solve this issue, some approaches, such as applying supercritical CO_2 [53, 54] or ultrasound [55] were conducted. However, these approaches were not improved OMLF dispersion. Thus, we should investigate

a novel preparation method, from industrial point of view, which is able to apply to the practical industrial production system.

In industrial plant, polymer powder is supplied to feeder in twin-screw extruder, and the fed polymer is heated and compounded inside of the barrel (Fig.1-4). It should be noted that the conventional extruder has several full flight section for the powder transportation. With getting overlooked flight screw section, I have examined the nano-composite formation possessing discrete dispersion of OMLFs *via* "solid-state processing" (Chapter 4 and 5) [56-58], which leads to successful delamination of OMLFs and broadens the scope of industrial application.

1-4. Structure and Characterization of PLF nano-composites

1-4-1. Structure of PLF nano-composite

Layered silicates and layered titanate have layer thickness in the order of 1 nm and very high aspect ratio (e.g., 10-1000), thus creating a much higher surface area for polymer/filler intercalation than in conventional composites. Depending on the strength of interfacial interaction between polymer matrix and layered filler (modified or not), two different types of PLF nano-composites are thermodynamically achievable (Figure 1-5) [20].

(1) Intercalated nano-composites: in an intercalated nano-composites, the insertion of polymer matrix into the layered filler structure occurs in a crystallographically regular fashion, regardless of the filler to polymer ratio. Properties of the composites typically resemble those of ceramic materials.

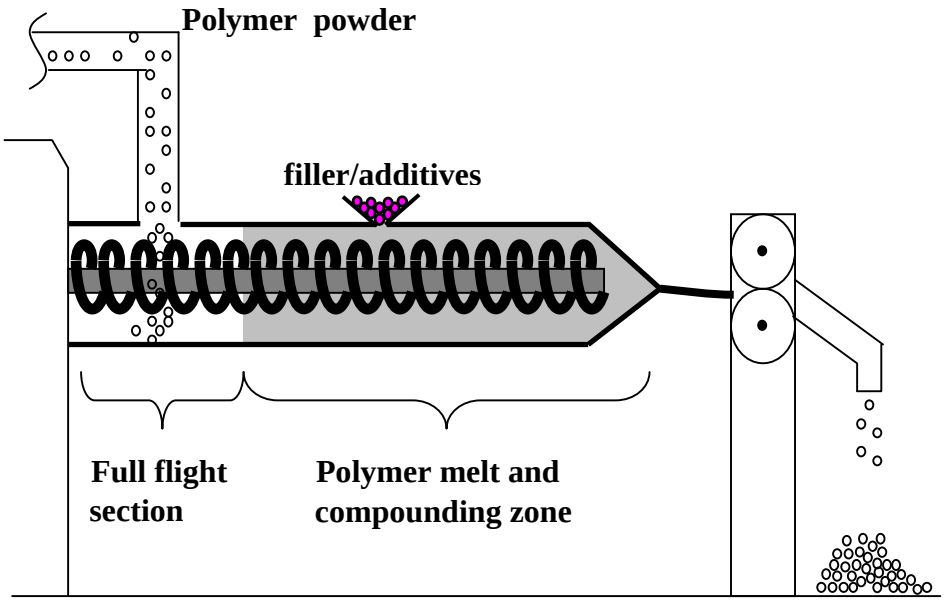

Figure 1-4. Illustration of twin-screw extruder. Full flight section is possibly available for solid-state processing.

(a)

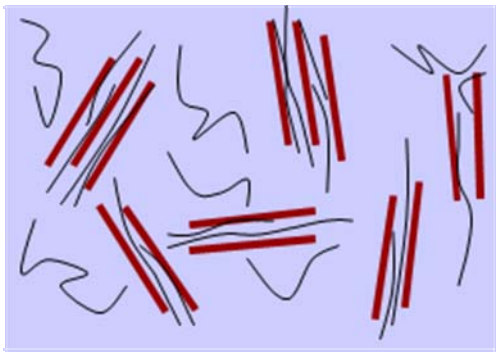

Intercalated

(b)

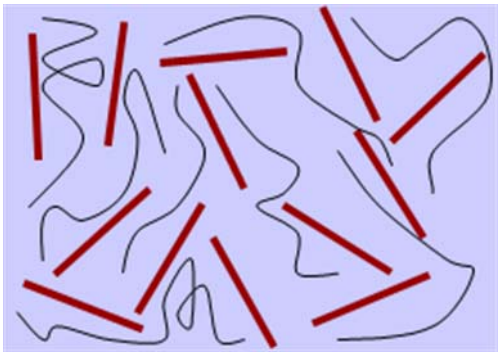

Exfoliated

Figure 1-5. Schematic illustration of two different types of thermodynamically achievable polymer/layered filler nano-composites.

(2) Exfoliated nano-composites: in exfoliated nano-composites, the individual filler layers are separated in a continuous polymer matrix by an average distance that totally depends on the layered filler loading. Usually, the clay content of an exfoliated nano-composite is much lower than that of an intercalated nano-composite.

1-4-2. Characterization of PLF nano-composites

The structure of the PLF nano-composites has typically been established using wide-angle X-ray diffraction (WAXD) analysis and transmission electron microscope (TEM) observations. Due to its ease of use and availability, WAXD is most commonly used to probe the PLF nano-composite structure and sometimes to study the kinetics of the polymer melt intercalation. By monitoring the position, shape and intensity of the basal reflections from the distributed filler layers, the nano-composite structure either intercalated or exfoliated may be identified. For example, in the case of exfoliated nano-composites, the extensive layer separation associated with the delamination of the original filler layers in the polymer matrix results in the eventual disappearance of any coherent X-ray diffraction from the distributed filler layers. On the other hand, for intercalated nano-composites, the finite layer expansion associated with the polymer intercalation results in the appearance of a new basal reflection corresponding to the variation of gallery height. Although, WAXD offers a convenient method to determine the interlayer spacing of the filler layers in the original layered fillers and in the intercalated nano-composites (within 1-4nm), however, little can be said about the spatial distribution of the filler layers or any structural inhomogeneities in the PLF nano-composites. Additionally, some layered fillers

initially do not exhibit well-defined basal reflection. Thus, peak broadening and intensity decreases are very difficult to study systematically. Therefore, conclusions concerning the mechanism of nano-composites formation and their structure based solely on WAXD patterns are only tentative.

On the other hand, TEM allows a qualitative understanding of the internal structure, spatial distribution of the various phases, and defect structure through direct visualization. However, special care must be exercised to guarantee a representative cross-section of the sample. The WAXD patterns and corresponding TEM images of two different types of nano-composites are presented in Figure 1-6.

1-5. Matrix polymers

Generally, polymer matrix for nano-composite preparation is determined by specification of the polymer usage. From scientific point of view, polymer matrix represented simple chemical structure has advantage to consider interaction between polymer matrix and nano-filler, polarity of the polymer and so on.

Polypropylene (PP) is one of the most widely used thermoplastic and consists from simple components, carbon and hydrogen. Because of the chemical structure, PP is classified into non-polar polymer. The polarity is the most important factor to achieve nano-filler dispersion. Therefore, maleic anhydrate grafted polypropylene (PP-g-MA), which has high polarity and compatibility with matrix PP is added to prepare PP-based nano-composite [53, 54]. However, PP-g-MA causes embrittlement for the result nano-composite materials, and the availability for

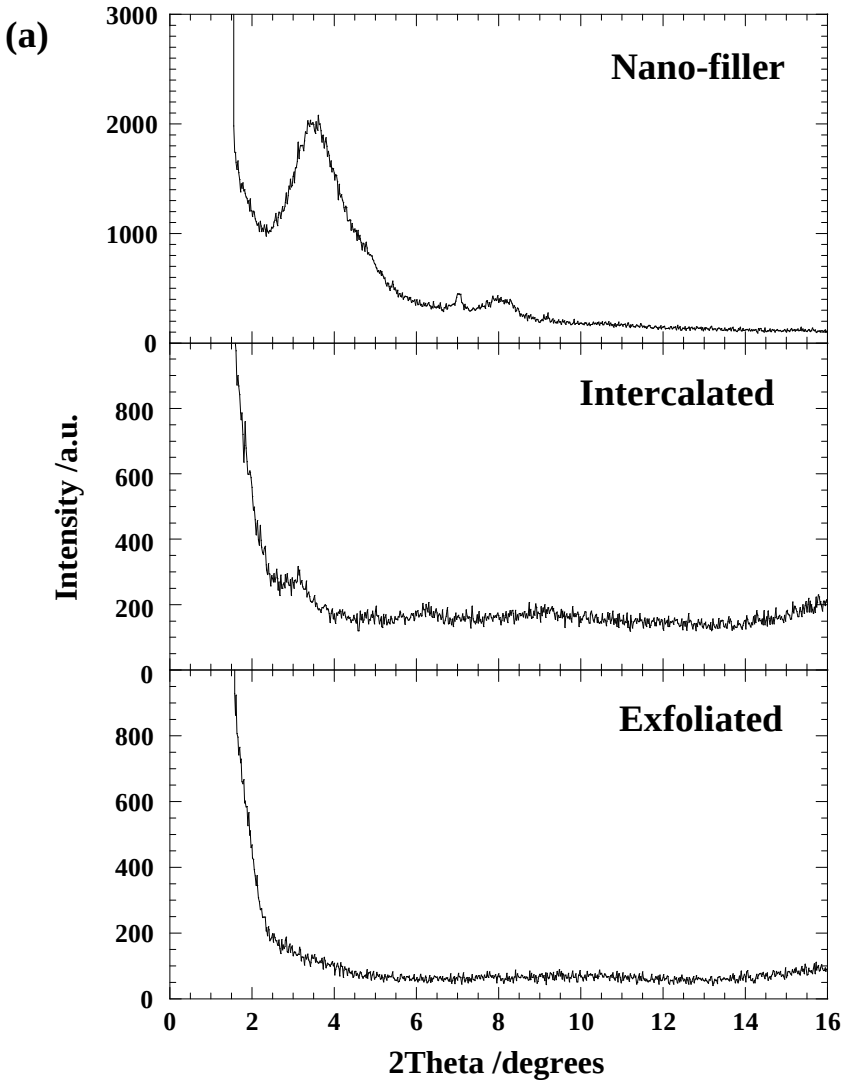

Figure 1-6. (a) WAXD patterns and (b) TEM images of two different types of nano-composite structures.

(b)

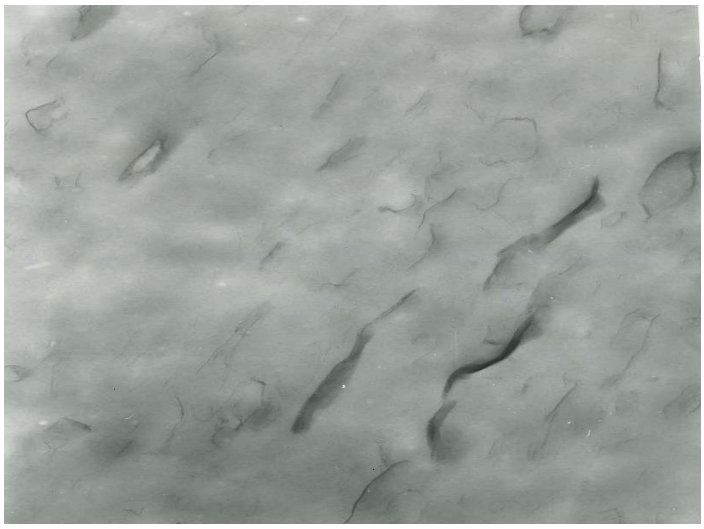

Intercalated **200 nm**

Exfoliated **200 nm**

Figure 1-6. *(Continued)*

the nano-composite is limited. Preparation for non-polar polymer based nano-composite without using compatibilizer is still challenging issue.

Poly(*p*-phenylene sulfide) (PPS) is a versatile high-performance engineering plastic having prominent heat resistance, chemical resistance, good mechanical properties, and rigidity. PPSonly consists of a rigid benzene ring and sulfur atom. So, it has possibilities of understanding polymer-filler interaction compared with other polymers. To the best of our knowledge, there are no studies on the preparation of PPS-based nano-composites containing various types of OMLFs.

1-6. Scope of this thesis

The main objective of this study is to bring out the factors that concerned with nano-composite formation and to feed back these factors for the preparation of the polymer nano-composite. For this purpose, I investigated fundamental study of the phase transition of the cationic surfactant located at the interlayer space in montmorillonite, and examined the intercalation behavior of the small molecules by using various types of nano-fillers, which have a strong impact on the explanation for the intercalation kinetics. I chose an optimal OMLF and conducted the PPS-based nano-composites preparation with and/or without shear processing. Furthermore, I have developed more innovative compounding process, i.e., solid-state processing, to delaminate the stacked-and-layered filler in the polymer matrix. And I adopted non-polar polymer as matrix to confirm the processing ability, and to investigate the effect of polarity of the matrix polymer on solid-state processing.

In Chapter 2, I investigated nonisothermal order-disorder transition behavior of alkylammonium ions (Fig. 1-3) in nano-confined space i.e., interlayer space of MMT, compared with crystallized dioctadecyl dimethyl ammonium bromide ($DC_{18}DM$-Br) through temperature modulated differential scanning calorimeter (TMDSC), WAXD, and FTIR.

In Chapter 3, I investigated the intercalation behavior of small molecules (Fig. 1-3), as a model compound for PPS, into various OMLFs interlayer evaluated from WAXD analysis. In the first part of Chapter 3, the effect of miscibility between small guest molecules and intercalants on the basis of DSC analysis was investigated. After that, the intercalation behavior of the molecules into the various types of OMLFs was discussed. In the remaining part, I chose an optimal OMLF and conducted the PPS-based nano-composites preparation with and without shear processing.

In the first part of Chapter 4, I discussed intercalation behavior with various polymers and OMLFs prepared by melt compound. The results show same trends as small molecules investigated in Chapter 3. In latter part, novel preparation methods, solid-state processing, to improve nano-filler dispersion and to delaminate the stacked-and-layered filler in PPS matrix was conducted. From the results, effectiveness of solid-state processing is clearly showed.

In Chapter 5, I also challenged to prepare non-polar polymer based nano-composite. It is considered that preparation for non-polar polymer-based nano-composite is difficult because polarity of matrix polymer is very important for nano-filler dispersion. Fortunately, I successfully prepared PP/OMLF nano-composite with solid-state processing. In this study, two thresholds during solid-state processing were found for OMLF dispersion.

Finally, I summarized the principal results and conclusions derived from this study in Chapter 6.

References

[1] Stewart R, *Plastics Engineering*, May 2004, 22.

[2] Cox H, Dearlove T, Rodges W, Verbrugge M, "Nanocomposite Systems for Automotive Applications", in 4th World Congress Nanocomposite 2004, San Francisco, Sep. 1-3, **2004**

[3] Okada A, Kawasumi M, Usuki A, Kojima Y, Kurauchi T, Kamigaito O, in D.W. Schaefer, J.E. Mark, Eds., *Polymer Based Molecular Composites*, Materials Research Society, Pittsburgh, **1990**, 171, 45.

[4] Usuki A, Kojima Y, Okada A, Fukushima Y, Kurauchi T, Kamigaito O, *J. Mater. Res.*, **1993**, 8, 1174-1178.

[5] Kojima Y, Usuki A, Kawasumi M, Okada A, Kurauchi T, Kamigaito O, *J. Polym. Sci. Part A: Polym. Chem.*, **1993**, 31, 983-986.

[6] Kojima Y, Usuki A, Kawasumi M, Okada A, Kurauchi T, Kamigaito O, Kaji K, *J. Polym. Sci. Part B: Polym. Phys.*, **1994**, 32, 625-630.

[7] Kojima Y, Usuki A, Kawasumi M, Okada A, Kurauchi T, Kamigaito O, Kaji K, *J. Polym. Sci. Part B: Polym. Phys.*, **1995**, 33, 1039-1045.

[8] Giannelis EP, *Appl. Organomet. Chem.*, **1998**, 12, 675-680.

[9] Gilman JW, *Appl. Clay Sci.*, **1999**, 15, 31-49.

[10] Ray SS, Yamada K, Okamoto M, Ueda K, *Nano Lett.*, **2002**, 2, 1093-1096

[11] Okamoto M, "Polymer/clay nanocomposites" in *Encyclopedia of Nanoscience and Nanotechnology*, H.S.Nalwa, Ed., ASP, California **2004**, Vol. 8, pp.791-843.

[12] Chen JS, Poliks MD, Ober CK, Zhang Y, Wiesner U, Giannelis EP, *Polymer*,**2002**, 43, 4895-4904.

[13] Ray SS, Okamoto K, Okamoto M, *Macromolecules*, **2003**, 36, 2355-2367.

[14] Soma I, *Filler Data Book for Practical Use*, Kogyo Chosakai Publishing Co., Ltd., **2004**.

[15] Hiroi R, Ray SS, Okamoto M, Shiroi T, *Macromol. Rapid Commun.*, **2004**, 25, 1359-1364.

[16] Yoshida O, Okamoto M, *Macromol. Rapid Commun.*, **2006**, 27, 751-757.

[17] Brindly SW, Brown G, Eds., *Crystal Structure of Clay Minerals and Their X-ray Diffraction*, Mineralogical Society, London, **1980**.

[18] Shen Z, Simon GP, Cheng YB, *Polymer*, **2002,** 43, 4251-4260.

[19] Li Y, Ishii H, *ACS Polymeric Materials Science and Engineering Fall Meeting*, **2001**, 85, 562-563.

[20] Hyun YH, Lim ST, Choi HJ, Jhon MS, *Macromolecules*, **2001**, 34, 8084-8093.

[21] Sukpiron N, Lerner MM, *Chem. Mater.*, **2001**, 13, 2179-2185.

[22] Vaia RA, Sauer BB, Tse OK, Giannelis EP, *J. Polym. Sci. Polym. Phys.*, **1997**, 35, 59-67.

[23] Aranda P, Ruiz-Hitzky E, *Chem. Mater.*, **1992**, 4, 1395-1403.

[24] Gendoya I, Lopez D, Alegria A, Mijangos C, *J. Polym. Sci. Polym. Phys.*, **2001**, 39, 1968-1975.

[25] Greenland DJ, *J. Colloid Sci.*, **1963**, 18, 647-664.

[26] Krishnamoorti R, Vaia RA, Giannelis EP, *Chem. Mater.*, **1996**, 8, 1728-1734.

[27] Blumstein A, *J. Polym. Sci. Part A Polym. Chem.*, **1965**, 3, 2653-2664.

[28] Vaia RA, Teukolsky RK, Giannelis EP, *Chem. Mater.*, **1994**, 6, 1017-1022.

[29] Vaia RA, Ishii H, Giannelis EP, *Chem. Mater.*, **1993**, 5, 1694-1696.

[30] Weimer MW, Chen H, Giannelis EP, Sogah DY, *J. Am. Chem. Soc.*, **1999**, 121, 1615-1616.

[31] Kim TH, Jang LW, Lee DC, Choi HJ, Jhon MS, *Macromol. Rapid Commun.*, **2002**, 23, 191-195.

[32] Becker O, Varley R, Simon G, *Polymer*, **2002**, 43, 4365-4373.

[33] Maiti P, Nam PH, Okamoto M, Hasegawa N, Usuki A, *Macromolecules*, **2002**, 35, 2042-2049.

[34] Kaempfer D, Thomann R, Mulhaupt R, *Polymer*, **2002**, 43, 2909-2916.

[35] Ke YC, Long CF, Qi ZN, *J. Appl. Polym. Sci.*, **1999**, 71, 1139-1146.

[36] Messersmith PB, Giannelis EP, *J. Polym. Sci. Part A: Polym. Chem.*, **1995**, 33, 1047-1057.

[37] Jimenez G, Ogata N, Kawai H, Ogihara T, *J. Appl. Polym. Sci.*, **1997**, 64, 2211-2220.

[38] Yao KJ, Song M, Hourston DJ, Luo DZ, *Polymer*, **2002**, 43, 1017-1020.

[39] Delozier DM, Orwoll RA, Cahoon JF, Johnston NJ, Smith JG, Connell JW, *Polymer*, **2002**, 43, 813-822.

[40] Li CY, Li L, Cai W, Kodjie SL, Tenneti KK, *Adv. Mater.*, **2005**, 17, 1198-1202.

[41] Zhang L, Tao T, Li C, *Polymer*, **2009**, 50, 3835-3840.

[42] Du F, Fisher JE, Winey KI, *J. Polym. Sci. Polym. Phys.*, **2003**, 41, 3333-3338.

[43] Vladimirov V, Betchev C, Vassiliou A, Papageprgiou G, Bikiaris D, *Comp. Sci. Tech.*, **2006**, 66, 2935-2944.

[44] Asuka K, Liu B, Terano M, Nitta K-H, *Macromol. Rapid Commun.*, **2006**, 27, 910-913.

[45] Nitta K-H, Asuka K, Liu B, Terano M, *Polymer*, **2006**, 47, 6457-6463.

[46] Fu BX, Yang L, Somani RH, Zong SX, Hsiao BS, Phillips S, Blanski R, Ruth P, *J.Polym.Sci. Polym. Phys.*, **2001**, 39, 2727-2739.

[47] Fu BX, Gelfer MY, Hsiao BS, Phillips S, Viers B, Blanski R, Ruth P, *Polymer*, **2003**, 44, 1499-1506.

[48] Fina A, Tabuani D, Peijs T, Camino G, *Polymer*, **2009**, 50, 218-226.

[49] Okamoto M, *Mater. Sci. Tech.*, **2006**, 22 (7), 756-779.

[50] Vaia RA, Ishii H, Giannelis EP, *Chem. Mater.*, **1993**, 5, 1694-1696.

[51] Kawasumi M, Hasegawa N, Kato M, Usuki A, Okada A, *Macromolecules*, **1997**, 30, 6333-6338.

[52] Kato M, Usuki A, Okada A, *J. Appl. Polym. Sci.*, **1997**, 66, 1781-1785.

[53] Yang K, Ozisik R, *Polymer*, **2006**, 47, 2849-2855.

[54] Bellair RJ, Manitiu M, Gulari E, Kannan RM, *J. Polym. Sci. Polym. Phys.*, **2010**, 48, 823-831.

[55] Lee EC, Mielewski DF, Baird RJ, *Polym. Eng. Sci.*, **2004**, 44, 1773-1782.

[56] Saito T, Okamoto M, Hiroi R, Yamamoto M, Shiroi T, *Macromole. Rapid Commun.*, **2006**, , 27, 1472-1475.

[57] Saito T, Okamoto M, Hiroi R, Yamamoto M, Shiroi T, *Polymer*, **2007**, 48, 4143-4151.

[58] Saito T, Okamoto M, *Polymer*, **2010**, 51, 4238-4242.

Chapter 2

Nonisothermal Order-Disorder Phase Transition of Alkylammonium Ions in Nano-confined Space

2-1. Introduction

Over the last few years, the utility of inorganic nanoscale particles as filler to enhance the polymer performance has been established. Of particular interest is recently developed nano-composite technology consisting of a polymer and organically modified layered silicate (organo-clay) because they often exhibit remarkably improved mechanical and various other materials properties when compared to those of virgin polymer or conventional composite (micro/macro-composites) [1-4]. The nano-composites and their self-assembly behavior have recently been approached to produce nano-scale polymeric materials [5]. Additionally, these nano-composites have been proposed as model systems to examine polymer structure and dynamics in confined environments [6-8].

The self-assembly and dynamics of the cationic surfactants intercalated in montmorillonite (MMT) [9-17] have been extensively investigated as well as molecular simulations [17-21]. The conformational disorder in the alkyl chains on MMT surfaces has been reported by Vaia et al. [9] as revealed by Fourier transform infrared (FTIR) spectroscopy. Li and Ishida [13,14] and Osman et al. [12,15] reported that the chain conformational order-disorder transition of the cationic surfactant in MMT galleries. At low temperature (~20 °C) the alkyl chains preferentially are in all-trans conformation. The conformational transition of the chains takes place with increasing temperature, leading to a disordered phase (at 60 °C), where the chains assume a random conformation. The observation of the phase transitions upon heating, variable chain conformation and metastable phases have been extensively investigated. The molecular simulations have helped to understand the molecular-level structure, chain conformation, tilt angle of the alkyl chains and the phase transitions. Heinz et al. [22] reported that about 4 out of 16 torsion angles were gauche in octadecyl trimethylammonium ions on mica

surfaces (C_{18}-mica) at 20 °C, whereas the number of gauche-bonds was increased to 5 at 100°C. The number of gauche-bonds remains steady with further increasing temperature. Assuming a homogeneous coverage of the entire surface area, the average molecular axis of the octadecyl trimethylammonium ions were inclined relative to the mica surface normal in the angles of 55 ° ± 2 °. This value well agrees with experimental data [23-25]. The simulation exhibited a major conformational change due to melting of the alkyl chains and an increased mobility of the C_{18}-ions across the surface cavities at elevated temperature. Brovelli et al. [25] discussed that the experimentally observed two distinct phase transition on heating. The first transition at 40 °C was due to breaking of the disordered C_{18} chains in the island structure [26] and the second transition at 60 °C was due to rearrangements of the C_{18}-ions on the surface. The concept packing density λ ($\cong A_C/A_S$) (surface saturation), which is given by the average cross-sectional area of an alkyl chain A_C in relation to the available surface area A_S, and its relation to conformational order were used to understand the behavior of alkyl chains on the surface [17,22]. They reported a simple relation between λ and the tilt angle θ for homogeneous layers is given by $\lambda = \cos \theta$.

The geometric parameter λ determines the preferred self-assembly structure into the MMT interlayer spaces. For MMT, A_S, is 1.404 nm^2 with layer charge of 0.333 [17,27]. The cross section of an all-trans alkyl chains perpendicular to its axis is $A_{C,\,trans}$= 0.188 nm^2 reported in the literature [17,27]. The λ value of C_{18}-MMT is low (~ 0.13). At low λ (< 0.2) the alkyl chains are oriented parrallel to the MMT surface having layer-by-layer structure, which leads to a high degree of conformational disorder and no reversible order-disorder transitions. At intermediate packing density ($0.2 < \lambda < 0.75$), alkyl chains adopt orientations with segmental tilt angles in the range from 78 ° to 42 °. The chain conformations are between liquid-like and crystalline. This simple model is independent of the alkyl chain length, the chemical nature of the surface and of

the cationic surfactant head group.

Despite extensive studies, the relation between packing density and chain dynamics under ordering transition is still sparse. Therefore, in this chapter, I aim to confirm the nonisothermal disorder-order phase transition (chain packing) kinetics and disorder transition (chain melting) behaviors including the conformational changes of the chain segment of the alkyl chains in confined space (nano-gallery space of the layered fillers). Knowledge of such investigations shall be useful not only in assessing how does the phase transitions appear to be fundamentally different from those observed in bulk, but also fundamental study for nano-composite formation with organically modified layered filler (OMLF).

2-2. Experimental Section

2-2-1. Materials

OMLF used in this study was montmorillonite (MMT) (cation exchange capacity (CEC) of 90 mequiv/100g, average length of 150-200 nm) intercalated with dioctadecyl dimethylammonium ($DC_{18}DM$) ions by ion exchange reaction [27], which will be hereafter defined as MMT-$DC_{18}DM$. The loading amount of the $DC_{18}DM$ cations, which was calculated from thermogravimetric analysis (TGA) was 29.5 wt% [27]. The overall degree of ion exchange was about 89%. The surface charge density is particularly important because it determines the interlayer structure of cationic surfactants as well as CEC. The characterizing method consists of total elemental analysis and the dimension of the unit cell [27]:

$$\text{Surface charge: } e^-/nm^2 = \zeta/ab \qquad (2\text{-}1)$$

where ζ is the layer charge (0.33 relative cation density for MMT [28]). a and b are cell parameters of MMT (a=5.18 Å, b=9.00 Å [27]). About 90 % of the interlayer Na^+ ions are replaced quantitatively by cationic surfactants [27]. The characteristic parameters of the nano-fillers are also summarized in Table 2-1. From these results, I can estimate the surface area per charge A_S, which is calculated to be 1.41 nm^2 for MMT. This estimation assumes that the cations are evenly distributed in a cubic array over the nano-filler surface and that half of the cations are located on the one side of the platelet and the other half reside on the other side. As reported by Heinz et al. [17], in the present study, the calculated λ value of MMT-$DC_{18}DM$ is ~ 0.27, corresponding to the intermediate packing density.

Table 2-1. Characteristic parameters of montmorillonite (MMT)

parameters	MMT
Chemical formula	$Na_{0.33}(Al_{1.67}Mg_{0.33})\ Si_4O_{10}(OH)_2$
Particle size[29] /nm	~100-200
BET area /m^2/g	~700
CEC [a)] /meq/100g	~90(90)
Area per charge/nm^2	1.41
Density /g/cm^3	2.50
Refractive index (n^{20}_D)	1.55
pH	7.5-10

[a)] Methylene blue adsorption method. The values in the parenthesis are calculated from chemical formula of nano-fillers.

For comparison, dioctadecyl dimethylammonium bromide ($DC_{18}DM$-Br), purchased from Aldrich, was used as a reference.

2-2-2. Characterization methods

The specimens were characterized by using temperature-modulated differential scanning calorimeter (TMDSC) (TA 2920; TA Instruments) under nitrogen at a heating and cooling rate of 5 °C/min with a heating/cooling cycle of the modulation period of 60s for an amplitude of +/-0.769 °C. The chain packing and/or crystallization temperature with cooling from melt (T_c), the melting temperature (T_m) and heat of fusion (ΔH), were calibrated with Indium before experiments.

WAXD analyses were performed using an Mxlabo X-ray diffractometer (MAC Science Co.; 3kW, graphite monochromator, CuKα radiation (λ_x=0.154nm), operated at 40kV and 20mA). Samples were scanned in fixed time mode with counting time of 2 s at room temperature under diffraction angle (2Θ) in the range of 1 ° to 70 °.

The crystalline texture of $DC_{18}DM$-Br during cooling process from melt state (~100 °C)

was also measured. The thin samples were crystallized on the Linkam hot stage mounted on a polarized optical microscope (POM) (Nikon OPTI-PHOTO2-POL). After the complete crystallization, the samples were observed using POM and fitted with a color-sensitive plate to determine the sign of birefringence, and the photographs were taken. The details regarding POM observation can be found in our previous paper [30].

Fourier transform infrared (FTIR) spectra were collected at 2 cm^{-1} nominal resolution using a Varian FTS7000 spectrometer equipped with a MCT detector in transmission mode. The spectra were obtained by averaging 32 scans with a mean collection length of 1 s per spectrum. The background spectra used for reduction were collected at the same temperature (*T*) range of 25-120 °C for DC_{18}DM-Br and 25-80 °C for MMT-DC_{18}DM, respectively, with the samples. The homogenous mixture of KBr powder and DC_{18}DM-Br (fine powder) or MMT- DC_{18}DM. (powder) in the weight ratio 98:2 were prepared. The mixtures were made into pellets having a thickness of ~ 400 μm, were placed in a homemade heating chamber and heated up to a temperature *T* with a heating/cooling rate of 200-300 °C /min. The collected data was processed with Grams/AI® software (Thermo Galactic Co., USA).

2-3. Results and Discussion

2-3-1. DSC scan and crystalline structure

Figure 2-1 shows the TMDSC thermograms of MMT-$DC_{18}DM$ and $DC_{18}DM$-Br from –50 °C to melt, cooling from molten state (~100-120 °C) and 2nd heating at a rate of 2.0 °C/min. For $DC_{18}DM$-Br, the formation of the maximum crystallization peak was obtained at 76.84 °C, accompanied with a small peak at 39.69 °C. For MMT-$DC_{18}DM$, the peak was much broader (35.55 °C) due to the disorder-order phase transition (chain packing) in the confined space [15,17,22]. Both chain packing temperatures (T_c) for MMT-$DC_{18}DM$ and crystallization temperature (T_c) from melt state for $DC_{18}DM$-Br sensitively depended on the cooling rate. A large shift was observed at chain melting point (T_m= 39.14 °C) and endothermic/exothermic heat behaviour of MMT-$DC_{18}DM$ (ΔH_f) when compared to the T_m of $DC_{18}DM$-Br crystals (86.66 °C). The depression of T_m in MMT-$DC_{18}DM$ increased due to the thermal stability of the ordered structure, formed during the cooling process. The enthalpy of phase transition was 20 % of the enthalpy of melting of $DC_{18}DM$-Br, which implied the breakage of the disordered alkyl chain structure. This speculation is in accord with the results reported by Heinz et al. [22].

The crystal structures of MMT-$DC_{18}DM$ and $DC_{18}DM$-Br were analyzed by WAXD as shown in Figure 2-2. The diffraction pattern of pristin MMT (MMT-Na^+) was taken as the reference to compare with the diffraction peaks of silicate layer.

In Figure 2-2 (a), the mean basal spacing of the (001) plane ($d_{(001)}$) is 3.57 nm (2Θ = 2.47 °). The interlayer distance was 2.65 nm, was estimated by subtracting the value of layer thickness (0.92 nm) of MMT [21]. This is an important point for the following discussion on the interlayer structure.

The molecular dimensions of various cationic surfactants were proposed by using a

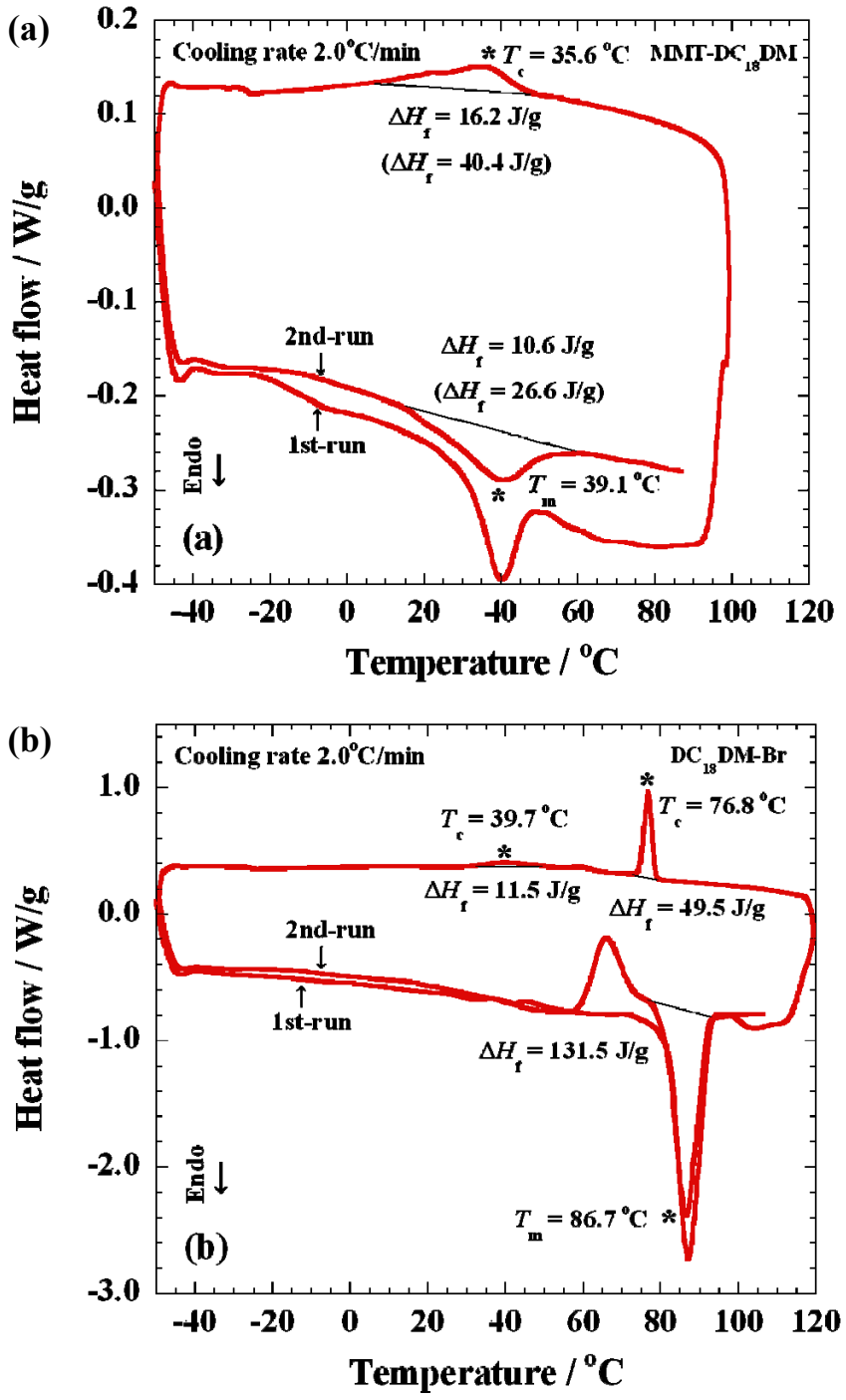

Figure 2-1. TMDSC scans for (a) MMT-DC_{18}DM and (b) DC_{18}DM-Br. The total endothermic and exothermic heat flows in the parenthesis indicate the total heat flows for 100 % cationic surfactant.

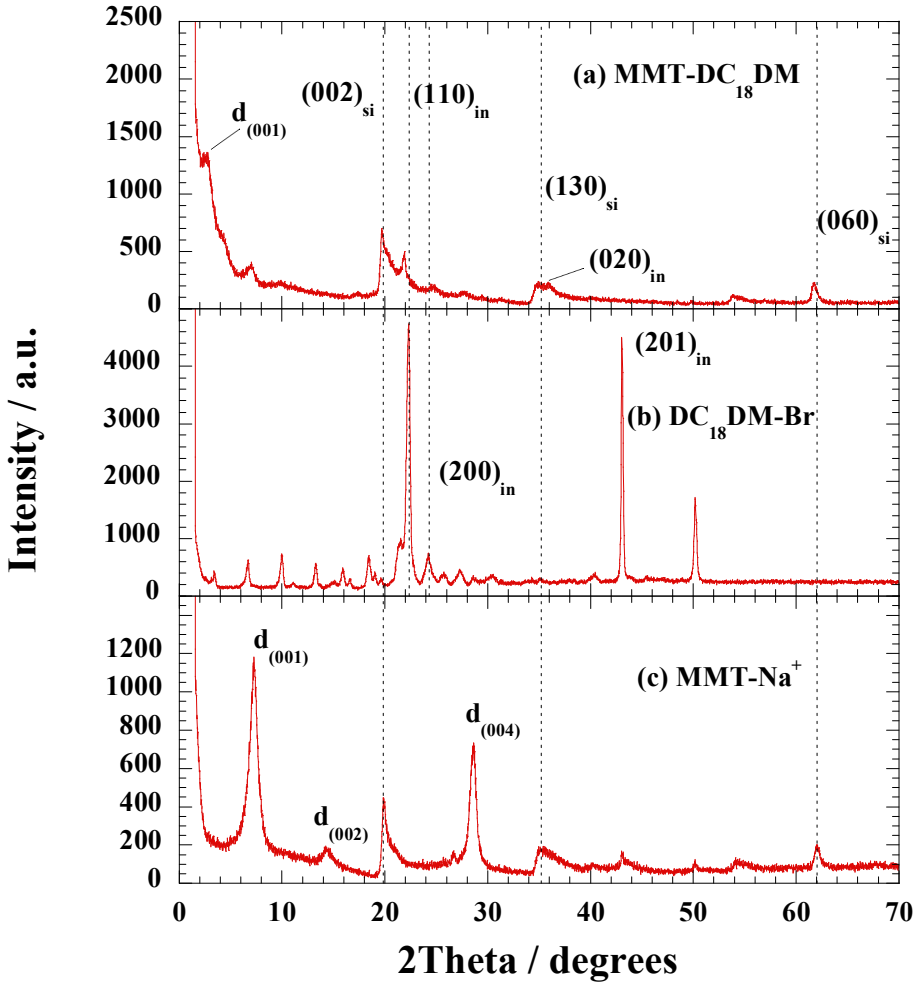

Figure 2-2. Typical WAXD profiles of (a) MMT-$DC_{18}DM$, (b) $DC_{18}DM$-Br and (c) pristin MMT (MMT-Na^+).

molecular dynamics program (MM2 in Quantum CAChe, Fujitsu Ltd.), by taking van der Waals radi into consideration. The structure optimization was based on minimization of the total energy of the molecular system. The calculated models of the cationic surfactant structures were presented in our previous paper [27]. For the $DC_{18}DM$ cation molecule, the length, thickness and width were 2.601, 0.372 and 0.372 nm respectively with an all-trans conformation. Since the length of the alkyl unit is more than 2 nm, the spacing (distance between exchange sites) of 1.188 nm do not allow the parallel layer arrangement of flat-lying chains [13,17] in the MMT nano-galleries.

The WAXD analysis coupled with an all-trans conformation of the cationic surfactant, it can assumed that the alkyl chains radiate away from the surface forming a one-layer extended paraffin type structure [31] without tilting to the silicate layers when I compared to the molecular modeling of the interlayer distance.

WAXD profiles of crystallized $DC_{18}DM$-Br during cooling process (see Figure 2-1(b)) from molted state (~ 120 °C) in Figure 2-2 (b) and the corresponding POM image is shown in Figure 2-3. The crystalline texture of $DC_{18}DM$-Br was evolved quickly during the cooling process. The assignment of the reflections associated with the crystalline structure was based on the orthorhombic unit cell (space group *Pnam*: a= 0.741 nm, b= 0.495 nm and c= 0.255 nm) and chain configurations [32]. The reflections at 2Θ=22.36°, 24.11° and 42.97°corresponds to $(110)_{in}$, $(200)_{in}$ and $(201)_{in}$ planes of the crystallite, respectively. For MMT-$DC_{18}DM$, these reflections are observed as small peaks except the evolution of $(201)_{in}$. The peak occurring from $(110)_{in}$ plane (parallel to the alkyl chains) is shifted towards the lower reflection angle and another reflection peak at 2Θ =36° (assigned to the reflection of $(020)_{in}$ plane) appears. The large inter-chain distances may be due to the formation of poor chain packing in the confined space.

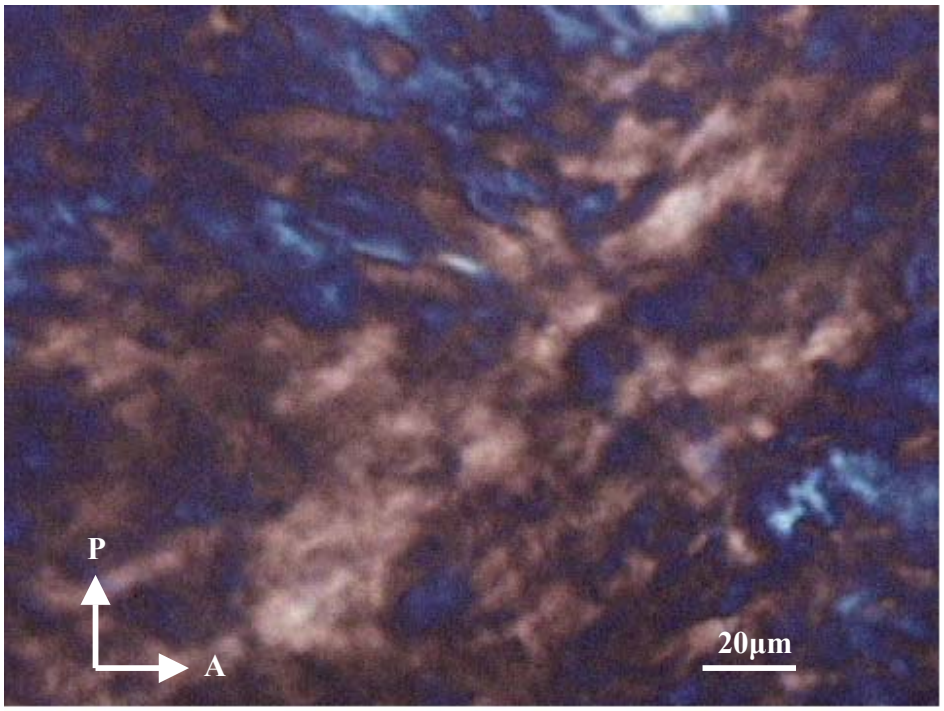

Figure 2-3. Polarized optical micrograph for crystallized $DC_{18}DM$-Br during cooling process.

In Figure 2-2 (c), the reflections at 2Θ =19.83°, 35.38° and 62.02° correspond to the planes $(002)_{si}$, $(130)_{si}$ and $(060)_{si}$ of the crystalline silicate lattice, respectively [33]. These reflections were clearly observed in Figure 2-2(a).

2-3-2. Temperature dependence of ordered structure development

The temperature dependence of WAXD profiles of MMT-DC_{18}DM with heating and cooling processes are shown in Figure 2-4. With increasing temperature the intensities from $(110)_{in}$ and $(200)_{in}$ gradually decreases without any peak shifts. The reflection from $(200)_{in}$ plane vanishes at around 60 °C and above. These features were summarized in the plot of intensity ratio against temperature. The intensity from $(002)_{si}$ plane was taken as a reference. The ratio of $I(110)_{in}/I(002)_{si}$, is related to the chain melting (heating process) and chain packing (cooling process) of the alkyl chains into the MMT galleries, rapidly decreased with temperature beyond 40 °C (corresponding to T_m [see Figure 2-1(a)]), and finally reached a constant value (~ 0.635). On cooling from melt (~ 80 °C) the same phenomena was observed too, can be termed as a reversible process. The ratio of $I(200)_{in}/I(002)_{si}$ showed a gradual decrease with temperature from the very beginning of the heating. Comparing to the heating process, the intensity ratio under cooling process is slightly lower and there is a hysteresis phenomenon.

On the other hand, through cyclic thermal treatment the interlayer spacing $d_{(001)}$ remained constant, whereas the intensity was found to be more sensitive to temperature. The intensity ratio of $I(001)_{MMT\text{-}DC18DM}/I(002)_{si}$ under cooling process showed a slightly higher value than that of the heating process. This feature seems to be a reversible process with some hysteresis.

FTIR spectroscopy was used to probe the conformational change and lateral chain-chain

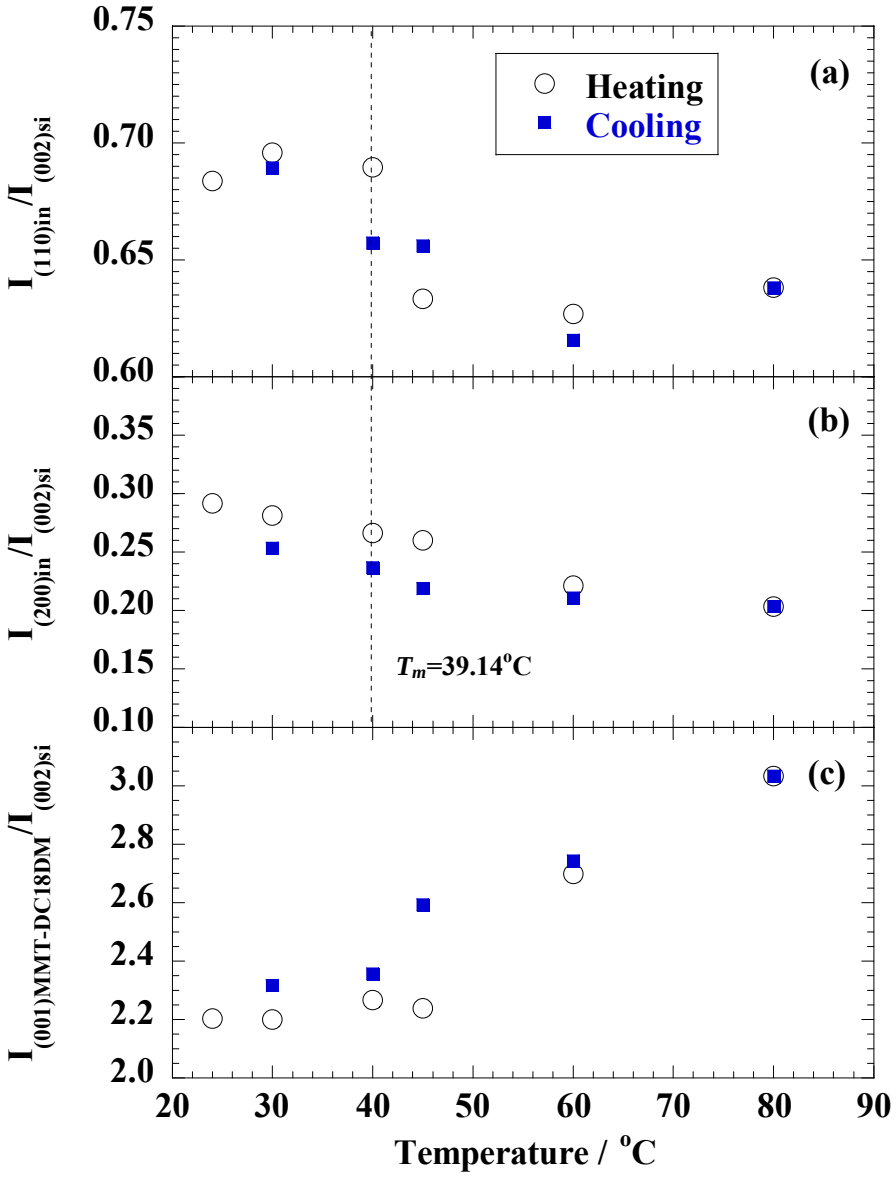

Figure 2-4. Temperature dependence of characteristic intensity ratios of (a) $I(110)_{in}/I(002)_{si}$, (b) $I(200)_{in}/I(002)_{si}$ and (c) $I(001)_{MMT\text{-}DC18DM}/I(002)_{si}$ with heating and cooling processes. The dashed line indicates T_m detected by TMDSC.

interaction. The frequency, width and intensity of the asymmetric ($\nu_{as}(CH_2)$) and symmetric ($\nu_s(CH_2)$) methylene stretching bands near 2920 and 2851 cm^{-1}, respectively, were sensitive to the gauche/trans conformer ratio. For example, in the melting of nonadecane, on going from the crystalline phase (all-trans conformation) to a disordered liquid state rich in gauche population, ($\nu_{as}(CH_2)$) and ($\nu_s(CH_2)$) were shifted from 2916 to 2923 cm^{-1} and from 2848 to 2853 cm^{-1}, respectively [11]. The similar shifts to higher frequencies were observed in both MMT-DC_{18}DM and DC_{18}DM-Br on heating across the transition temperatures (= T_m) detected by TMDSC (Figure 1), suggesting the conformational changes in alkyl chains. For MMT-DC_{18}DM, a band of ($\nu_{as}(CH_2)$) exhibited higher frequency (2921.1 cm^{-1}) than that of DC_{18}DM-Br (2919.2 cm^{-1}), suggesting a higher population of the gauche conformers. The temperature dependence of the bandwidth (full width at half-maximum: FWHM) are shown in Figure 2-5. The bandwidth is closely proportional to the degree of molecular mobility. For MMT-DC_{18}DM, at 25 °C, the bandwidths at both characteristic bands ($\nu_{as}(CH_2)$) and ($\nu_s(CH_2)$) were wider than those of DC_{18}DM-Br, whereas its variation with increasing temperature exhibited narrow values (4 cm^{-1} for ($\nu_{as}(CH_2)$) and 5 cm^{-1} for ($\nu_s(CH_2)$), respectively) when compared with those of DC_{18}DM-Br (11 cm^{-1} for ($\nu_{as}(CH_2)$) and 7 cm^{-1} for ($\nu_s(CH_2)$). These results conclude the formation of enhanced gauche conformers and the poor chain packing of the ordered alkyl chains in MMT-DC_{18}DM when compared to the crystallized DC_{18}DM-Br. Upon heating, the mobility of the alkyl chains is enhanced owing to the chain melting in the confined space. The alkyl chains are tethered to the silicate surface on one end and the translational freedom of the chains is limited due to the ion-dipole interaction between the head group of $N^+(CH_3)_2$ and silicate surface. In addition, the pressure drop (Δp) into the nano-galleries[27,29], which makes the chain mobility more difficult, is also an important parameter. The estimated pressure difference (~ -24MPa) was

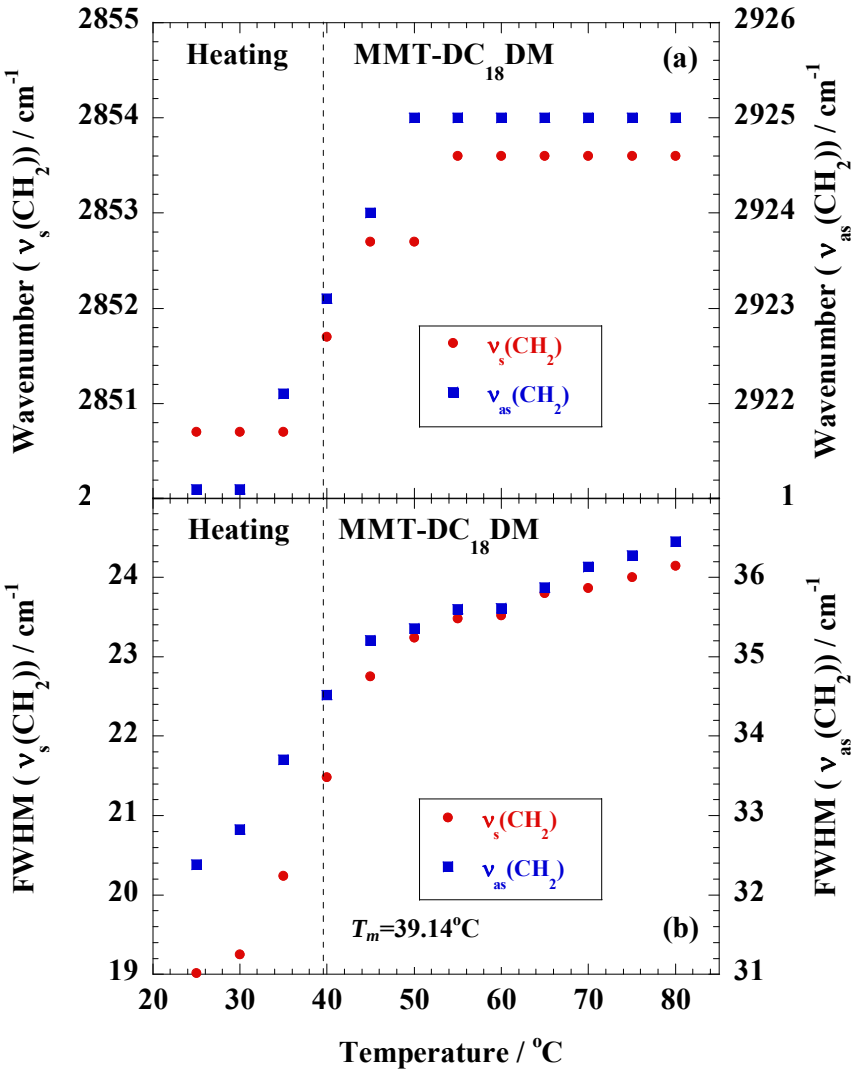

Figure 2-5. Temperature variations of frequency shifts and FWHM for heating process for MMT-DC_{18}DM ((a) and (b)), and DC_{18}DM-Br ((c) and (d)). The dashed line indicates T_m detected by TMDSC.

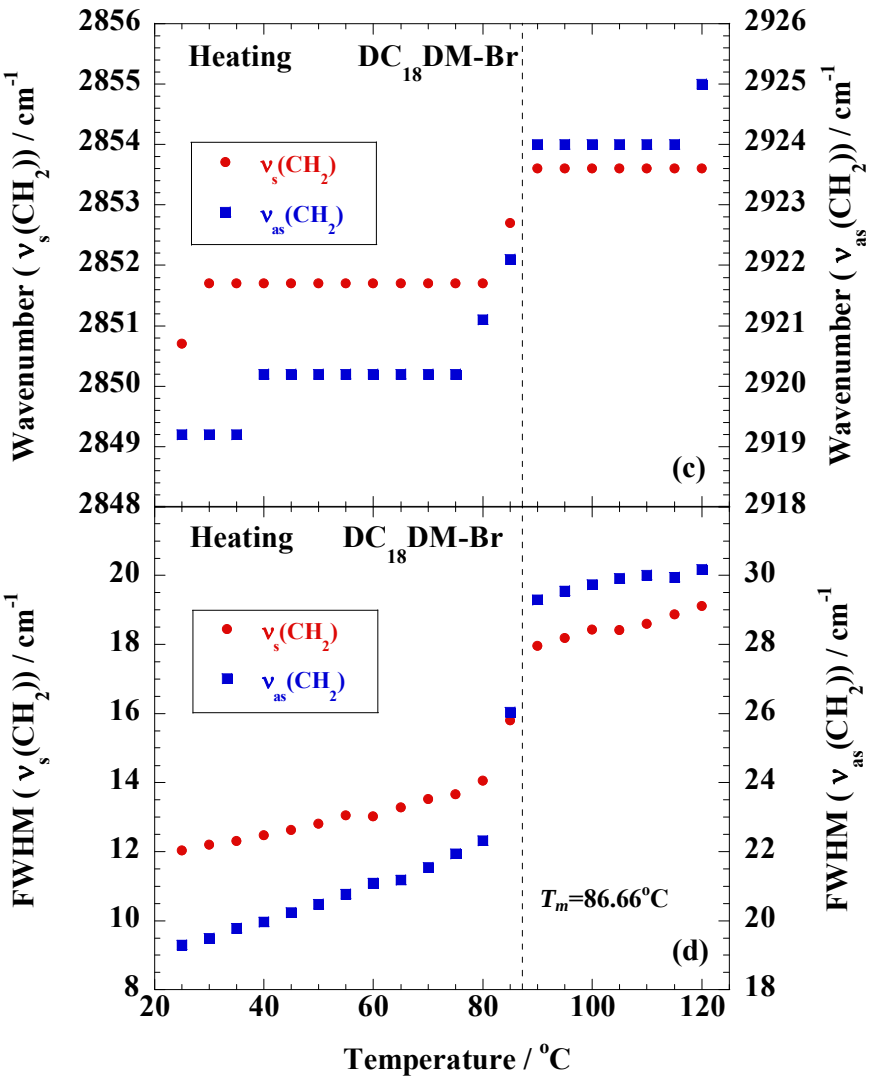

Figure 2-5. *(Continued)*

much larger than the atmospheric pressure (~ 0.1MPa). For these reasons, another interesting feature related with the confined alkyl chains is shown in Figure 2-5. For $DC_{18}DM$-Br, the sharp changes in peak maxima and FWHM were seen around T_m of the crystallized alkyl chains (indicated with dashed lines of Figure 2-5) in the bulk. On the other hand, for MMT-$DC_{18}DM$, the confinement effects lead to a more steady increase up to 80 °C

Figure 2-6 shows the comparison of the characteristic band ($\nu_{as}(CH_2)$) for heating and cooling processes. For MMT-$DC_{18}DM$ and $DC_{18}DM$-Br, the hysteresis phenomena were observed in both cases, i.e. the peak maxima in the cooling process exhibits higher frequency when compared to the heating process owing to the difference between T_m and T_c (indicated with dashed lines of Figure 2-6). For the variation of FWHM, the same trend was found in both systems (Fig. 2-7). This means that the temperature dependence of the conformational changes and the mobility of the alkyl chains agree well with the thermal transition temperatures as revealed by TMDSC.

2-3-3. Ordering kinetics and crystallization kinetics

To understand the disorder-order phase transition kinetics of the alkyl chains in MMT-$DC_{18}DM$, differential scanning calorimeter was used to estimate the overall transitions under nonisothermal process. The broadening of the crystallization peak occurred with increase of cooling rate in the bulk crystallization of $DC_{18}DM$-Br. On the other hand, the MMT-$DC_{18}DM$, the chain packing peak profile remained the same with the increase of cooling rate. The effect of confined molecules ($DC_{18}DM$s) on the nonisothermal phase transition can be detected from this analysis. Figure 2-8 shows the cooling rate dependence of T_c and ΔH_f. For MMT-$DC_{18}DM$, T_c value showed a gradual decrease with the cooling rate (increasing up to 5 °C/min), beyond which

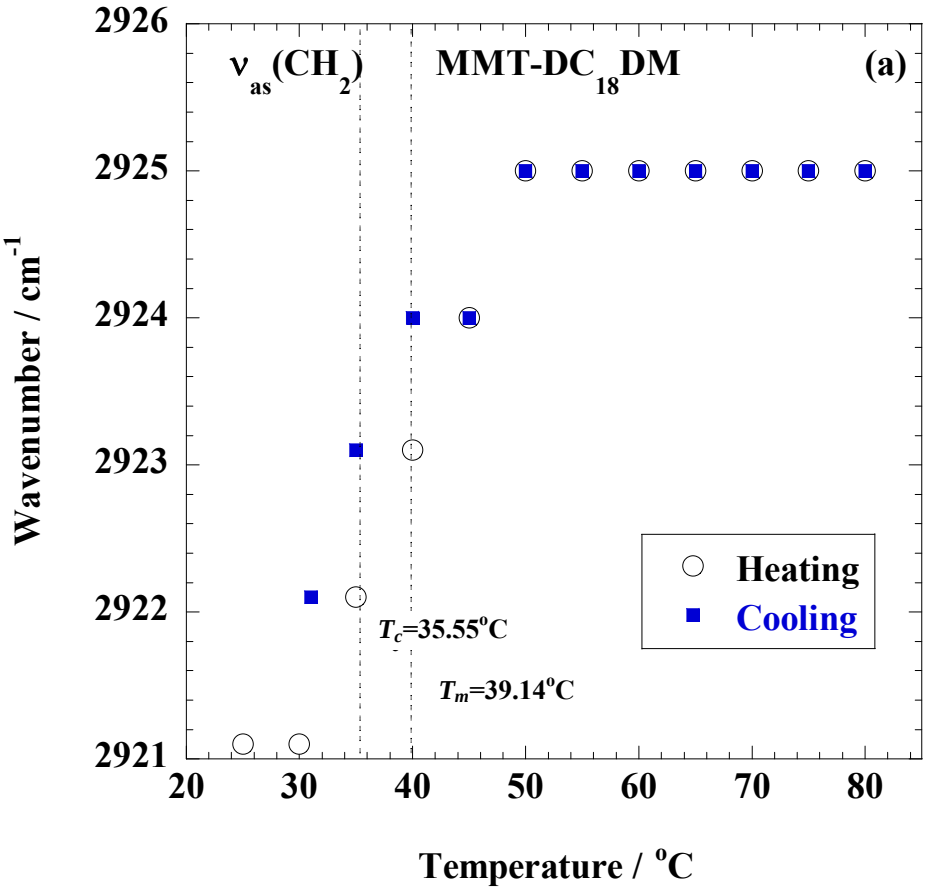

Figure 2-6. Temperature variations of frequency shifts in characteristic band ($\nu_{as}(CH_2)$) upon cyclic thermal treatment for (a) MMT-DC_{18}DM and (b) DC_{18}DM-Br. The dashed lines indicate T_c and T_m detected by TMDSC.

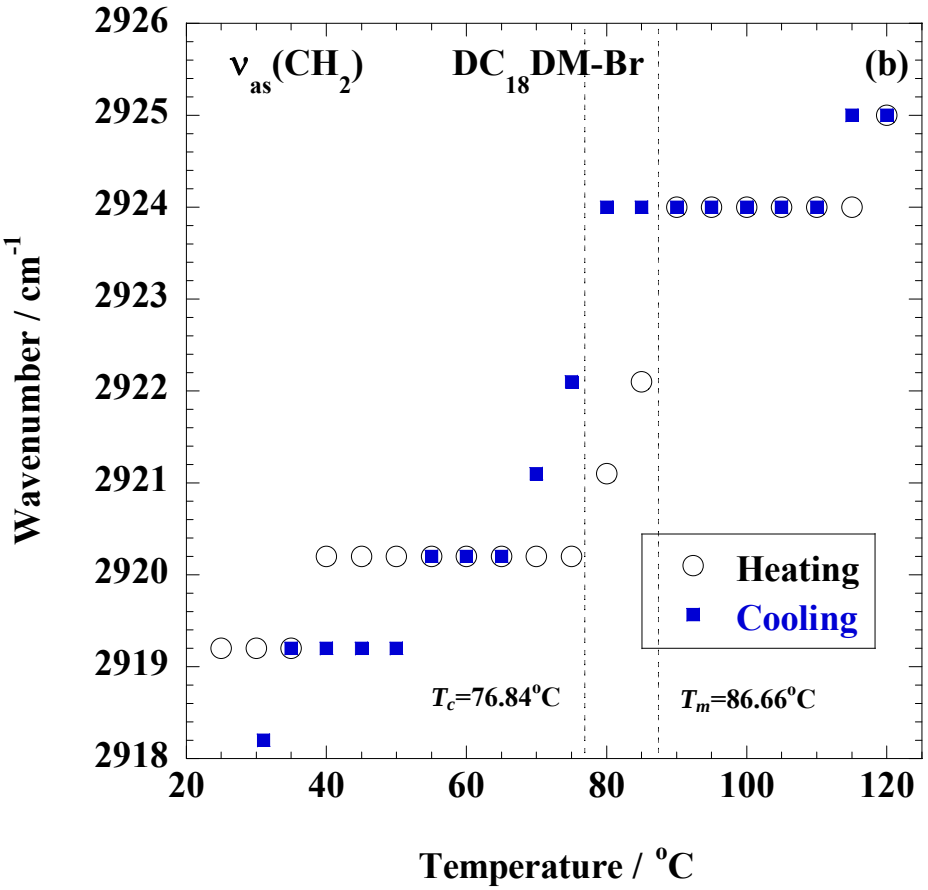

Figure 2-6. *(Continued)*

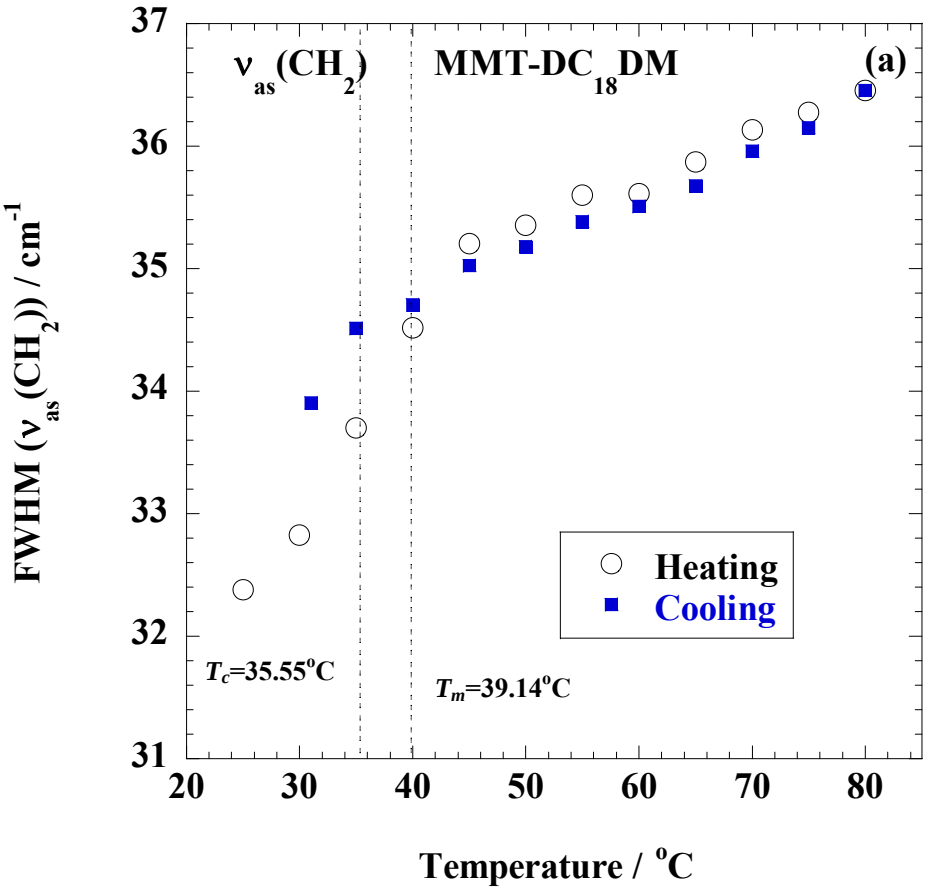

Figure 2-7. Temperature variations of FWHM for characteristic band ($\nu_{as}(CH_2)$) upon cyclic thermal treatment for (a) MMT-DC_{18}DM and (b) DC_{18}DM-Br. The dashed lines indicate T_c and T_m detected by TMDSC.

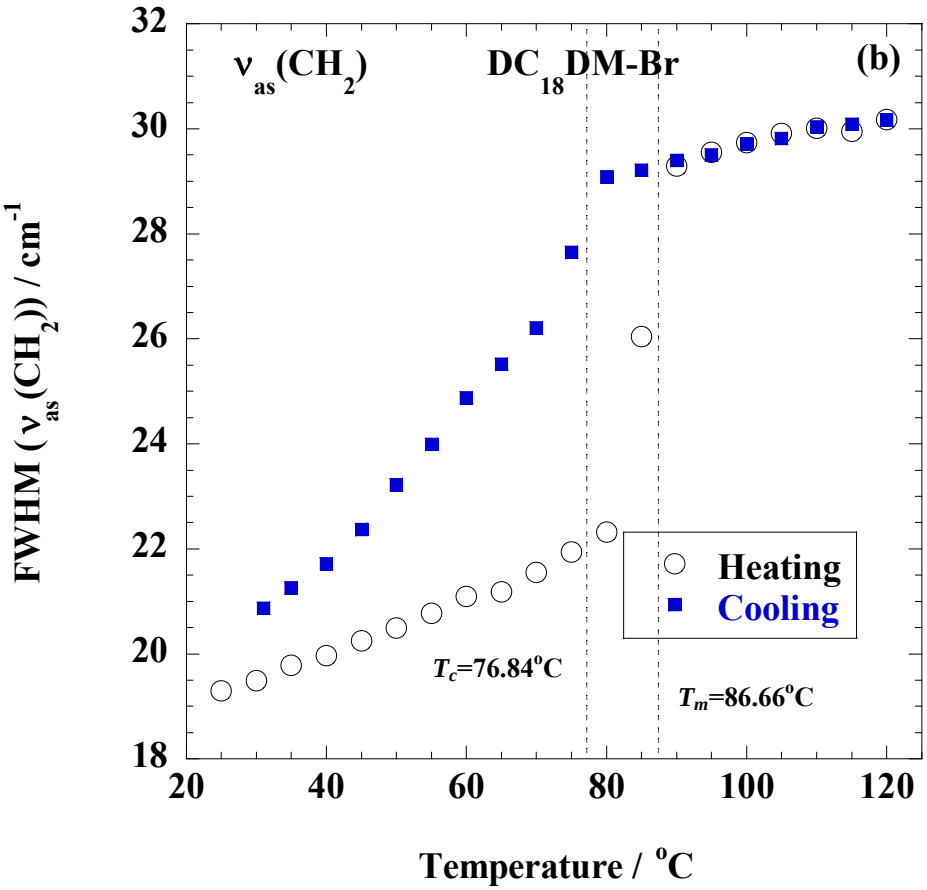

Figure 2-7. *(Continued)*

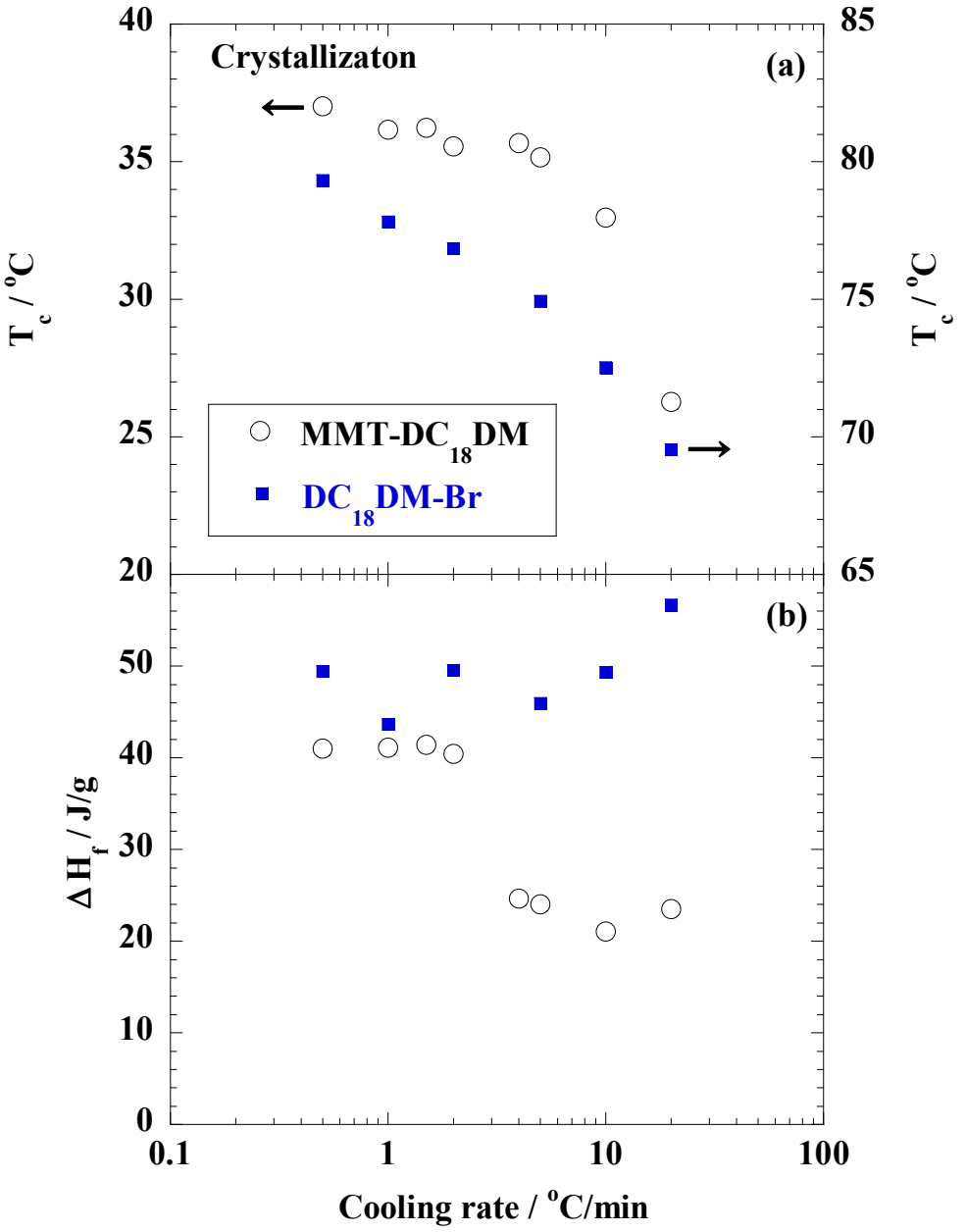

Figure 2-8. Cooling rate dependence of (a) T_c and (b) ΔH_f for MMT-DC_{18}DM and DC_{18}DM-Br.

the temperature rapidly decreased with the rapid decrease in ΔH_f. On the other hand, the $DC_{18}DM$-Br T_c decreased steadily up to 20 °C/min and ΔH_f first stood almost constant (~ 46 J/g), later increased steadily, implying that the occurrence normal crystallization in the bulk. Thus, the crystallization is controlled by the degree of the supercooling ($\equiv T_m - T_c$), such as the polymer melt crystallization [34]. I can conclude that the phase transition in the confined space is more obvious as opposed to the bulk crystallization.

Figure 2-9 shows the time variation of the relative degree of the ordering during phase transition ($\Delta H_f(t)/\Delta H_f(\text{total})$). This was calculated from the ratio area of the exotherms up to time (t) divided by the total exotherm area, i.e.:

$$\Delta H_f(t) / \Delta H_f(total) = \frac{\int_{t_0}^{t} (dH_f / dt)dt}{\int_{t_0}^{\infty} (dH_f / dt)dt} \qquad (2\text{-}2)$$

where (dH_f/dt) is the heat flow rate and t_0 is onset time, at which the ordering and/or crystallization starts. The development of the transition showed a characteristic sigmoidal dependence on time for the samples. Furthermore, the curves in the bulk crystallization ($DC_{18}DM$-Br) exhibited much faster transition as compared with those of MMT-$DC_{18}DM$. The phase transition *half-time* $t_{1/2}$ with the reduced intensity reaches 1/2, I defined $1/t_{1/2}$ as a measure of the overall transition rate at each characteristic curve in Figure 2-9 (indicating the arrow), and plotted it in Figure 2-10 against cooling rate. Interestingly, the estimated overall rate (0.40-4.35 s^{-1}) for MMT-$DC_{18}DM$ coincides with the cooling rate in the range between 0.5 and 5.0 °C/min, beyond which they deviated to a downward trend. The downward deviation agreed well with the cooling rate dependence of T_c and ΔH_f (Fig. 2-8). In contrast, the $DC_{18}DM$-Br

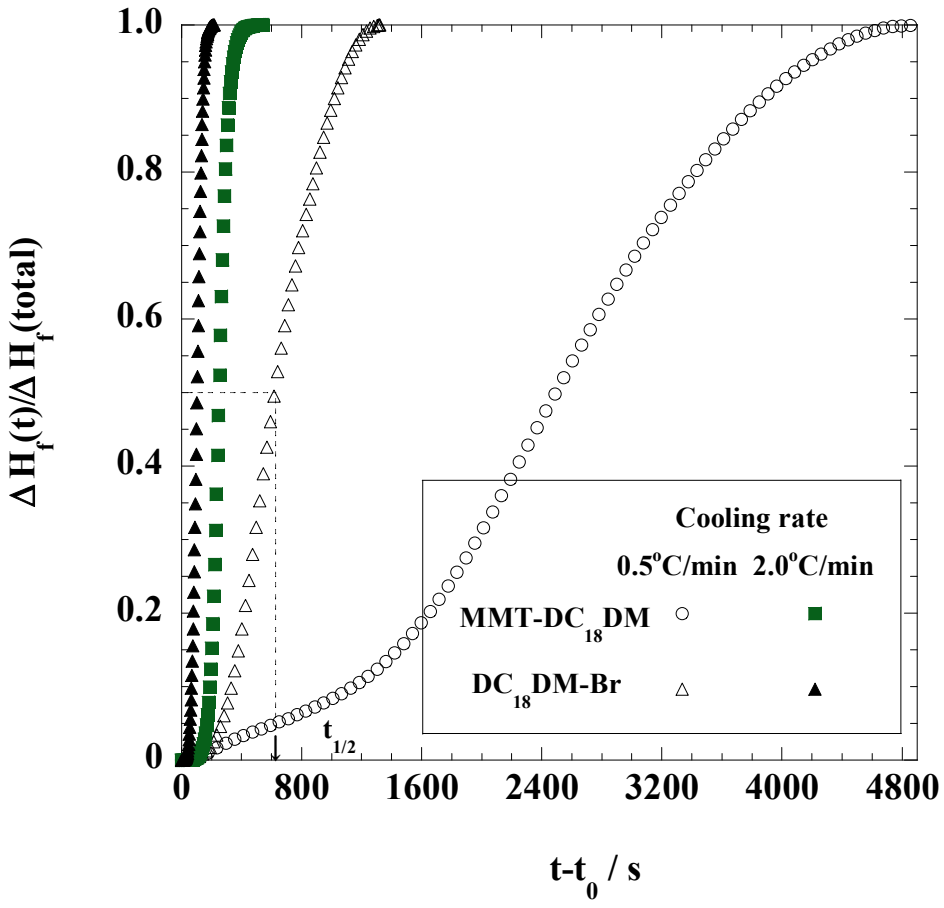

Figure 2-9. Time variation of reduced degree of the degree of ordering ($\Delta H_f(t)/\Delta H_f(\text{total})$) at two different cooling rate (0.5 and 2.0 °C/min). The dashed line indicates the phase transition half-time $t_{1/2}$.

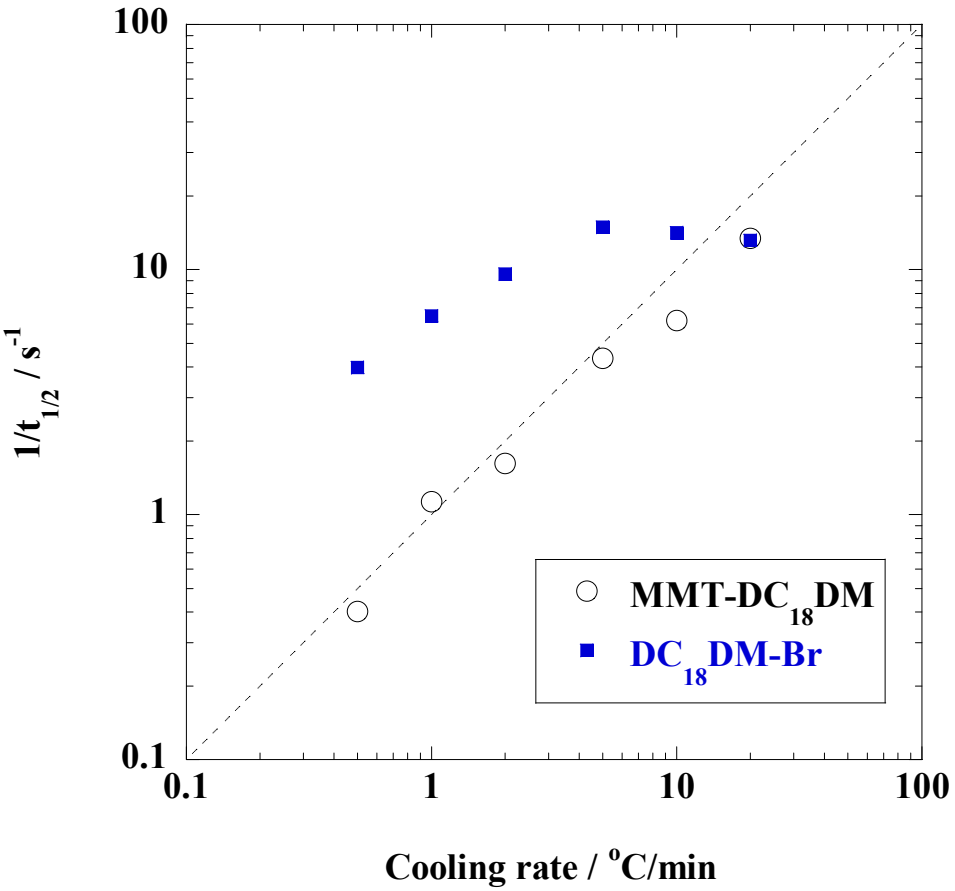

Figure 2-10. Cooling rate dependence of overall phase transition rate ($1/t_{1/2}$). The dashed line indicates the linear relation between x- and y-axes.

values showed a large value one order higher in magnitude as compared with those of MMT-$DC_{18}DM$, later reached a constant value (13.2 s^{-1}). The confined molecules ($DC_{18}DMs$) in one or two dimensional order exhibit significant contribution to enhance the nonisothermal phase transition (chain packing) at higher cooling rate (~ 5.0-20.0 °C/min) despite the some downward deviation. As discussed above, this is presumably due to the poor chain packing for the ordered alkyl chains in MMT-$DC_{18}DM$.

To confirm the ordering kinetics of the nonisothermal transition behavior of the cationic surfactants in MMT upon confinement, Arrhenius plot was constructed with the cooling rate *versus* reciprocal of the absolute phase transition (chain packing) temperature, $1/T_c$ as shown in Figure 2-11.

Ozawa-Flynn-Wall method based on Doyle's approximation [35,36] can be used to find the effective activation energy and is expressed as follow:

$$\text{Cooling rate} \sim \exp(1.052E_a / RT_c) \qquad (2\text{-}3)$$

where E_a is the activation energy for the nonisothermal phase transition, RT_c is the thermal energy. For both the cases examined, the plots conformed to two straight lines in the different T_c regime. The slope that reflects the activation energy of the nonisothermal process was reduced when the cooling rate was beyond 5.0 °C/min. For example, in the polymer melt crystallization, the E_a value decreased upon increasing the crystallization temperature throughout both glass and melt crystallization regions [37]. In Figures 2-11, similar changes are found at a cooling rate of 5.0 °C/min. This feature is superficially similar to the result as shown in Figures 2-8 and 2-10. For MMT-$DC_{18}DM$, the significant change in E_a (= 947±5 to 110±20 kJ/mol) was found when

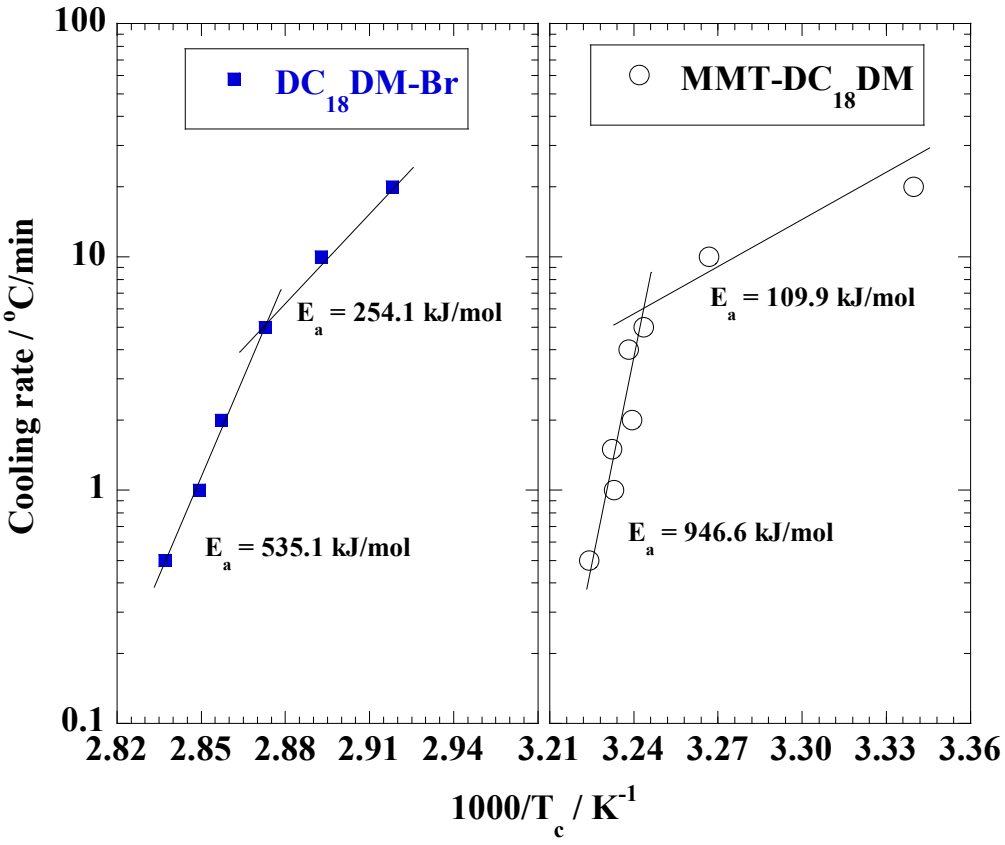

Figure 2-11. Arrhenius plots of cooling rate *versus* reciplocal of the absolute phase transition temperature, $1/T_c$. The solid line is calculated by linear regression.

compared with that of $DC_{18}DM$-Br (E_a= 535±5 to 254±12 kJ/mol, which is almost the same (~ 200-400 kJ/mol) in the polymer melt crystallization based on isoconversional analysis reported by Vyazovkin and Sbirrazzouli [38]). This indicates a possible change in the disorder-order phase transition mechanism. A significant decrease in E_a is correlated with the nonisothermal ordering associated with the poor chain packing of the alkyl chains and its molecular mobility in MMT-$DC_{18}DM$. In other words, the promoted chain packing in different T_c ranges (cooling rate > 5.0 °C/min) showed much lower energy barrier (E_a= 110±20 kJ/mol) as shown in Figure 2-10.

2-4. Conclusions

I have examined the detailed nonisothermal ordering kinetics and disorder transition (chain melting) behavior including the conformational changes of the chain segment of the alkyl chains in the confined space (nano-gallery space in MMT). The chain packing and melting of the confined alkyl chains in MMT-$DC_{18}DM$ is a reversible process with some hysteresis owing to the difference between T_m and T_c. The formation of gauche conformers was enhanced and the poor chain packing took place for the alkyl chains in MMT-$DC_{18}DM$ as compared with those of the crystallized $DC_{18}DM$-Br in bulk.

Via order-disorder transition kinetic, it was found that the ordering in the confined space was more obvious as opposed to the bulk crystallization. For $DC_{18}DM$-Br, the overall crystallization rates exhibited large value one order higher in magnitude when compared to MMT-$DC_{18}DM$. However, these values were strongly affected by the increase of the cooling rate and later achieved a constant value. The confined molecules ($DC_{18}DMs$) in one or two dimensional order exhibited significant contribution to enhance the nonisothermal ordering (chain packing) for a higher cooling rate.

References

[1] Sinha Ray S, Okamoto M, *Prog. Polym. Sci.*, **2003**, 28, 1539-1641.

[2] Gao F, *Materials Today*, **2004**, 7(11), 50-55.

[3] Okada A, Usuki A, *Macromol. Mater. Eng.*, **2006**, 291, 1449-1476.

[4] Hussain F, Hojjati M, Okamoto M, Gorga RE, *J. Composite Mater.*, **2006**, 40, 1511-1575.

[5] Vaia RA, Wagner HD, *Materials Today*, **2004**, 7(11), 32-37.

[6] Krishnamoorti R, Vaia RA, Giannelis EP, *Chem. Mater.*, **1996**, 8, 1728-1734

[7] Vaia RA, Giannelis EP, *Macromolecules*, **1997**, 30, 8000-8009.

[8] Rao Y, Pochan JM, *Macromolecules*, **2007**, 40, 290-296.

[9] Vaia RA, Teukolsky RK, Giannelis EP, *Chem. Mater.*, **1994**, 6, 1017-1022.

[10] Vaia RA, Giannelis EP, *Macromolecules*, **1997**, 30, 7990-7999.

[11] Osman MA, Seyfang G, Suter UW, *J. Phys. Chem. B.*, **2000**, 104, 4433-4439.

[12] Osman MA, Ernst M, Meier BH, Suter UW, *J. Phys. Chem. B.*, **2002**, 106, 653-662.

[13] Li Y, Ishida H, *Chem. Mater.*, **2002**, 14, 1398-1404.

[14] Li Y, Ishida H, *Langmuir*, **2003**, 19, 2479-2484.

[15] Osman MA, Ploetze M, Skrabal P, *J. Phys. Chem. B.*, **2004**, 108, 2580-2588.

[16] Lagaly G, Ogawa M, Dekany I, *Clay Mineral Organic Interactions. Handbook of Clay Science*. Elsevier, Amsterdam, **2006**, Chapter 7.3, 309-377.

[17] Heinz H, Vaia RA, Farmer BL, *Langmuir*, **2008**, 24, 3727-3733.

[18] Heinz H, Koerner H, Anderson KL, Vaia RA, Farmer BL, *Chem. Mater.*, **2005**, 17, 5658-5669.

[19] He H, Galy J, Gerard JF, *J. Phys. Chem. B.*, **2005**, 109, 13301-13306.

[20] Heinz H, Vaia RA, Farmer BL, *J. Chem. Phys.*, **2006**, 124, 224713-224719.

[21] Heinz H, Vaia RA, Krishnamoorti R, Farmer BL, *Chem. Mater*., **2007**, 19, 59-68.

[22] Heinz H, Castelijns HJ, Suter UW, *J. Am. Chem. Soc*., **2003**, 125, 9500-9510.

[23] Nuzzo RG, Dubois LH, Allara DL, *J. Am. Chem. Soc*., **1990**, 112, 558-569.

[24] Binder H, Kohlstrunk B, Brenn U, Schwieger W, Klose G, *Colloid Polym. Sci*., **1998**, 276, 1098-1109.

[25] Brovelli D, Casei WR, Hähner G, *J. Colloid Interface Sci*., **1999**, 216, 418-423.

[26] Fujii M, Li B, Fukuda K, Kato T, Seimiya T, *Langmuir*, **1999**, 15, 3689-3692.

[27] Yoshida O, Okamoto M, *Macromol. Rapid Commun*., **2006**, 27, 751-757.

[28] Bailey SW, *In Reviews in Mineralogy, Mineralogical Society of America*, Chelsea, MI, **1998**, Vol. 19.

[29] Yoshida O, Okamoto M, *J. Polym. Eng*., **2006**, 26, 919-940.

[30] Kubo H, Sato H, Okamoto M, Kotaka T, *Polymer*, **1998**, 39, 501-503.

[31] Lagaly G, *Clays Clay Minerals*, **1970**, 16, 1-46.

[32] Bunn CW, *Trans. Faraday Soc*., **1939**, 35, 482-491

[33] Okamoto M, Taguchi H, Sato H, Kotaka T, Tateyama H, *Langmuir*, **2000**, 16, 4055-4058.

[34] Asai K, Okamoto M, Tashiro K, *Polymer*, **2008**, 49, 4298-4306.

[35] Ozawa T, *J. Therm. Anal. Calorim*., **1970**, 2, 301-324.

[36] Moroni A, Mijovic J, Pearce E, Foun CC, *J. Appl. Polym. Sci*., **1986**, 32, 3761-3773.

[37] Vyazovkin,S, Dranca I, *Macromol. Chem. Phys*., **2006**, 207, 20-25.

[38] Vyazovkin S, Sbirrazzuoli N, *Macromol. Rapid Commun*., **2006**, 27, 1515-1532.

Chapter 3

Intercalation of Diphenyl sulfide into Nano-galleries and Preparation of Poly(*p*-phenylenesulfide)-based Nano-composites

3-1. Introduction

Continued progress in nano-scale controlling as well as an improved understanding of the physicochemical phenomena at the nano-galleries of the layered silicates, have contributed to the rapid development of polymer/layered silicate nano-composites [1].

In order to understand the thermodynamic issue associated with the nano-composites formation, Vaia et al. applied mean-field statistical lattice model, and they found conclusions based on the mean field theory nicely agree with the experimental results [2, 3]. In the study, the entropy loss associated with confinement of a polymer melt is not prohibited to nano-composite formation because an entropy gain associated with the layer separation balances the entropy loss of polymer intercalation, resulting in a net entropy change near to zero. Thus, from the theoretical model, the outcome of nano-composite formation via polymer melt intercalation depends on energetic factors, which may be determined from the surface energies of the polymer and organically modified layered filler (OMLF).

Nevertheless, we have often faced the problem that the nano-composite shows fine and homogeneous distribution of the nano-particles in polymer matrix (e.g., poly(L-lactide)) without clear peak shift of the mean interlayer spacing of the (001) plane as revealed by wide-angle X-ray diffraction (WAXD) analysis [4]. Furthermore we sometimes encounter a decreasing of the interlayer spacing compared with that of pristine OMLF, despite very fine dispersion of the silicate particles. To the best of our knowledge, the mechanism of the direct melt intercalation in the nano-composite formation is very complicated, and is not very well explored in literatures.

In this regard, we reported that an optimal interlayer structure on OMLF is most favorable for nano-composite formation with respect to the number per area and size of surfactant (intercalant) chains [5, 6]. In the study, we supported the interdigitated layer structure model of

the OMLF, where the intercalants are oriented with some inclination to the host layer in the interlayer space. Details regarding this model and explanation are presented in references [5, 6]. Past studies [7, 8] have shown that the all-trans conformation of the alkyl chains was preferentially adopted and was ordered in two-dimensional lattice when using high-surface charge density clay (such as vermiculite and mica). Osman reported that the average molecular axis of a di-octadecyl di-methylammonium cation intercalant is inclined to the mica surface by ca. 50° [7]. The interdigitated layer structure is of particular important to understand the intercalation kinetics that can predict final nano-composite morphology and overall materials properties.

In this chapter, in order to prove the importance of the interdigitated layer structure in the direct (melt) intercalation, I report the intercalation of diphenyl sulfide (DFS) molecules into nano-galleries based on OMLFs consisting of different types of intercalants and nano-fillers with different surface charge density as a reference system of the poly(*p*-phenylenesulfide) (PPS)-based nano-composite. Although there is no direct correlation between small molecules and macromolecules, the intercalation behavior of the small molecules have a strong impact on the explanation for the intercalation kinetics. I chose an optimal OMLF and conducted the PPS-based nano-composites preparation with and/or without shear processing.

3-2. Experimental Section

The various types of OMLFs having different types of intercalants used in this study, were synthesized by replacing Na^+ and K^+ ions in different nano-fillers with alkylammonium and alkylphosphonium cations [4, 9]. *n*-hexadecyl tri-*n*-butyl phosphonium, *n*-octyl triphenyl phosphonium (C_{12}TPP), *N*-(cocoalkyl)-*N*,*N*-[bis(2-hydroxyethyl)]-*N*-methyl ammonium (qC_{14}(OH)), and octadecyl benzyl di-methyl ammonium ($C_{18}Me_2Bz$) cations are miscible with DFS as revealed by melting temperature depression of DFS (T_m=-21.49°C) (Table 3-1), while octadecylammonium (ODA), octadecyl tri-methylammonium (C_{18}TM) cations are immiscible with DFS. Both ODA·Cl^- and C_{18}TM·Cl^- did not dissolve in DFS. The layer titanate (HTO) is a new nano-filler having highly surface charge density [5] compared with conventional layered silicates (synthetic fluorine hectorite (*syn*-FH) and montmorillonite (MMT)) (Table 3-2). The mixtures of DFS, purchased from Aldrich, and various OMLFs in weight ratio 70/30 were prepared. The mixtures were stirred for 1 h to obtain homogeneous mixtures and allowed to stand in sealed glass tubes for 3 h at room temperature. The resultant products were isolated by repeated filtration, washed with methanol, and dried at room temperature [10]. A PPS *fine* powder (M_n=1.0x10^4g/mol, T_m=285 °C), which is source from Aldrich, was used. The PPS-based nano-composites preparation was conducted via melt compounding operated at 300 °C for 3 min. The extruded samples were dried under vacuum at 120°C for 6 h to remove water. The dried nano-composites were then converted into sheets with a thickness of 0.7 to 2 mm by pressing with ≈1.5 MPa at 300 °C for 1min using a hot press. To estimate effect of the shear on the nano-filler dispersion, I also conducted nano-composite preparation without shear processing (just annealed at 300 °C for 30 s). Both types of the sample sheets were then quickly quenched between glass plates and subjected to the characterizations.

Table 3-1. Melting temperature depression and endothermic heat flow (melting enthalpy) in mixtures of intercalants and DFS (10/90 weight ratio)

	DFS	DFS/ $C_{16}TBPCl^-$	DFS/ $C_{18}Me_2BzCl^-$	DFS/ $C_{12}TPPCl^-$
T_m [a] / °C	-21.49	-23.12	-22.47	-23.25
ΔH [a] / J/g	45.06	43.73	37.78	36.46

[a] Heating rate is 5 °C/min.

Table 3-2. Characteristic parameters of nano-fillers

parameters	HTO	*syn*-FH	MMT
Chemical formula	$H_{1.07}Ti_{1.73}O_{3.95}\cdot 0.5H_2O$	$Na_{0.66}Mg_{2.6}Si_4O_{10}(F)_2$	$Na_{0.33}(Al_{1.67}Mg_{0.33})Si_4O_{10}(OH)_2$
Particle size /nm	~100-200	~100-200	~100-200
BET area /m^2/g	~2400	~800	~700
CEC [a] /meq/100g	~200 (660)	~120 (170)	~90(90)
Surface charge: e^- [b]/nm^2	1.26	0.971	0.708
Density /g/cm^3	2.40	2.50	2.50

[a] Methylene blue adsorption method. The values in the parenthesis are calculated from chemical formula of nano-fillers.
[b] Surface charge density =layer charge/unite cell parameters, *a* and *b* [5, 6, 11, 13].

The nano-structure analyses of wide-angle X-ray diffraction (WAXD) and transmission electron microscopy (TEM) were carried out using the same apparatus as in the previous articles [4, 9]. To investigate the micro-scale morphology of the nano-composites, I also used polarizing optical microscope (POM). The mixture of PPS *fine* powder and OMLFs was first sandwiched between two pieces of cover glass and placed on a laboratory hot plate at above T_m of PPS for 30s to obtain a thin film of ~30 μm in thickness. The molten film was then rapidly put on a thermostatted hot-stage (>T_m) (Linkam RTVMS, Linkam Scientific Instruments, Ltd.) mounted on a POM (Nikon OPTIPHOTO2-POL). Here I briefly describe molecular modeling of the

intercalants. By aid of computer simulation, we proposed the molecular dimensions of two different intercalants using the molecular dynamics program (MM2 in Quantum CAChe, Fujitsu Ltd.) in consideration of van der Waales radi. Optimization of structure is based on minimization of the total energy of the molecular system [6].

3-3. Results and Discussion

3-3-1. Intercalation of DFS molecules into nano-galleries

WAXD patterns for the typical examples of nano-filler powders are presented in Figure 1. The mean interlayer spacing of the (001) plane ($d_{(001)}$) for the HTO modified by C_{16}TBP [HTO-C_{16}TBP] obtained by WAXD measurements is 2.31nm (diffraction angle, $2\Theta = 3.82°$). The appearances of small peaks observed at $2\Theta = 7.60°$, 11.36°, 15.08° and 18.88° were confirmed that these reflections are due to (002) up to (005) plane of HTO-C_{16}TBP. HTO-C_{16}TBP intercalated with DFS [HTO-C_{16}TBP/DFS] exhibits well-ordered suprastructure proved by WAXD with diffraction maxima up to the seventh order due to the high-surface charge density of the HTO layers compared with that of MMT (see Figure 3-3a).

Despite the immiscibility between ODA and DFS, we can see the layer expansion in MMT-ODA after mixing with DFS, indicating the DFS intercalation into nano-galleries. MMT-ODA/DFS profile shows less-ordered interlayer structure compared with that of HTO-C_{16}TBP/DFS. That is, the coherent order of the silicate layers (MMT) is much lower in each HTO-based OMLFs intercalated with DFS molecules presumably due to the different surface charge density.

In Figure 3-2, I discuss the change of the interlayer opening, which is estimated after subtraction of the layer thickness value of 0.374 nm for HTO [11], 0.98 nm for *syn*-FH [12] and 0.96 nm for MMT [13]. The intercalation of DFS molecules successfully takes place regardless of the miscibility between DFS and intercalants. Obviously we can observe the strong correlation between initial interlayer opening and layer expansion (=Δ opening) after mixing with DFS. That is, the smaller initial opening leads to the larger interlayer expansion. In other words, the smaller interlayer opening caused by the lower surface charge density and/or short chain length of the

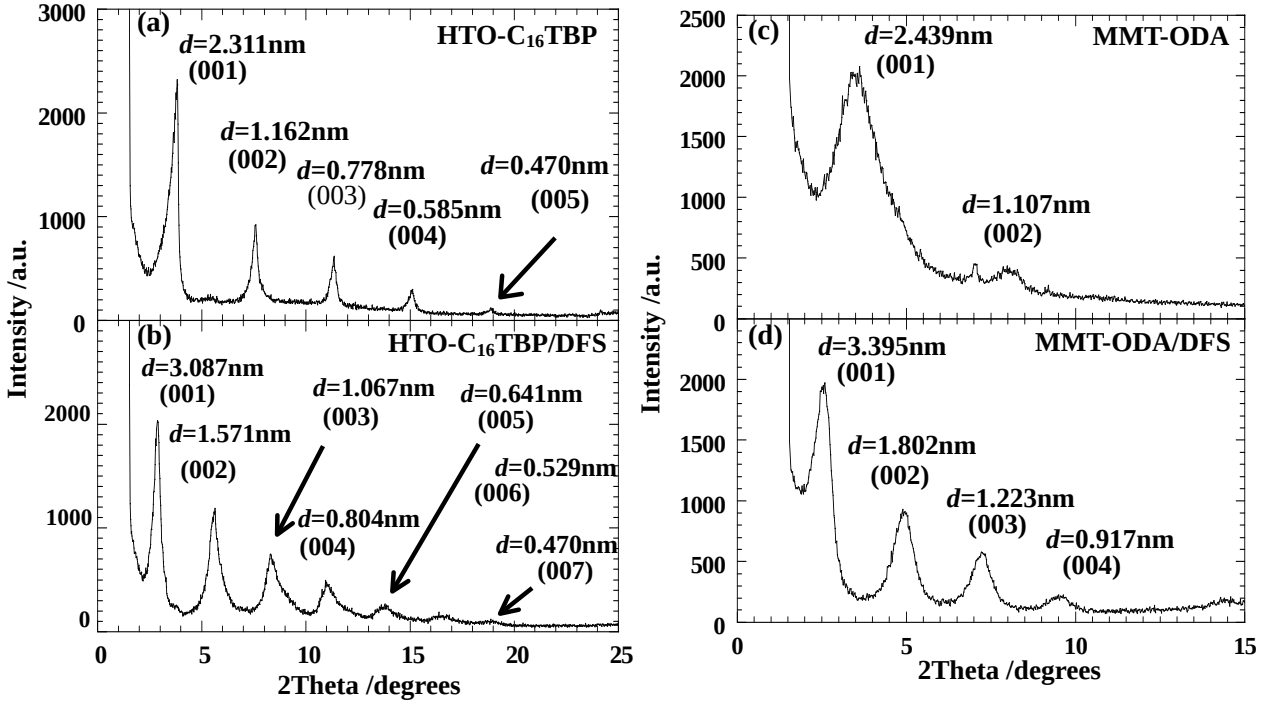

Figure 3-1. WAXD patterns of (a) HTO-C_{16}TBP, (b) HTO-C_{16}TBP intercalated with DFS, (c) MMT-ODA and (d) MMT-ODA intercalated with DFS.

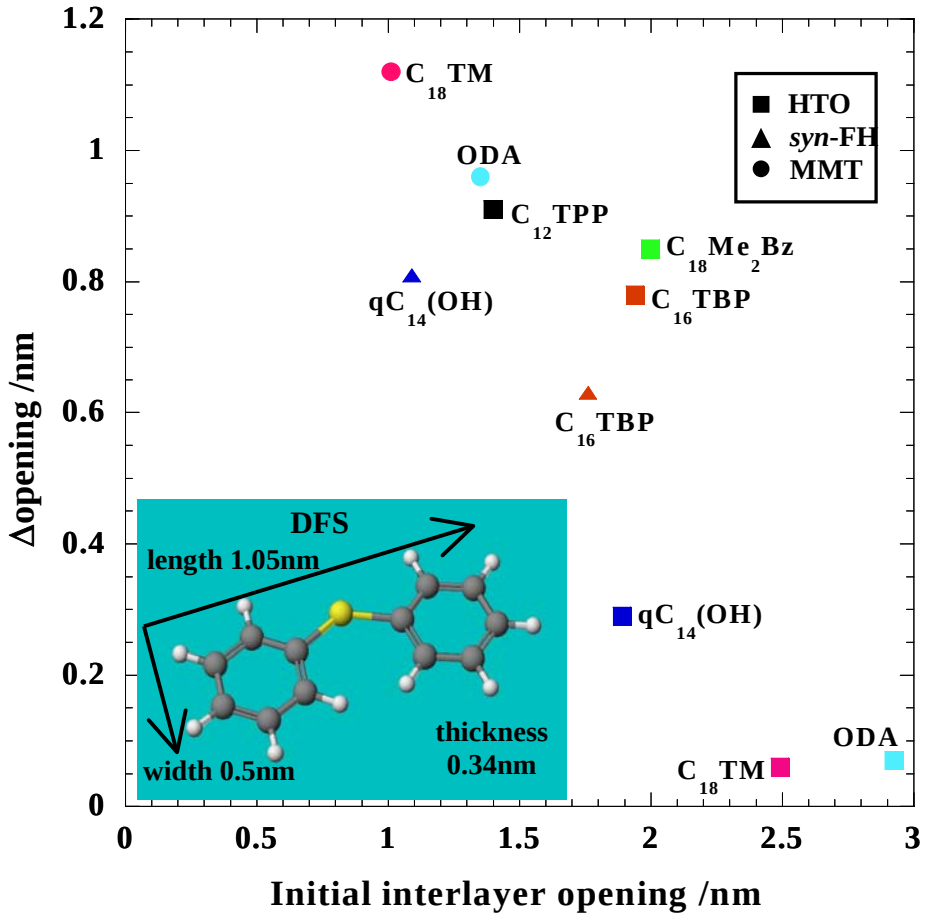

Figure 3-2. Plot of initial interlayer opening versus Δ opening for various OMLFs intercalated with DFS. The inset shows molecular dimensions of DFS calculated using a molecular dinamic program (MM2 in Quantum CAChe, Fujitsu Ltd.), taking van der Waales radi into consideration.

intercalant (e.g., qC_{14}(OH) and C_{12}TPP) promotes the large amount of the intercalation of DFS molecules, probably due to the configuration with small tilt angle of the intercalant into the nano-galleries. This feature has been observed in the results of polyester-based nano-composites prepared by different OMLFs intercalated with different intercalants [5, 6].

One more interesting feature is the absolute value of Δ opening. For HTO-ODA/DFS and HTO-C_{18}TM/DFS, the absolute value of Δ opening (0.07 nm (2.4%) and 0.06 nm (2.4%), respectively) is lower than the molecular dimension of DFS (length, width and thickness are 1.05 nm, 0.5 nm and 0.34 nm, respectively) (see the inset in Figure 3-2). This suggests that the DFS molecules can not penetrate into galleries when we compare the apparent interlayer expansion (=Δ opening). It is necessary to understand the meaning of the interlayer expansion in the intercalation. As explained in the first part, we have to take the interdigitated layer structure into consideration. This structure may imply the different orientation angle of the intercalants can adopt when DFS molecules penetrate into the galleries. Apparently, the interdigitated layer structure may provide a balance between DFS penetration and different orientation angle of the intercalants.

From these results, the entropic contribution of the intercalants, which leads to the entropy gain associated with the layer expansion after intercalation of the small molecules and/or polymer chains, may not be significant due to the interdigitated layer structure. Presumably the penetration takes place by the pressure drop into the nano-galleries generated by the two platelets.

3-3-2. Effect of surface charge density on intercalation

For MMT-C_{16}TBP/DFS, the peaks arising from (001) and (002) reflections of

MMT-C_{16}TBP disappear and the layer structure is destroyed as shown in Figure 3-3. The delamination and swelling of the MMT layers are retained in the sample. The swelling behavior of the MMT layers was observed by the naked eye. However the complete exfoliation of the silicate layers is not judged from WAXD analysis. On the other hand, *syn*-FH, which has higher surface charge density compared with that of MMT, shows intercalated layer structure like a HTO-C_{16}TBP/DFS (Figures 3-3c and 3-3d). This feature has been observed in the result of the OMLF modified with qC_{14}(OH). For the same intercalant into the different nano-fillers (e.g., comparison among MMT, *syn*-FH and HTO), *syn*-FH- qC_{14}(OH)/DFS exhibits a large value of Δ opening compared with that of HTO-qC_{14}(OH)/DFS. MMT-qC_{14}(OH)/DFS shows the delamination behavior when comparing with *syn*-FH-qC_{14}(OH)/DFS and HTO-qC_{14}(OH)/DFS (The data is not shown here). This indicates that the OMLFs having lower surface charge density leads to a lower coherent order of the layer structure and the layer structure is presumably destroyed when the OMLFs are modified by some intercalant, which is miscible with matrix.

3-3-3. PPS-based nano-composite formation

I conducted nano-composite preparation without shear processing. Figure 3-4 shows the morphologies of PPS-based nano-composites prepared by annealing at 300 °C for 30 s (without shear processing). The OMLS content in the nano-composites was 5wt%. The alkylphosphonium cation as a intercalant has an advantage for the thermal stability than alkylammonium one [6, 14]. It is clear from the POM photographs that stacked-and-agglomerated structure of layers are evident in PPS/*syn*-FH-C_{16}TBP system, while good dispersion appears in PPS/MMT-C_{16}TBP systems. The internal structure of the nano-composites in the nano-meter scale was directly observed *via* TEM analyses.

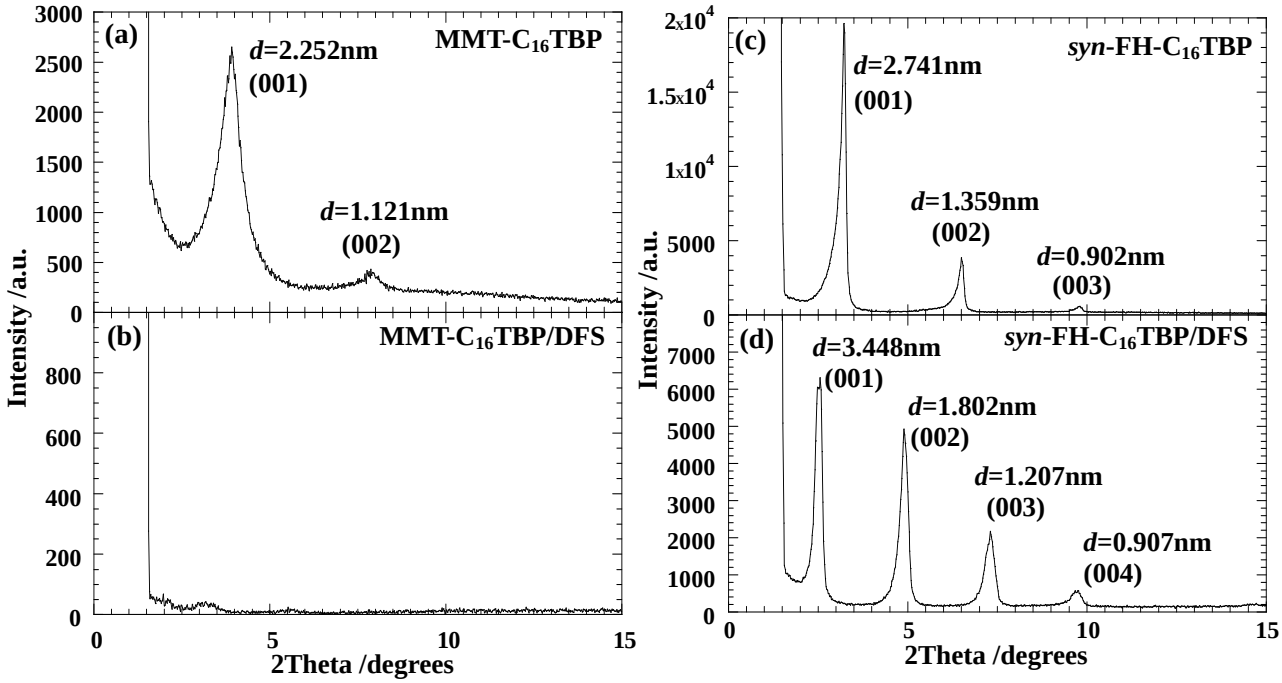

Figure 3-3. WAXD patterns of (a) MMT-C_{16}TBP, (b) MMT-C_{16}TBP intercalated with DFS, (c) *syn*-FH-C_{16}TBP and (d) *syn*-FH-C_{16}TBP intercalated with DFS.

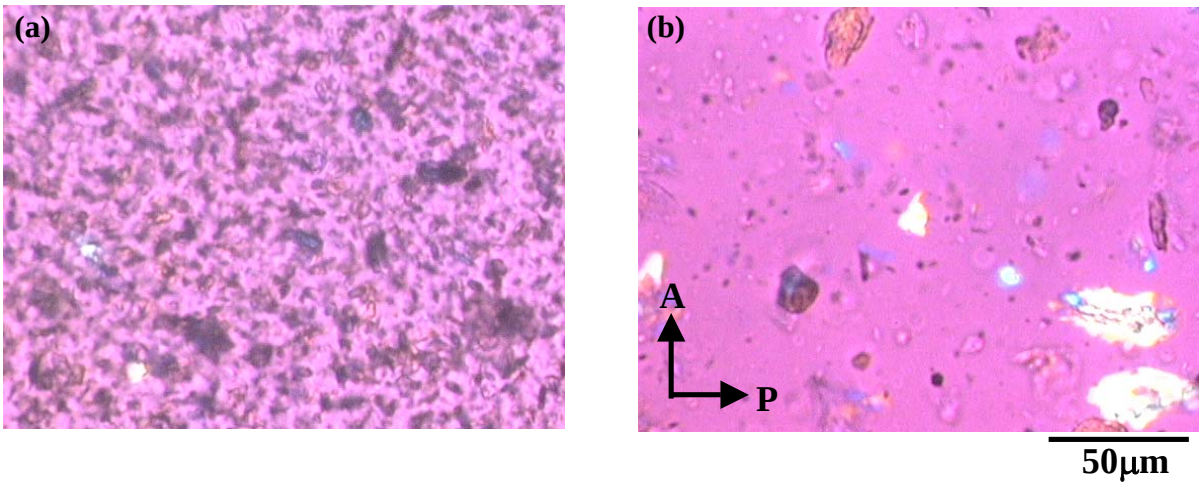

Figure 3-4. Polarized optical micrographs of (a) PPS/*syn*-FH-C_{16}TBP and (b) PPS/MMT-C_{16}TBP prepared by annealing at 300 °C for 30 s (without shear processing).

Figure 3-5a shows the results of TEM bright field images of PPS/*syn*-FH-C_{16}TBP systems corresponding to the POM experiments, in which dark entities are the cross section of the layered nano-fillers. The large agglomerated tactoids of about 300nm thickness are seen in Figure 3-5a. On the other hand, Figures 3-5b and 3-5c show the observation of discrete silicate layers. We can observe the aggregated feature of the silicate layers in Figure 3-5c. An aggregated particle contains several discrete silicate layers with finer dispersion. For PPS/MMT-C_{16}TBP prepared by annealing without shear processing, the annealing promotes the delamination of the stacked MMT layers. The estimated zero-shear viscosity of the PPS melt (M_n=1.0x10^4g/mol) at 300 °C (fitted with Ellis model) was 60 Pa s [15]. The intercalation of PPS molecules takes place presumably due to the low viscosity. This feature very greatly resembles to the intercalation behavior in OMLS/DFS systems at room temperature. The existences and/or disappearances of sharp Bragg peaks ((001) and (002) planes) in PPS-based nano-composites prepared without shear processing clearly indicate the dispersed behavior of the silicate layers in the PPS matrix (see Figure 3-6).

Figure 3-7 shows the results of TEM bright field images of the nano-composites prepared by melt compounding with shear (operated at 300 °C for 3 min). For PPS/*syn*-FH-C_{16}TBP, we still observe large stacked silicate layers in the nano-composites, whereas, in PPS/MMT-C_{16}TBP, more homogeneously and finely dispersed layer structure is developed when comparing with the corresponding to the nano-composite prepared without shear processing (see Figures 3-5b and 3-5c).

I estimate the form factors obtained from TEM images, i.e. average value of the particle length (L), thickness (D) of the dispersed partiles and the correlation length (ξ) between them. The details of the evaluation were described in our previous paper [9]. The results are

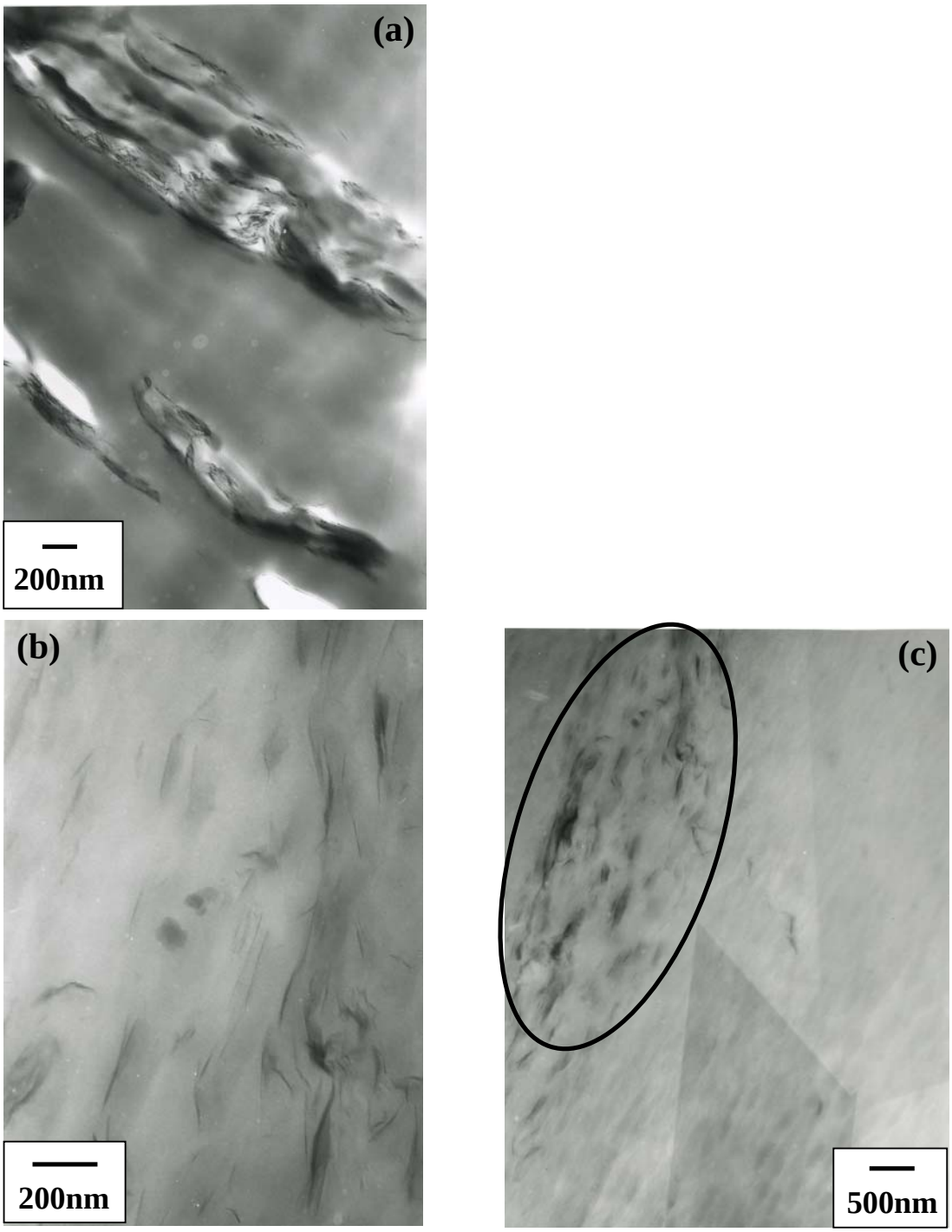

Figure 3-5. Bright filed TEM images of (a) PPS/*syn*-FH-C_{16}TBP, (b) and (c) PPS/MMT-C_{16}TBP prepared by annealing at 300 °C for 30 s (without shear processing). The dark entities are the cross section and/or face of intercalated-and-stacked silicate layers, and the bright areas are the matrix. The circled area indicates the aggregated particles contain many discrete silicate layers with finer dispersion (see text).

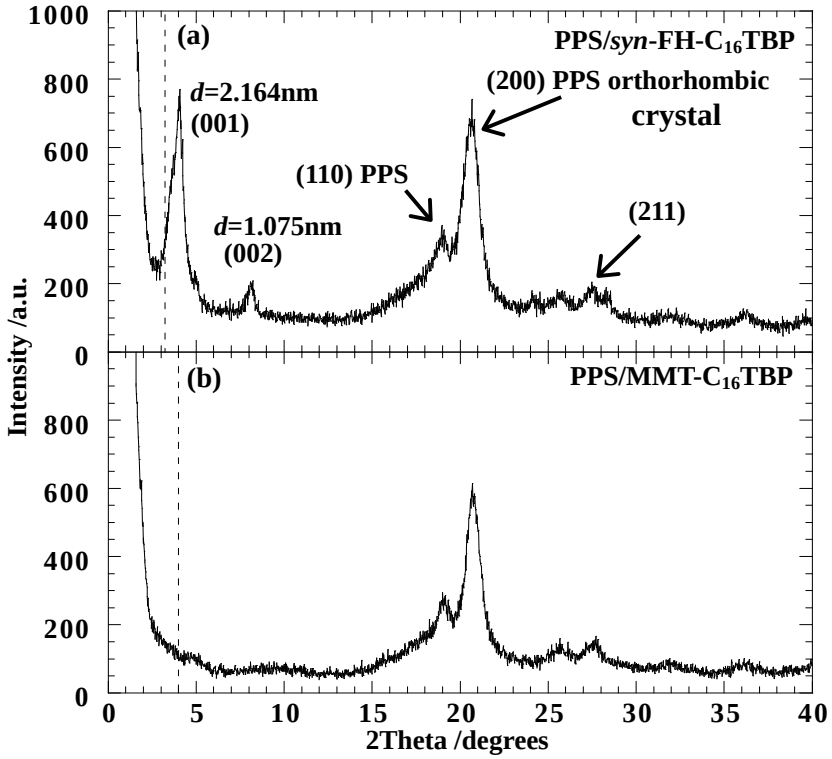

Figure 3-6. WAXD patterns for PPS-based nanocomposites prepared by (a) *syn*-FH-C_{16}TBP and (b) MMT- C_{16}TBP without shear processing. The dashed line in each figure indicates the location of silicate (001) reflection of each OMLS. The strong diffraction peaks at 2Θ=15-30° are assigned to the orthohombic crystal of PPS.

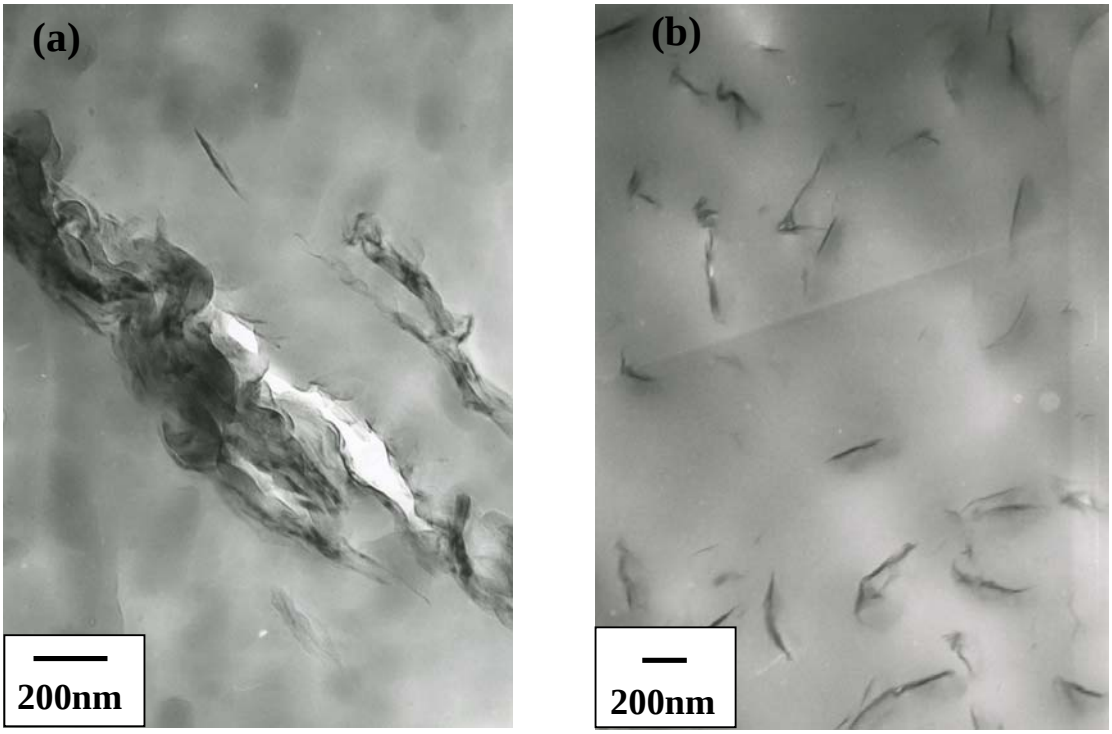

Figure 3-7. Bright filed TEM images of (a) PPS/*syn*-FH-C_{16}TBP, (b) PPS/MMT-C_{16}TBP prepared by melt compounding with shear (operated at 300 °C for 3 min).

Table 3-3. Form factors of two nano-composites obtained from TEM observation

PPS/MMT-C_{16}TBP	Without shear [a)]	With shear
L /nm	130±50	270±100
D /nm	9±5	22±10
ξ /nm	100±80	350±200

[a)] The values are obtained from Figure 5b

presented in Table 3-3. For PPS/MMT-C_{16}TBP prepared by annealing without shear processing, *L* and *D* are in the range of (130±50)nm and (9±5)nm, respectively.

On the other hand, PPS/MMT-C_{16}TBP prepared by shear processing exhibits a large value of *L* (270±100nm) with almost double of stacking of the silicate layers (*D*=22±10nm). ξ value of the nano-composite without processing (100±80nm) is lower than the value of the shear processed one (350±200nm). In case of annealing (without shear), the values are obtained from Figure 3-5b. PPS/MMT-C_{16}TBP after shear processing exhibits some staked-and-flocculated silicate layers in the nano-composite presumably due to the thermal decomposition of the intercalant (C_{16}TBP) at 300 °C. However, more uniform dispersion of the layers seems to be attained due to the shear processing (cf. Figure 3-5c and Figure 3-7b). That is, the delamination of the stacked nano-fillers is governed by the initial interlayer opening, which is controlled by the surface charge density and molecular dimension of the intercalant, while the uniform dispersion of the nano-fillers was affected by the shear processing. The shear stress may have little effect on the delamination of OMLFs in the preparation of PPS-based nano-composite.

3-4. Conclusions

Intercalation of DFS molecules into nano-galleries having different initial interlayer opening was discussed. The small interlayer opening caused by the low surface charge density promoted the large amount of the intercalation of DFS molecules regardless of the miscibility between DFS and intercalants. For this reason, PPS-based nano-composite prepared with MMT-C_{16}TBP without shear processing exhibited finer dispersion. The delamination of the MMT layers was attained when comparing with the nano-composite prepared with *syn*-FH-C_{16}TBP. This approach can be extended to prepare polymeric nano-composites with finer dispersion of the nano-fillers.

Note and References

[1] Okamoto M, *Mater. Sci. Tech.*, **2006**, 22, 756-779.

[2] Vaia RA, Giannelis EP, *Macromolecules*, **1997**, 30, 7990.

[3] Vaia RA, Giannelis EP, *Macromolecules*, **1997**, 30, 8000.

[4] Hiroi R, Sinha Ray S, Okamoto M, Shiroi T, *Macromol. Rapid Commun.*, **2004**, 25, 1359-1364.

[5] Yoshida O, Okamoto M, *Macromol. Rapid Commun.*, **2006**, 27, 751-757.

[6] Yoshida O, Okamoto M, *J. Polym. Eng.*, **2006**, 26, 919-940.

[7] Osman MA, Ernst M, Meier BH, Suter UW, *J. Phys. Chem. B*, **2002**, 106, 653-662.

[8] Osman MA, Ploetze M, Skrabal P, *J. Phys. Chem. B*, **2004**, 108, 2580-2588.

[9] Sinha Ray S, Yamada K, Okamoto M, Ogami A, Ueda K, *Chem. Mater.*, **2003**, 15, 1456-65.

[10] When these OMLNs are washed with methanol, no change in the WAXD profiles is observed.

[11] Nakano S, Sasaki T, Takemura K, Watanabe M, *Chem. Mater.*, **1998**, 10, 2044-46.

[12] Tateyama H, Nishimura S, Tsunematsu K, Jinnai K, Adachi Y, Kimura M, *Clays Clay Miner.*, **1992**, 40, 180-185.

[13] Lagaly G, *Clays Clay Miner.*, **1970**, 16, 1-46.

[14] Maiti P, Okamoto M, Yamada K, Ueda K, Okamoto K, *Chem. Mater.*, **2002**, 14, 4654-4661.

[15] Maiti P, Okamoto M, Kotaka T, *Polymer*, **2001**, 42, 9827-9835.

Chapter 4

Poly(*p*-phenylenesulfide)-based Nano-composite Formation: Delamination of Organically Modified Layered Filler via Solid-state Processing

4-1. Introduction

A significant amount of work has already been done on various aspects of polymeric nano-composite containing organically modified layered fillers (OMLFs) [1]. However, complete exfoliation of OMLFs in continuous polymer matrix is still challenging issue because it could not be satisfactorily attained. We know, by now, that the complete exfoliation is not feasible after melt intercalation with appropriate shear. Delamination of stacked layered fillers in polymeric nano-composite is the ultimate target for controlling better overall materials properties. Thus, we are far from the goal of understanding the mechanisms of the nano-structure control and the preparation of the nano-composite with discrete dispersion of the nano-fillers. From this reason, a novel preparation method is currently in progress.

The effect of the supercritical CO_2 (sc-CO_2) fed to the tandem extruder on the dispersion of organically modified montmorillonite (MMT) with different intercalants into Nylon 6 matrix was examined [2]. In the absence of sc-CO_2, pressure improved the MMT-clay delamination by reducing the free volume of the polymer and increasing the interaction between chains and ultimately increasing the viscosity. Using sc-CO_2 did not improve the clay dispersion due to the decreasing the melt viscosity.

Another interesting approach for the delamination of OMLFs is an ultrasound in the preparation of nano-composites. The effect of the *in-situ* ultrasound on the polymer/MMT melt phase is reported [3]. An effective method to enhance the dispersion, intercalation and exfoliation of OMLFs in thermoplastic-based nano-composites is reported. The same experiment was done in another report for polypropylene (PP)-base nano-composite preparation [4]. The maximum power output and frequency of the ultrasonic generator are 300W and 20kHz, respectively. They described the fine dispersion of silicate layers in PP matrix after ultrasonic treatment (100W).

However, the ultrasonic oscillations exhibited a little effect on the delamination of OMLFs as revealed by transmission electron microscope (TEM) observation. Thus, the compounding with an assist from sc-CO_2 fluids and ultra-sonication did not improve the state of the nano-filler dispersion once a critical morphology was established. That is, the dispersion of the nano-filler in the polymer matrix is governed by judicious choice of OMLF.

In this regard, we also reported that an optimal interlayer structure on OMLF is most favorable for nano-composite formation with respect to the number per area and size of surfactant (intercalant) chains [5]. The shear stress has little effect on the delamination of the layer as compared with the optimal interlayer structure on OMLF [6]. This reasoning is consistent with the intercalated structure reported by so many nano-composite researchers, who can prepare only intercalated (not exfoliated) nano-composites via simple melt extrusion technique [1].

Although the intercalation technology of the polymer melt is developed along with the current industrial process, such as extrusion and injection molding, we have to develop more innovative compounding process, especially in the preparation of the nano-composites possessing discrete dispersion of the nano-fillers.

Very recently, Wang et al. [7] reported the exfoliation of talc fillers by solid-state shear processing using pan-type mill, to prepare PP/talc nano-composites. Although the delamination of talc fillers was not achieved in the nano-composite as revealed by TEM images, no indication of the layer correlation was observed in wide-angle X-ray diffraction (WAXD). The solid-state shear processing may be an innovative technique to delaminate the layered fillers in overcoming the pressure drop (Δp) within the nano-galleries. Because Δp within the nano-galleries makes the polymer penetration more difficult and provides the formation of intercalated structure (coherent order of the layers) without delamination [5, 8].

In this Chapter, I discuss the effect of Δp for polymer nano-composite preparation through melt compounding process and challenge solid-state processing to delaminate the stacked, layered filler in the polymer matrix. I report a novel method for the nano-scale control of the dispersed layered fillers.

4-2. Experimental

OMLF used in this study was synthetic fluorine hectorite (*syn*-FH) modified with *n*-hexadecyl tri-*n*-butyl phosphonium ($C_{16}TBP^+$) cation. The alkylphosphonium cation as an intercalant has an advantage for the thermal stability than alkylammonium one [8, 9]. A poly(*p*-phenylenesulfide) (PPS) *fine* powder (M_n=1.0x10^4 g/mol, T_m=285 °C and average particle size=5 μm), purchased from Aldrich, was used as a polymer matrix. The homogeneous mixture of PPS and OMLF in the weight ratio 95:5 was prepared. I conducted the solid-state processing using thermostatted hot-press (Techno Supply Co.). The mixtures were subjected to a hot-press at two different temperatures of ambient temperature (~25 °C) and 150 °C, below T_m of PPS powder (i.e., PPS is still at the solid-state), and three different applying pressures of 7, 14 and 33MPa at each temperature for 30s. Since the melting temperature of the intercalant ($C_{16}TBP^+$) into the nano-galleries was –23.5 °C, for two different temperatures, we can observe the effect of layer delamination at each temperature. The solid-state processing was conducted 15 times. The recovered sheet was about 1 mm thickness and was kept at room temperature prior to the measurements.

The nano-structure analyses of wide-angle X-ray diffraction (WAXD) and transmission electron microscopy (TEM) were carried out using the same apparatus as in the previous articles [10, 11]. To investigate the micro-scale morphology of the nano-composites, I also used polarizing optical microscope (POM). Because TEM micrograph cover a small area, which might not be entirely representative for the overall microstructure of the sample. The recovered sheets were first sandwiched between two pieces of cover glass and placed on a laboratory hot plate at above T_m of PPS for 30s. The molten film was then rapidly put on a thermostatted hot-stage (300 °C) (Linkam RTVMS, Linkam Scientific Instruments, Ltd.) mounted on a POM (Nikon

OPTIPHOTO2-POL). For analyzing the features of the micrographs, I carried out fast Fourier transform (FFT) analysis on digitally saved images of POM micrographs using the commercial image analysis software (Ultimage®, Graftek, France) [12], which allowed to provide us information equivalent to the scattering analyses.

For comparison, the PPS-based nano-composite preparation was conducted via conventional melt compounding operated at 300 °C for 3 min [6]. The extruded samples were dried under vacuum at 120 °C for 6 h to remove water. The dried nano-composite was then converted into sheets with a thickness of 0.7 to 2 mm by pressing with ≈1.5 MPa at 300 °C for 1 min using a hot-press.

4-3. Results and Discussion

4-3-1. Intercalation behavior between various polymers and OMLFs

To understand intercalation behavior of polymer chain, applying stress into OMLF nano-galleries is considered. The pressure drop difference (Δp) into the nano-galleries is generated by the liquids having large surface tension into two platelets [13]. Δp is given by

$$\Delta p = \gamma\left(\frac{1}{R} - \frac{\cos\theta}{H/2}\right) \qquad (4\text{-}1)$$

where γ is the surface tension of the intercalant, R is the radius of the disk if we assume all platelets are of identical disk form, θ is the contact angle (< 90°), and H is the distance between two disks, corresponding to the interlayer opening (Figure 4-1). When the value of H is much smaller than the value of R, i.e. nano-gallery, the value of Δp become negative, suggesting that the attractive force is generated between two disks. The attractive force F is defined as [13]

$$F = \pi R^2 \Delta p + 2\pi R\gamma \sin\theta \qquad (4\text{-}2)$$

We consider here Δp in order to prove the validity of the above model in case of the melt intercalation, with value of γ is 50mN/m (average value of H_2O and $C_{18}H_{38}$), R is 50nm, H is 2nm (≅ final interlayer opening [5, 6, 8]), and θ is less than 90° because the intercalant wets the layer surface fully due presumably to the attractive interaction between negative charges of the layers and alkylammonium or alkylphosphonium cations. Therefore, the calculated value of Δp is equal to -24MPa (F=1.7x10^{-7}N) by assuming θ of 60°. This value is quite large value compared to that

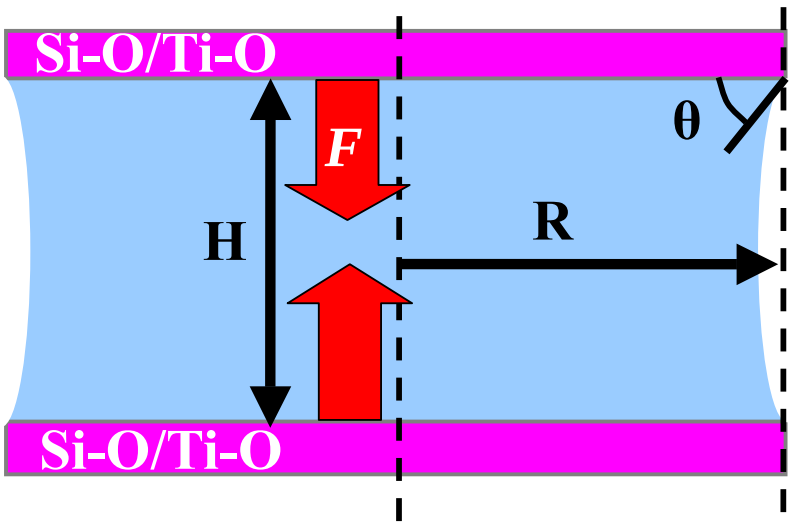

Figure 4-1. Schematic illustration of pressure drop generated by the liquids having large surface tension into two platelets.

of atmospheric pressure (≅ 0.1MPa). This pressure difference may make the polymer penetration more difficult and provides a good balance between the polymer penetration (interlayer expansion) and formation of intercalated structure (coherent order of the layers). Figures 4-2 and 4-3 summarize the layer expansion after preparation of various nano-composites, i.e. initial layer opening, layer expansion (after subtraction of the initial layer opening), and final layer opening. All nano-composites in the figures were prepared by melt compounding operated at 150 ℃ for poly(butylene succinate) (PBS) [14, 15], 190 ℃ for poly(vinylidene fluoride) (PVDF), 200 ℃ for PP [16], 210 ℃ for poly(L-lactide) (PLA) [17, 18], 240 ℃ for sulfonated poly(ethylene terephthalate) copolymer (PES) [8], 240 ℃ for poly[styrene-co-(maleic anhydride)］(SMA) [19] and 300 ℃ for PPS.

An interesting feature in the polymer melt intercalation into the nano-galleries is the final interlayer opening. As seen in Figure 4-2, the interlayer expansion (=Δ opening) depends on the initial interlayer opening after melt intercalation. The smaller initial opening leads to the larger interlayer expansion. The intercalation of polymer chains takes place successfully, regardless of the polymer matrices, the miscibility between polymer and intercalants, and Lewis-acid strength of the intercalants. At the same time, the smaller initial opening gives almost same final interlayer opening (≅ 1.8-2.2 nm) (Figure 4-3). In other words, the final interlayer opening does not depend on the initial opening. And the results support the discussion for pressure drop.

Furthermore, this pressure difference should be compared to the shear stress during melt compounding. In case of the preparation of PLA-based nano-composites, the shear stress (~0.1MPa at 175 ℃ [20]) is much lower than the pressure difference (~–24MPa), suggesting the shear stress have little effect on the delamination (exfoliation) of the layers. This

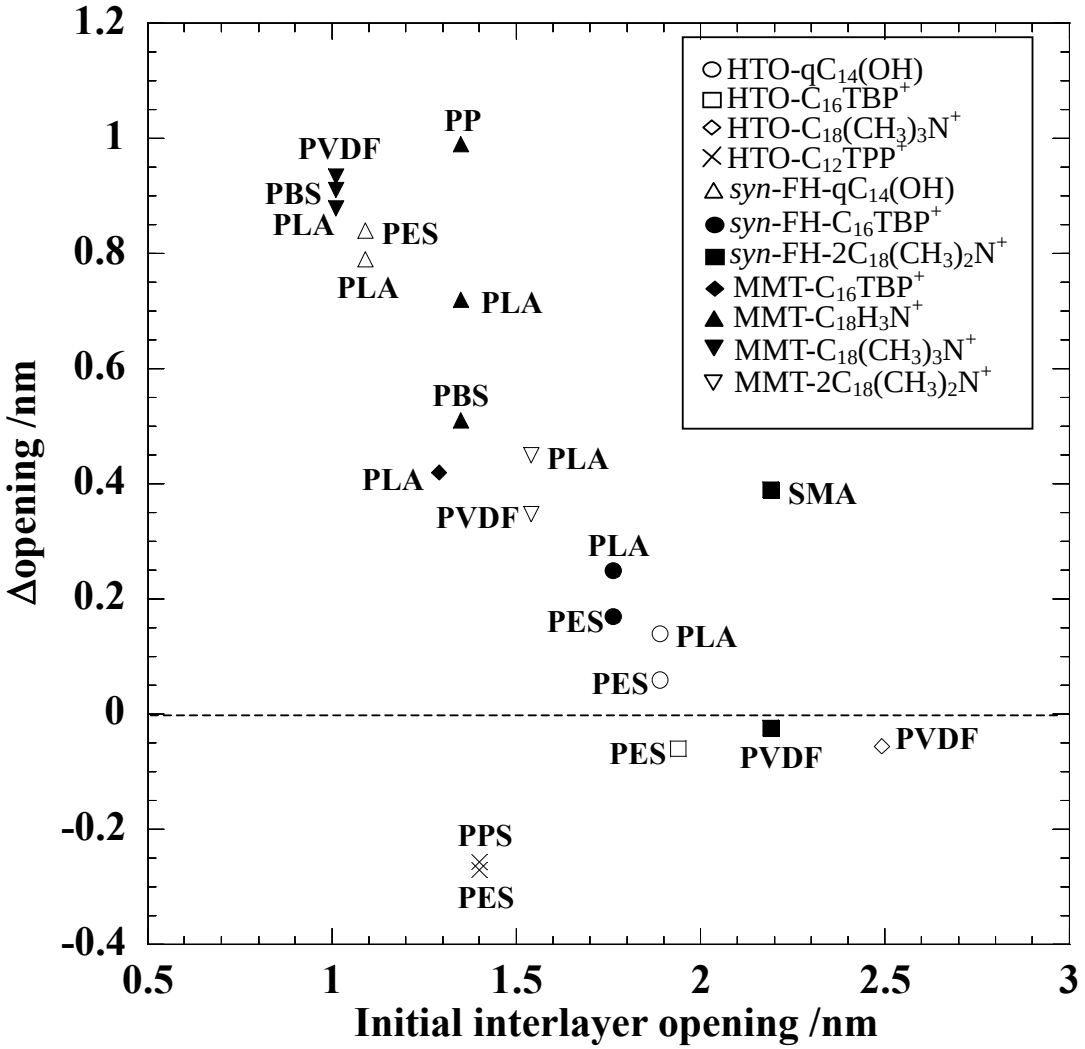

Figure 4-2. Plot of initial interlayer opening versus Δ opening for various OMLFs intercalated with poly(butylene succinate) (PBS), poly(vinylidene fluoride) (PVDF), polypropylene (PP), poly(L-lactide) (PLA), sulfonated poly(ethylene terephthalate) copolymer (PES), poly[styrene-co-(maleic anhydride)] (SMA) and PPS after melt intercalation. Layered titanate (HTO), *syn*-FH and MMT are intercalated with various intercalants; eg., *N*-(cocoalkyl)-*N*,*N*-[bis(2-hydroxyethyl)]-*N*-methyl ammonium ($qC_{14}(OH)$), octadecylammonium ($C_{18}H_3N^+$), octadecyl tri-methylammonium ($C_{18}(CH_3)_3N^+$), dioctadecyldimethylammonium ($2C_{18}(CH_3)_2N^+$), and *n*-octyl *tri*-phenyl phosphonium cations ($C_{12}TPP^+$) cations.

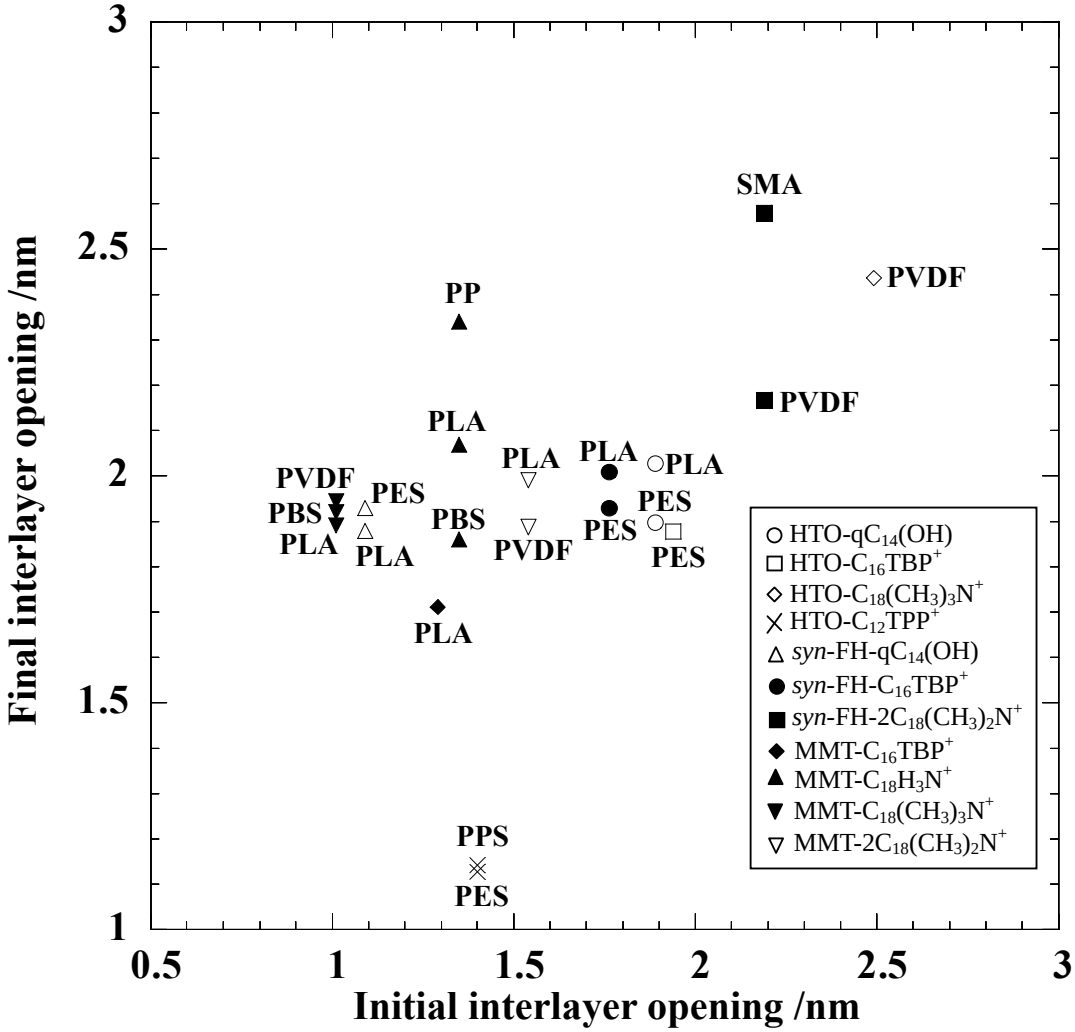

Figure 4-3. Plot of initial interlayer opening versus final layer opening for various OMLFs after preparation of nano-composites.

reasoning is consistent with the intercalated structure reported by so many nano-composite researchers, who can prepare only intercalated (not exfoliated) nano-composites via simple melt extrusion technique [1].

4-3-2. PPS-based nano-composites formation with or without shear compounding

To clarify the effect of shear stress during melt compounding process, I conducted nano-composite preparation with or without shear processing. Figure 4-4 (a) shows TEM image of PPS-based nano-composites prepared by annealing at 300 °C for 30 s (without shear processing). That is, this sample (mixture) is unprocessed mixture of PPS and OMLF just before solid-state processing. It is clear from the TEM image that stacked-and-agglomerated structures of layers are evident in PPS/*syn*-FH-$C_{16}TBP^+$ system. The large agglomerated tactoids of about 300nm thickness are seen in Figure 4-4 (a). Figure 4-4 (b) shows the results of the nano-composite prepared by melt compounding with shear (operated at 300 °C for 3 min). For PPS/*syn*-FH-$C_{16}TBP^+$, we still observe large stacked silicate layers in the nano-composite. Despite shear processing at 300 °C, the nano-composite exhibits some staked-and-flocculated silicate layers in the PPS matrix [6]. On the other hand, when we use MMT intercalated with $C_{16}TBP^+$, a more homogeneously and finely dispersed layer structure is developed in PPS/MMT-$C_{16}TBP^+$ system, with and without shear processing (Figure 3-5 (b), (c), and Figure 3-6 (b)) [6]. This indicates that the OMLFs having lower surface charge density (ζ) (i.e., MMT (ζ=0.780e^-/nm^2) rather than *syn*-FH (ζ=0.971e^-/nm^2)) leads to a lower coherent order of the layer structure and the layer structure is presumably destroyed when the OMLFs are modified by some intercalant, which is miscible with polymer matrix.

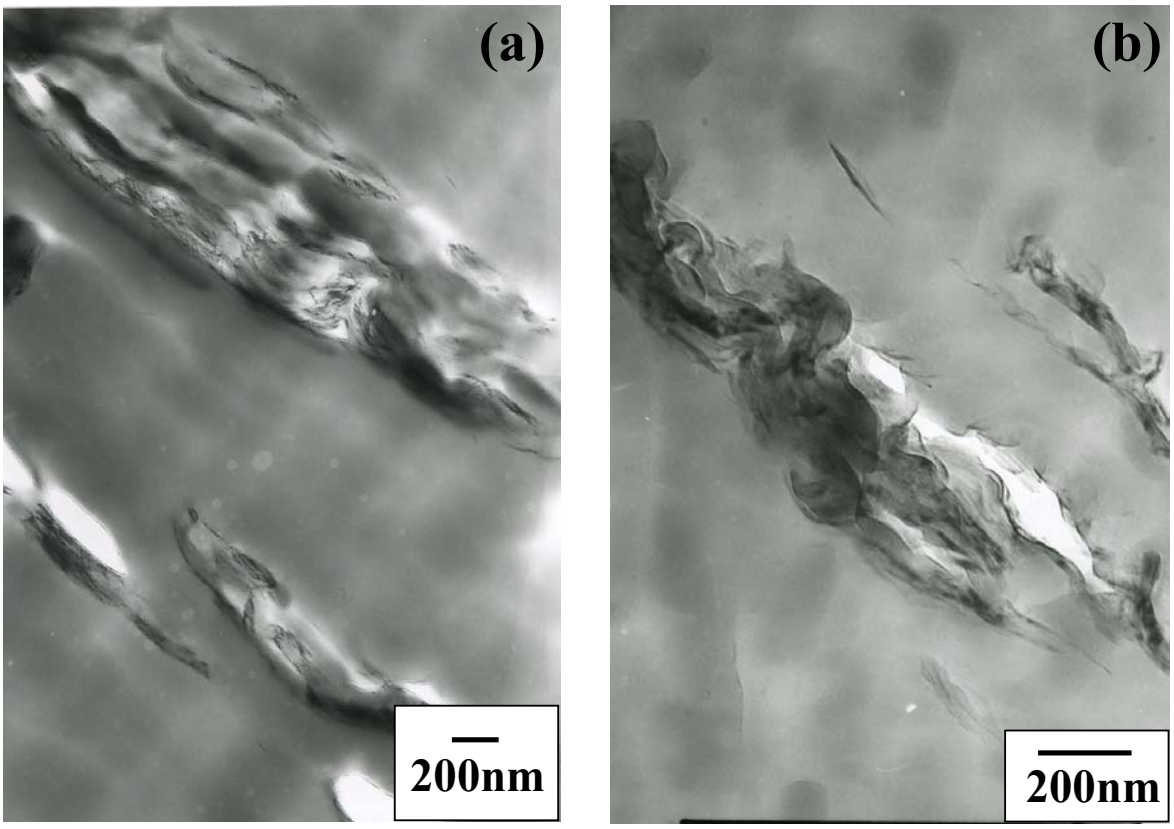

Figure 4-4. Bright field TEM images of (a) PPS/*syn*-FH-$C_{16}TBP^+$ (95:5 wt./wt.) mixture before solid-state processing. The samples are prepared by annealing at 300 ^oC for 30 s (without shear processing), and (b) PPS/*syn*-FH-$C_{16}TBP^+$ prepared by melt compounding with shear (operated at 300 ^oC for 3 min). The dark entities are the cross section and/or face of intercalated-and-stacked silicate layers, and the bright areas are the matrix.

4-3-3. PPS-based nano-composite formation via solid-state processing

4-3-3-1. Variation of WAXD profiles

WAXD patterns, in the range of diffraction angle 2Θ =1-10°, for the typical examples of nano-filler powders are presented in Figure 4-5 (a). The mean interlayer spacing of the (001) plane ($d_{(001)}$) for the *syn*-FH that was modified by $C_{16}TBP^+$ [*syn*-FH-$C_{16}TBP^+$] obtained by WAXD measurements is 2.74 nm (2Θ = 3.22 °). The appearances of small peaks observed at 2Θ = 7.60° and 11.36° were confirmed that these reflections are due to (002) and (003) planes of *syn*-FH-$C_{16}TBP^+$. *syn*-FH-$C_{16}TBP^+$ exhibits well-ordered layered structure proved by WAXD with diffraction maxima up to the third order. Figure 4-5 (b) shows the result of the mixture of PPS and *syn*-FH-$C_{16}TBP^+$ (95:5 wt./wt.). The intensity of the WAXD peaks is decreased sharply due to the diluent effect. On the contrary, after solid-state processing with applying pressure of 33MPa at 150 °C, the WAXD pattern of the mixture is almost featureless diffraction, only exhibiting a broad and weak reflection (Figure 4-5 (c)), possibly because of the layer disorder or collapse of the layer structure. The silicate concentration does not contribute to the featureless diffraction because of the comparison with Figure 4-5 (b).

In Figure 4-6, the whole view of the WAXD patterns just after solid-state processing. For all processed samples, the intensity of the (001) plane of the *syn*-FH-$C_{16}TBP^+$ decreases with loading pressure. For the samples with applying pressure of 33 MPa, the WAXD pattern of the mixture is almost featureless diffraction as mentioned before, only exhibiting an orthorhombic unit cell of the crystallized PPS [21]. The diffraction peaks at 2Θ=19.0°, 20.5°, 25.5° and 27.5° correspond to the planes of (110), (111/200), (112) and (211), respectively. The significant difference in the WAXD profiles among the processing condition is not observed.

Figure 4-7 exhibits WAXD patterns for the typical examples of both processed and

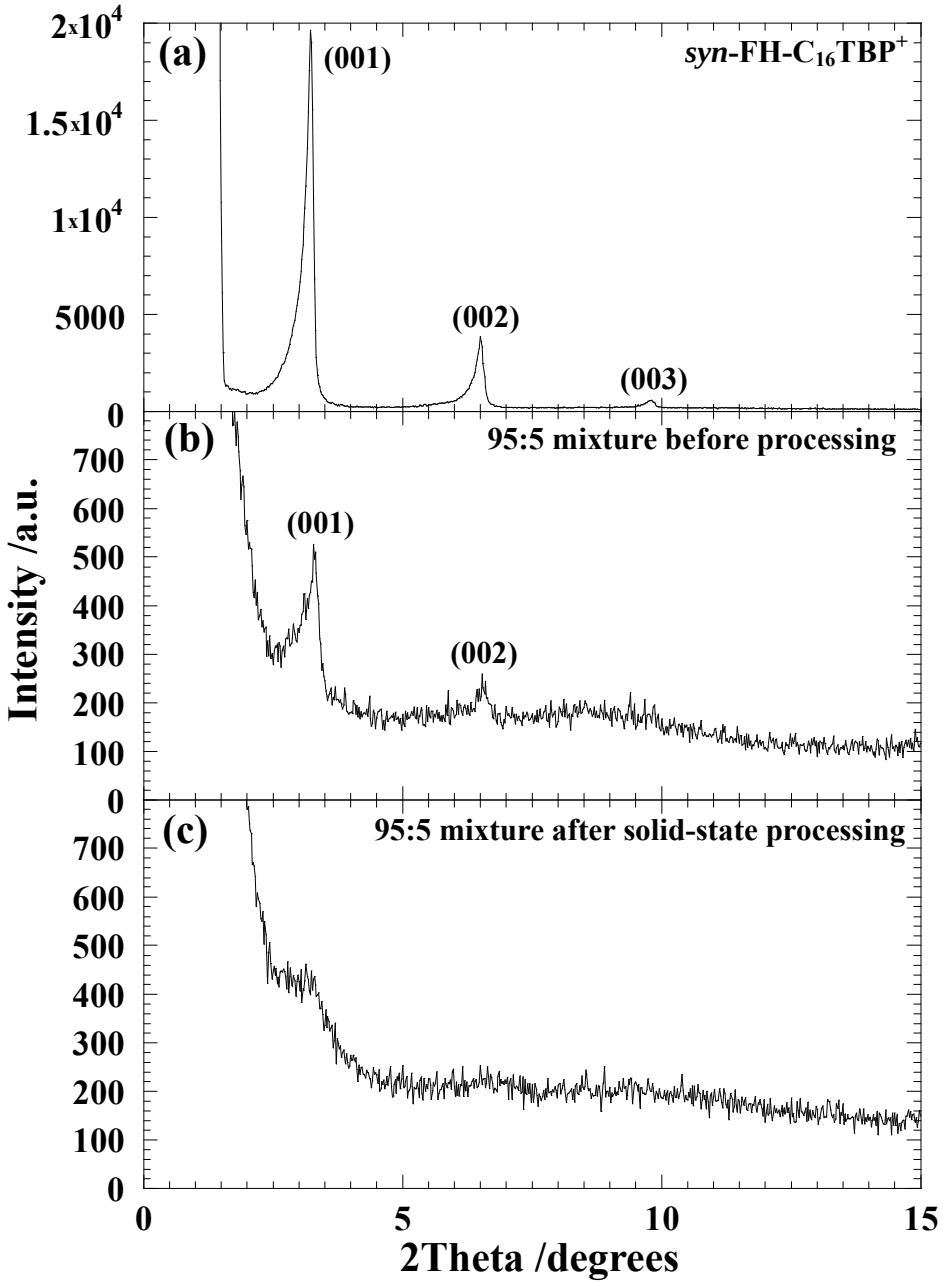

Figure 4-5. WAXD patterns of (a) *syn*-FH-$C_{16}TBP^+$, (b) mixture of PPS and *syn*-FH-$C_{16}TBP^+$ (95:5 wt./wt.) before solid-state processing and (c) processed mixture of PPS and *syn*-FH-$C_{16}TBP^+$ (95:5 wt./wt.) with applying pressure of 33 MPa at 150 ^oC.

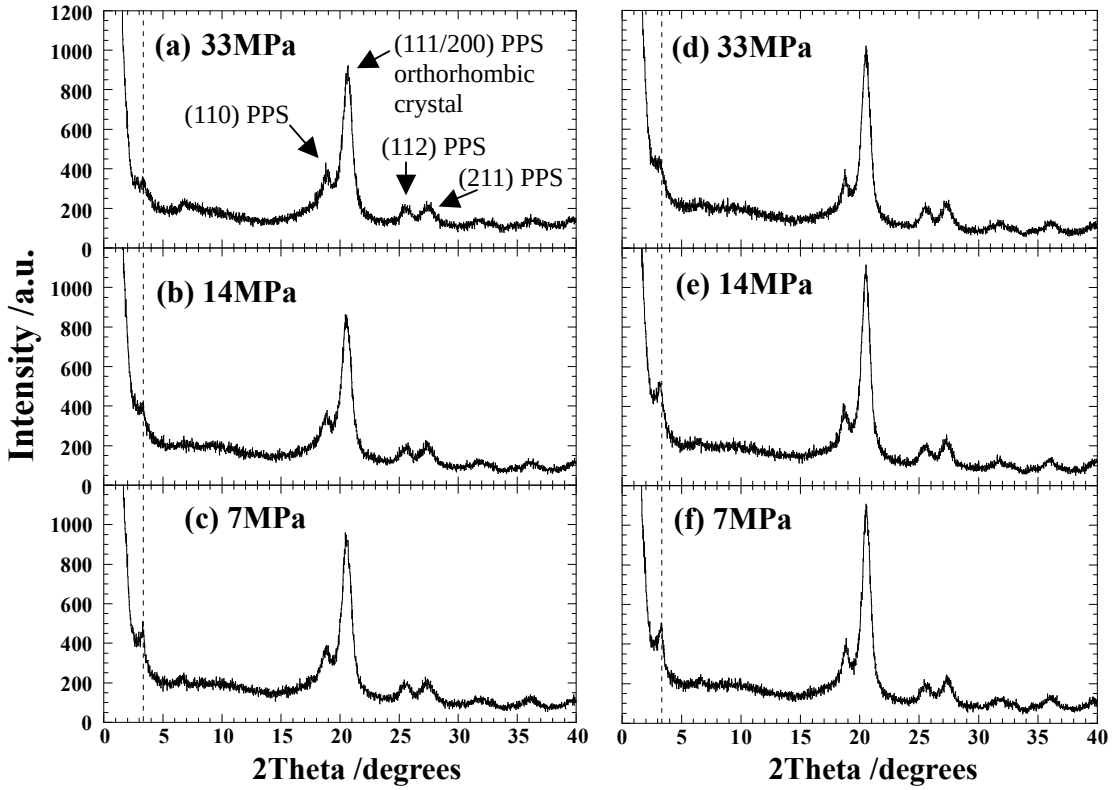

Figure 4-6. WAXD patterns for solid-state processed mixture with applying pressure of (a) 33MPa at room temperature (r.t.), (b) 14 MPa at r.t., (c) 7 MPa at r.t., (d) 33 MPa at 150 ^{o}C, (e) 14 MPa at 150 ^{o}C, and (f) 7 MPa at 150 ^{o}C. The dashed lines in each figure are the (001) peak position of *syn*-FH-$C_{16}TBP^{+}$ before solid-state processing. The strong diffraction peaks at 2Θ=15-30^{o} are assigned to the orthorhombic crystal of PPS.

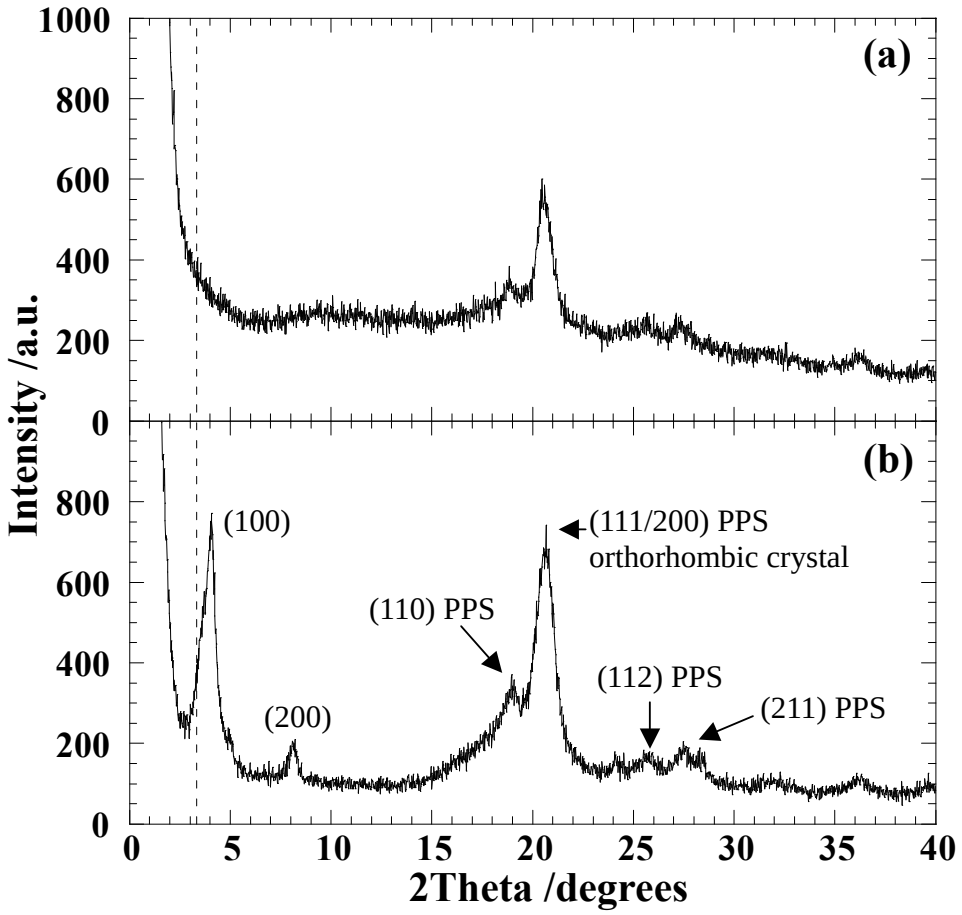

Figure 4-7. WAXD patterns after annealing at 300 ^{o}C for 30 s: (a) solid-state processed mixture with applying pressure of 33MPa at 150 ^{o}C and (b) unprocessed mixture. All profiles were taken at room temperature. The dashed line in each figure indicates the location of silicate (001) reflection of each OMLF. The strong diffraction peaks at 2Θ=15-30^{o} are assigned to the orthorhombic crystal of PPS.

unprocessed mixtures after annealing at 300 °C for 30s (without shear stress). The profiles were taken at room temperature. We can see a large effect of the processing on the collapse of the layer structure of OMLF. After annealing, the disappearance of sharp Bragg peaks [(001) and (002) planes] in OMLS clearly indicate the dispersed behavior of the silicate layers in the PPS matrix (Figure 4-7 (a)). We confirmed that this behavior is essentially the same at any other processed mixtures. In the case of the unprocessed mixture corresponding to the TEM image of Figure 4-4 (a), the interlayer shrinkage takes place after annealing without the thermal decomposition of the intercalant (Figure 4-7 (b)) [8]. The apparent interlayer expansion/shrinkage was deeply discussed in our previous articles [5, 6, 8]. Such discussion is beyond the objects of this chapter.

It is interesting to note that the disappearance of the peaks after annealing at 300 °C. For explaining this remarkable difference of the profiles (cf. Figure 4-6 (d) *vs* Figure 4-7 (a)), we speculate the large layer slippage takes place during processing due to the lubrication between the two platelets, where the intercalants are liquid state. With decreasing the value of *R* (Figure 1) by mechanically approach, the reduction of the attractive force, accompanying the polymer penetration into the nano-galleries and leading to a high level of the dispersion of the OMLF is expected. This discussion is further supported by the morphology observation.

4-3-3-2. Morphology

To elucidate the morphologies before and after solid-state processing, I conducted POM observation at 300 °C.

Figure 4-8 shows the POM photographs with their FFT patterns of the mixtures prepared by annealing at 300 °C for 30 s (without shear processing). It is clear from the POM photographs that stacked-and-agglomerated structures of layers are evident in the un-processed mixture

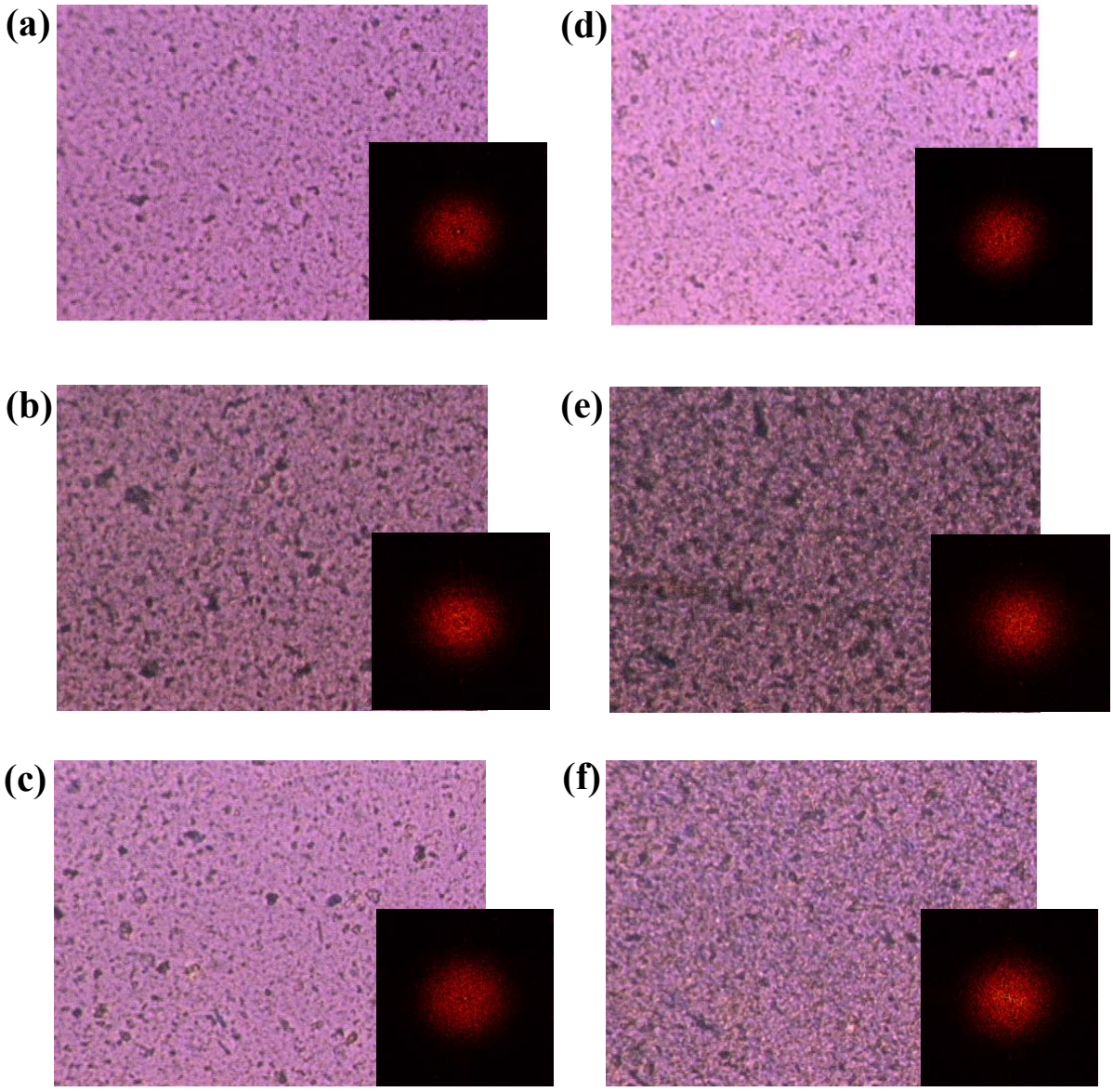

Figure 4-8. Polarized optical micrographs for solid-state processed mixtures with applying pressure of (a) 33MPa at room temperature (r.t.), (b) 14 MPa at r.t., (c) 7 MPa at r.t., (d) 33 MPa at 150 ^{o}C, (e) 14 MPa at 150 ^{o}C, and (f) 7 MPa at 150 ^{o}C. Micrographs of (g) a mixture before solid-state processing and (h) a mixture prepared by melt compounding with shear. All micrographs were taken at 300 ^{o}C just after annealing for 30 s (without shear processing). The inset in each picture is a computed FFT spectrum of the micrograph.

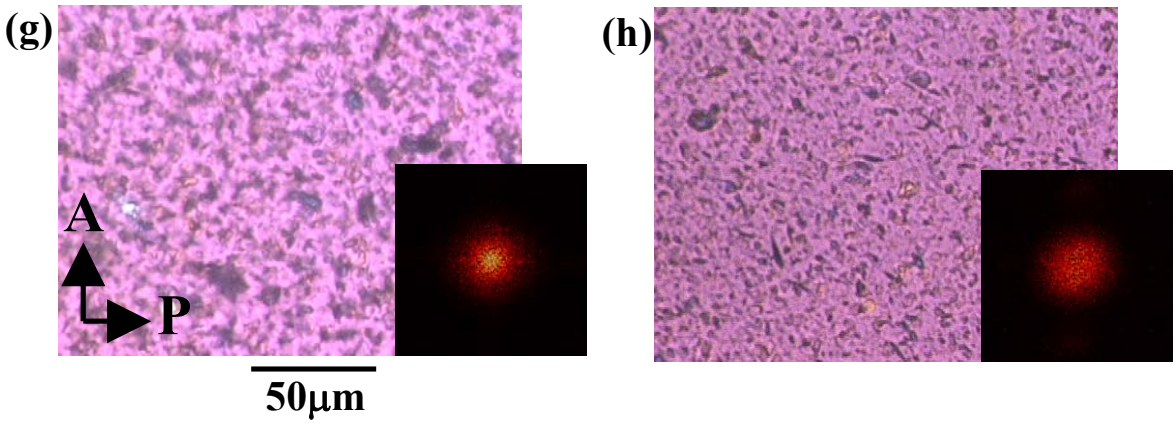

Figure 4-8. *(Continued)*

(Figure 4-8 (g)) and melt compounded sample (Figure 4-8 (g)), whereas a good dispersion appears in the processed sample (Figure 4-8(a)-(f)). The FFT pattern shows weak scattering with isotropy (halo) compared with that of un-processed mixture. This indicates that the particles size of the dispersed nano-filler becomes smaller during solid-state processing. There is no significant difference in the FFT patterns between processing temperatures. For high applying pressure (33 MPa), however, the FFT patterns exhibits more weak scattering feature compared with that of low pressure condition (7 MPa). The dispersion state in the nano-meter scale was directly observed *via* TEM analyses.

Figure 4-9 shows the results of TEM bright field images of the mixtures corresponding to the POM experiments, in which dark entities are the cross section of layered nano-fillers. The disorder and delaminated silicate layer structure with the thickness of 40-80 nm are observed in each TEM image compared with unprocessed or melt compounded sample (cf. Figure 4-4 (a) and (b)). This is a unique observation of the discrete silicate layers. I estimated the form factors obtained from TEM images, i.e. average value of the particle length (L), thickness (D), of the dispersed particles and the correlation length (ξ) between the particles. The details of the evaluation were described in our previous paper [11]. The results are presented in Table 4-1. The values of L are estimated by the limitation of the area of the micrograph due to the magnification factor. Therefore, these values are not so significant compared with that of D. However, the dispersed structure of layered fillers having extremely large value of L is evident in the large layer slippage. For processing at 150 °C the D value decreases with decreasing applying pressure, while at low temperature condition (~ 25 °C) the value exhibits opposite trend with applying pressure. The intercalants into nano-galleries act as a lubricant at processing temperature. Above the glass transition temperature of matrix PPS (T_g=~ 80 °C), the solid-state processing provides

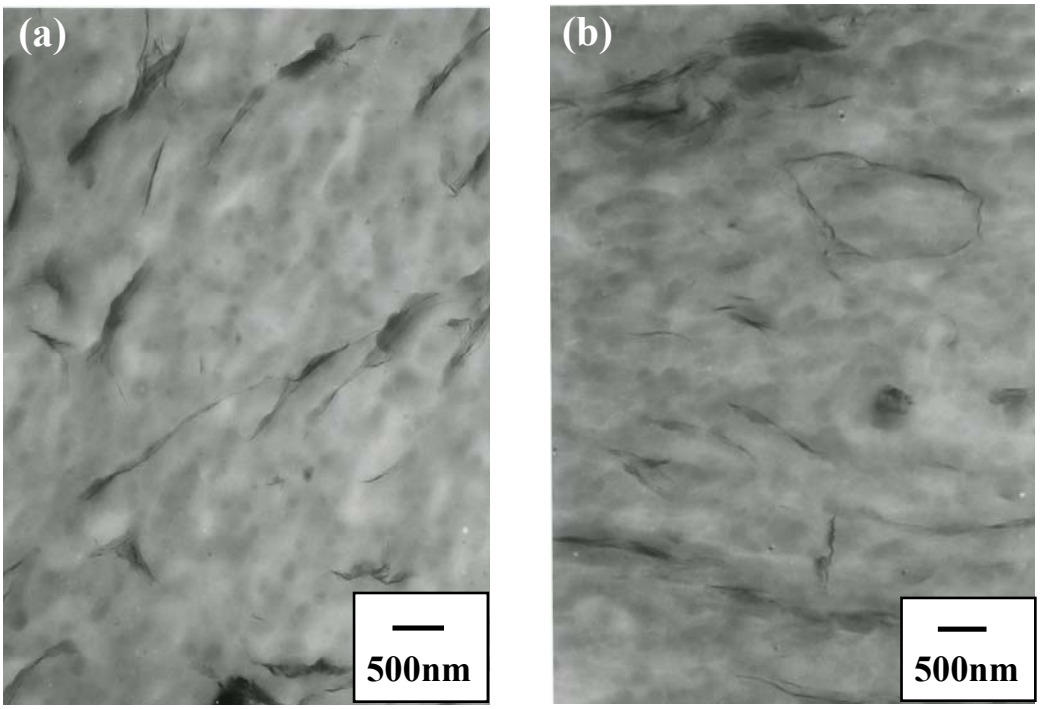

Figure 4-9. Bright field TEM images of samples after solid-state processed mixture with applying pressure (a) 33MPa at room temperature (r.t.), (b) 14 MPa at r.t., (c) 7 MPa at r.t., (d) 33 MPa at 150 ^{o}C, (e) 14 MPa at 150 ^{o}C, and (f) 7 MPa at 150 ^{o}C. All samples are prepared by annealing at 300 ^{o}C for 30 s (without shear processing). The dark entities are cross section and/or face of intercalated-and-stacked silicate layers, and the bright areas are the matrix.

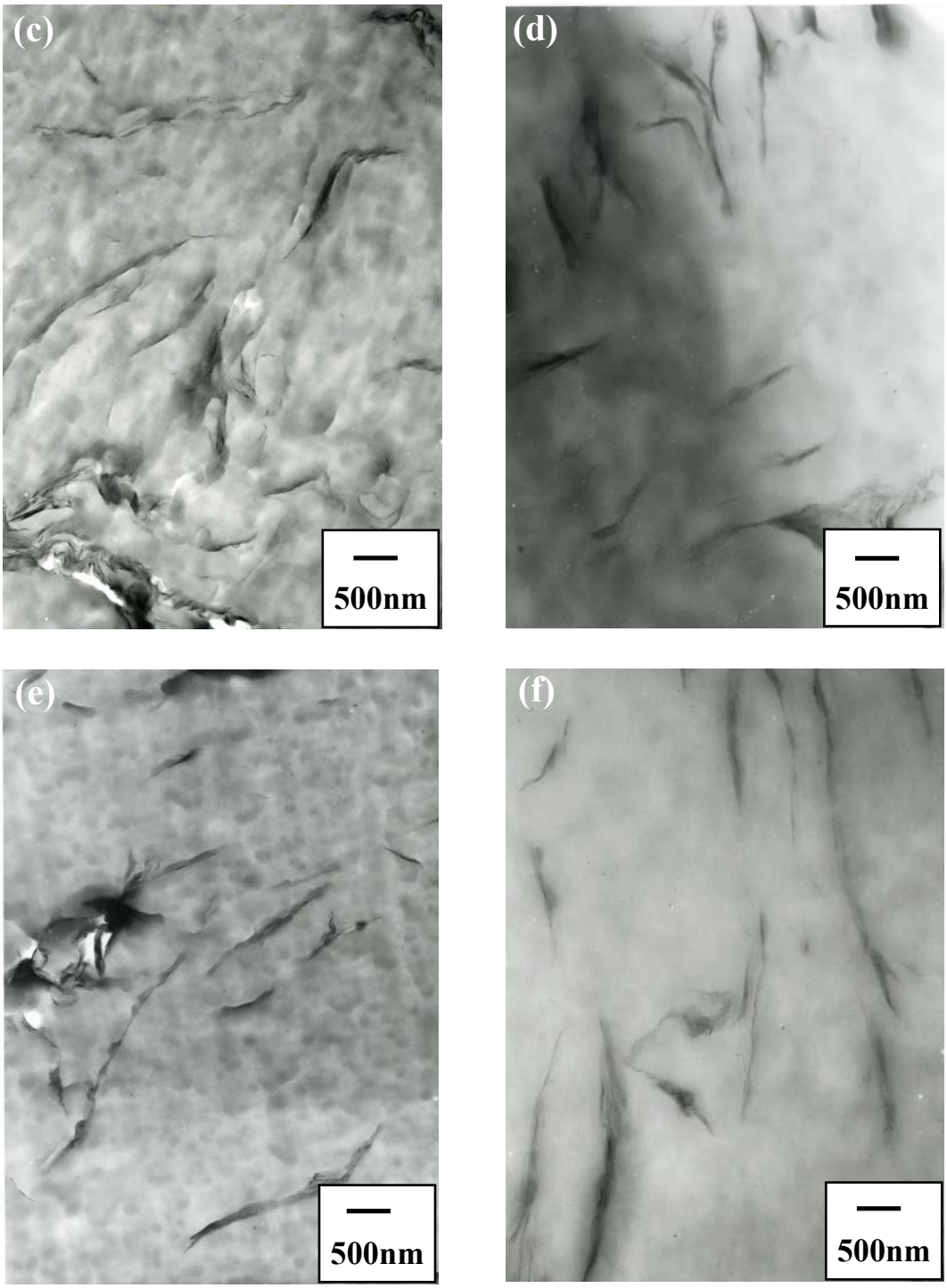

Figure 4-9. *(Continued)*

Table 4-1. Form factors of PPS-based nano-composites prepared via solid-state processing with various conditions

Temperature	Parameters	33 MPa	14 MPa	7 MPa
150°C	*L* /nm	1340*	1250*	1300*
	D /nm	97 ± 10	72 ± 10	69 ± 10
	ξ /nm	784 ± 100	725 ± 100	632 ± 100
Room temperature	*L* /nm	1120*	1340*	860*
	D /nm	45 ± 10	47 ± 10	78 ± 10
	ξ /nm	760 ± 100	770 ± 100	620 ± 100

* Some nano-fillers have large value of *L* (more than 2μm).

small effect because of the softening of PPS compared with low temperature condition (~ 25 °C). The adaptive temperature protocol for the processing might be above T_m of the intercalants and below T_g of the matrix polymer. Therefore, the applying pressure might be more important factor than the processing temperature at low temperature condition.

From these facts, the solid-state processing is extremely effective method to collapse the stacked structure. This processing leads to the layer delamination accompanying the discrete dispersion.

4-4. Conclusions

I have described a novel and economic method for the nano-scale control of the dispersed layered fillers via solid-state processing. The effect of the different temperatures and applying pressures on the delaminating behavior of the nano-fillers was examined. This processing led to delaminate of the silicate layers and attained the discrete dispersion. This approach can be extended to prepare polymeric nano-composites with delamination of the nano-fillers in overcoming the pressure drop within the nano-galleries. In this study, the applying pressure might be more important factor than the processing temperature at low temperature condition (below T_g of PPS).

References

[1] Sinha Ray S, Okamoto M, *Prog. Polym. Sci.*, **2003**, 28, 1539-1641.

[2] Yang K, Ozisik R, *Polymer*, **2006**, 47, 2849-2855.

[3] Lee EC, Mielewski DF, Baird RJ, *Polym. Eng. Sci.*, **2004**, 44, 1773-1782.

[4] Zhao L, Li J, Guo S, Du Q, *Polymer*, **2006**, 47, 2460-2469.

[5] Yoshida O, Okamoto M, *Macromol. Rapid Commun.*, **2006**, 27, 751-757.

[6] Saito T, Okamoto M, Hiroi R, Yamamoto M, Shiroi T, *Macromol. Mater. Eng.*, **2006**, 291, 1367-1374.

[7] Shao W, Wang Q, Li K, *Polym. Eng. Sci.* **2005**, 45, 451-457.

[8] Yoshida O, Okamoto M, *J. Polym. Eng.*, **2006**, 26, 919-940.

[9] Maiti P, Okamoto M, Yamada K, Ueda K, Okamoto K, *Chem. Mater.* **2002**, 14, 4654-4661.

[10] Hiroi R, Sinha Ray S, Okamoto M, Shiroi T, *Macromol. Rapid Commun.* **2004**, 25, 1359-1364.

[11] Sinha Ray S, Yamada K, Okamoto M, Ogami A, Ueda K, *Chem. Mater.* **2003**, 15, 1456-1465.

[12] Kim YH, Okamoto M, Kotaka T, *Macromolecules*, **2000**, 33, 8113-8116.

[13] Atkins PW, *Physical Chemistry*, Oxford Unv. Press Oxford, **1998**.

[14] Sinha Ray S, Okamoto K, Okamoto M, *Macromolecules*, **2003**, 36, 2355-2367.

[15] Okamoto K, Sinha Ray S, Okamoto M, *J. Polym. Sci. Part B: Polym. Phys.*, **2003**, 41, 3160-3172.

[16] Nam PH, Maiti P, Okamoto M, Kotaka T, Hasegawa N, Usuki A, *Polymer*, **2001**, 42, 9633-9640.

[17] Sinha Ray S, Maiti P, Okamoto M, Yamada K, Ueda K, *Macromolecules*, **2002**, 35,

3104-3110.

[18] Sinha Ray S, Yamada K, Okamoto M, Fujimoto Y, Ogami A, Ueda K, *Polymer*, **2003**, 44, 6633-6646.

[19] Ito Y, Yamashita M, Okamoto M, *Macromol. Mater. Eng.*, **2006**, 291, 773-783.

[20] Sinha Ray S, Yamada K, Okamoto M, Ueda K. *Polymer*, **2003**, 44, 857-866.

[21] Tabor BJ, Marge EP, Boo J, *Euro. Polym. J.*, **1971**, 7, 1127-1128.

Chapter 5

Polypropylene-based Nano-composite Formation: Delamination of Organically Modified Layered Filler via Solid-state Processing

5-1. Introduction

A significant amount of work has already done on various aspects of polymeric nano-composite containing organically modified layered fillers (OMLFs) [1]. However, complete delamination of OMLFs in continuous polymer matrix is still challenging issue because it could not be satisfactorily attained. Gardolinski and Lagaly [2] described a very distinctive definition of delamination and exfoliation in aim to avoid the controversial use of these terms. Exfoliation is defined as the decomposition of large aggregates into smaller particles, whereas delamination denotes the process of separation of the individual layers of the particles at the nano-scale.

To the best of our knowledge, so far, the complete delamination is not feasible after melt intercalation with appropriate shear. Only a few examples of this type can be found in the literature [3, 4], but many published photographs show very small regions in the melt compound where partially exfoliation occurred [1]. Delamination of stacked layered fillers in polymeric nano-composite is the ultimate target for controlling better overall materials' properties. Thus, we are far from the goal of understanding the mechanisms of the nano-structure control and the preparation of the nano-composite with discrete dispersion of the nano-fillers. From this reason, a novel preparation method is currently in progress.

Some methods for the delamination of OMLFs were conducted by using supercritical CO_2 [5, 6]. The effect of the supercritical CO_2 (sc-CO_2) fed to the tandem extruder on the dispersion of organically modified montmorillonite (MMT) with different intercalants into Nylon 6 matrix was examined [6]. In the absence of sc-CO_2, pressure improved the MMT-clay delamination by reducing the free volume of the polymer and increasing the interaction between chains and ultimately increasing the viscosity. Using sc-CO_2 did not improve the clay dispersion due to the decreasing the melt viscosity. Another interesting approach for the delamination of

OMLFs is an ultrasound in the preparation of nano-composites. The effect of the *in-situ* ultrasound on the polymer/MMT melt phase is reported [7].

An effective method to enhance the dispersion, intercalation and exfoliation of OMLFs in thermoplastic-based nano-composites is reported. The same experiment was done in another report for polypropylene (PP)-base nano-composite preparation [8]. The maximum power output and frequency of the ultrasonic generator are 300W and 20kHz, respectively. They described the fine dispersion of silicate layers in PP matrix after ultrasonic treatment (100W). However, the ultrasonic oscillations exhibited a little effect on the delamination of OMLFs as revealed by transmission electron microscope (TEM) observation. Thus, the compounding with an assist from sc-CO_2 fluids and ultra-sonication did not improve the state of the nano-filler dispersion once a critical morphology was established. That is, the dispersion of the nano-filler in the polymer matrix is governed by judicious choice of OMLF.

Although the intercalation technology of the polymer melt is developed along with the current industrial process, such as extrusion and injection molding, we have to develop more innovative compounding process, especially in the preparation of the nano-composites possessing discrete dispersion of the nano-fillers.

In this regard, we have reported solid-state processing of poly(*p*-phenylenesulfide) (PPS)-based nano-composites to delaminate the stacked, layered filler in the polymer matrix [9, 10]. The mixture of PPS and organically modified layered filler (OMLF) (95:5 wt./wt.) was subjected to the processing using thermostatted hot-press at ambient temperature and 150 °C, below T_m of PPS (i.e., PPS matrix is still at the solid-state), and applying pressures of 7, 14 and 33MPa for 30s. The mixture exhibited disorder and delaminated layer structure with the thickness of 40-80 nm into PPS matrix. The solid-state processing led to delaminate of the silicate layers

and attained the discrete dispersion. Similarly, Wang et al. [11-13] reported the exfoliation of talc fillers by solid-state shear processing using pan-type mill, to prepare PP/talc nano-composites, in which the delamination of talc fillers was not achieved in the nano-composite as revealed by TEM images.

Torkelson et al. [14] demonstrated that a continuous scalable solid-state shear pulverization (SSSP) could result in well-dispersed unmodified graphite in PP, leading to a 100% increase in modulus as compared with neat PP. High shear and compressive forces result in repeated fragmentation and fusion of polymer in the solid-state producing excellent mixing and dispersion of nano-fillers in the nano-composites [15].

The solid-state shear processing may be an innovative technique to delaminate the layered fillers in overcoming the pressure drop (Δp) within the nano-galleries [10]. Therefore, successful delamination of OMLFs could broaden the scope of application of this procedure. The objective of this work is to gain insight into the solid-state processing for the preparation of nano-composites based on PP having finely dispersed layered fillers.

5-2. Experimental Section

Organically modified layered filler (OMLF) used in this study was montmorillonite (MMT, Hojun Co., Ltd.) modified with *n*-hexadecyl tri-*n*-butyl phosphonium (C_{16}TBP) cation. A polypropylene (PP) *fine* powder (average particle size ~5μm, T_m = 151 °C), purchased from Seishin enterprise Co., Ltd. The homogeneous mixture of PP and OMLF in the weight ratio 95/5 was prepared. I have ground the mixture with pestle and mortar for 8 h at 65 °C (well below T_m of PP matrix powder). We call the process "solid-state processing" because PP matrix is solid state. After solid-state processing, the mixture of PP and OMLF was melt compounded using miniature mixer of gram scale (MINI-MAX Molder CS-183, Custom Scientific Instruments Inc.) and to convert into sheet for the characterization.

The nano-structure analyses of wide-angle X-ray diffraction (WAXD) were performed for the PP/OMLF mixture and corresponding nano-composite sheets by using MXlabo X-ray diffractometer (MAC Science Co., CuKα radiation, wavelength λ = 0.154 nm) and Ultima IV X-ray diffractometer (Rigaku Co., CuKα radiation, wavelength λ = 0.154 nm), and transmission electron microscopy (TEM) were carried out using the same apparatus as in the previous articles [9]. To investigate the micro-scale morphology of the nano-composites, I also used polarizing optical microscope (POM). The detail of POM observation is in our previous paper [10]. For analyzing the features of the micrographs, I carried out fast Fourier transform (FFT) analysis on digitally saved images of POM and TEM micrographs using the commercial image analysis software (Ultimage®, Graftek, France) [16], which allowed to provide us information equivalent to the scattering analyses.

For comparison, the PP-based nano-composite preparation was conducted via conventional melt compounding operated at 180 °C for 3 min [17]. The ejected samples were

dried under vacuum at 80 °C for 6 h to remove water. The dried nano-composite was then converted into sheets with a thickness of 0.7 to 2 mm by pressing with ≈1.5 MPa at 180 °C for 1 min using a laboratory hot-press (Mini Test Press-10, Toyo Seiki Seisaku-sho, Ltd.). Furthermore, instead of using alumina mortar, I carried out solid-state processing using internal mixer (Laboplastomill V4C150, Toyo Seiki Seisaku-sho, Ltd.) with a rotating speed of 50 rpm at 50°C for 5 h.

5-3. Results and Discussion

5-3-1 Solid-state processing with alumina mortar

WAXD patterns for the mixture powder of PP and OMLF (95:5 wt./wt.) are presented in Figure 5-1a. The mean interlayer spacing of the (001) plane ($d_{(001)}$) for the MMT that was modified by C_{16}TBP [MMT-C_{16}TBP] obtained by WAXD measurements is 2.26 nm (diffraction angle, 2Θ = 3.90 °). Actually, there is a large anisotropy of the stacked silicate layers. The size of the some of the stacked-silicate layers appears to reach about 50-100 nm in lengths and the interlayer distance as revealed by TEM observation is about 3 nm (see Figure 5-4a and c). This value is virtually same as compared to WAXD data.

After solid-state processing for 2 h, a small remnant shoulder is observed around 2Θ ≅ 4.00 ° (Fig. 5-1c). In the following processing from 3 to 8 h, the peak was almost featureless diffraction, only exhibiting the monoclinic (α-form)/triclinic (γ-form) unit cells of the crystallized PP [18].

Figure 5-2 shows the time variation of $d_{(001)}$ and corresponding intensity normalized by α(110)/γ(111) peak of PP during processing. With increasing processing time the intensity from $d_{(001)}$ gradually decreases with peak shift to lower angle (layer shrinkage). Beyond 4 h, the layer spacing finally reached a constant value (~ 2.05 nm) possibly due to the change of the interdigitated layer structure of the MMT-C_{16}TBP [19]. The structure may suggest that the different orientation angle could adopt, giving a decreasing of the basal spacing during processing.

To elucidate the morphologies before and after solid-state processing, I conducted POM observation at 180 °C. Figure 5-3a shows the POM photograph of the mixtures prepared by

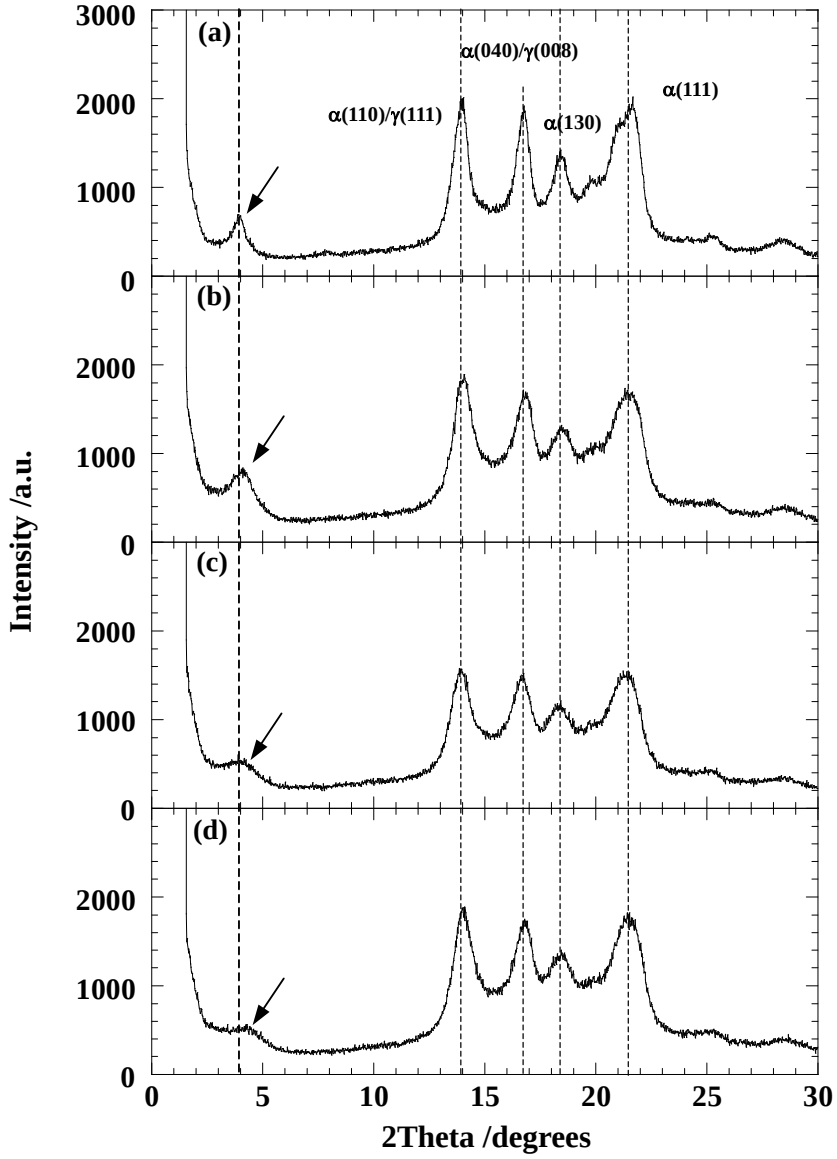

Figure 5-1. WAXD patterns of (a) mixture of PP and OMLF (95:5 wt./wt.) before solid-state processing, (b), (c) and (d) processed mixture of PP/OMLF at 65 °C for 1, 2 and 8 h, respectively. Arrows in each panel indicate $d_{(001)}$ peak of OMLF.

The strong diffraction peaks at 2Θ=15-25 ° are assigned to the monoclinic (α-form)/triclinic (γ-form) unit cells of the crystallized PP.

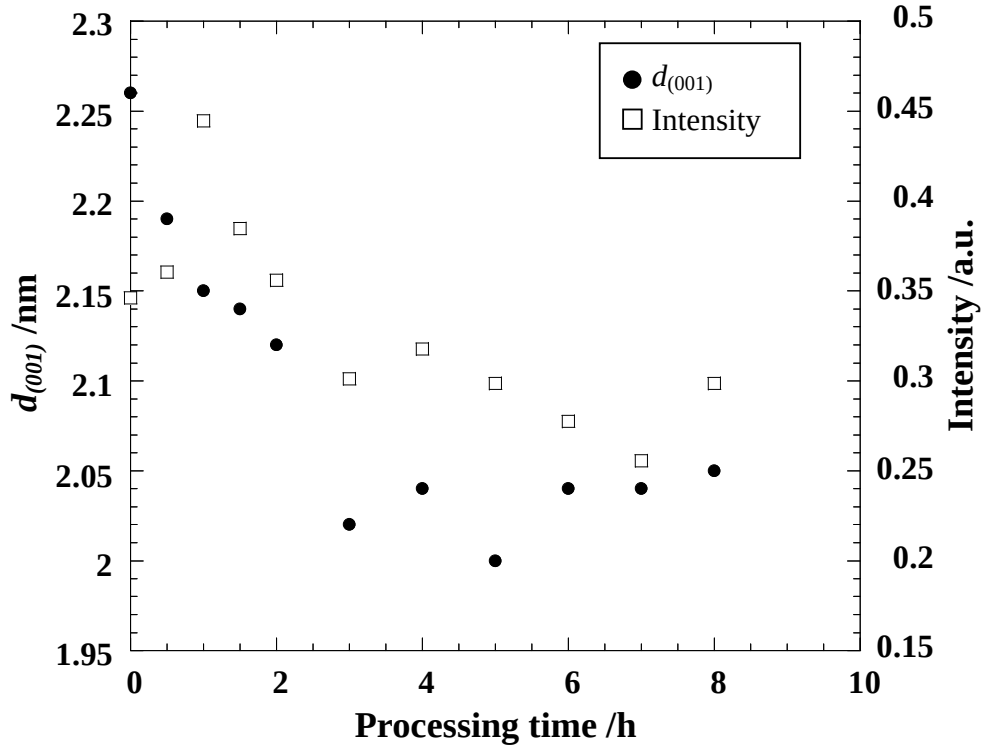

Figure 5-2. Time variation of $d_{(001)}$ and corresponding intensity during processing. Intensity is normalized by $\alpha(110)/\gamma(111)$ peak.

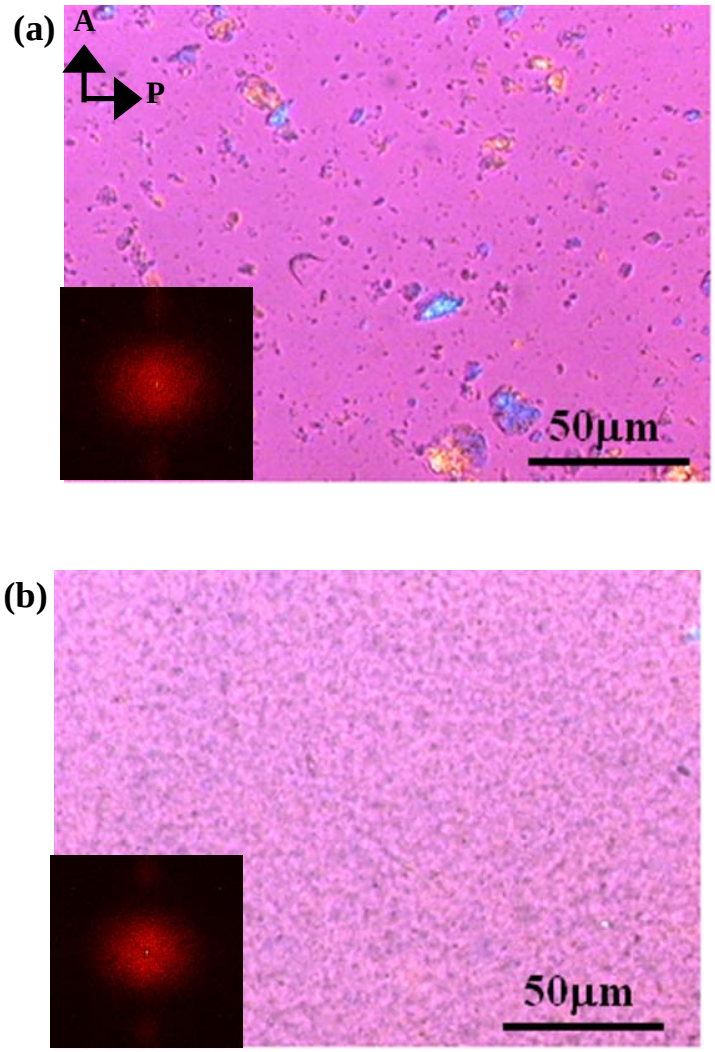

Figure 5-3. POM photographs of the mixture (a) unprocessed sample and (b) after solid-state processing for 8 h. Both micrographs were taken at 180 °C just after annealing for 30 s. The inset in each image is a computed FFT spectrum of the micrograph.

melt compounding and annealing at 180 °C for 30 s. It is clear from the POM photographs that stacked-and-agglomerated structure of layers is evident in the melt compounded sample, whereas a good dispersion appears in the processed sample for 8 h (Fig. 5-3b). The FFT pattern shows weak scattering with isotropy (halo) as compared with that of unprocessed sample (i.e., melt compounded sample). This indicates that the particles size of the dispersed nano-filler becomes smaller during solid-state processing. The dispersion state in the nano-meter scale was directly observed *via* TEM analysis.

Figure 5-4 shows the results of TEM bright field images and their FFT patterns of the melt compounded mixtures corresponding to the POM experiments, in which dark entities are the cross section of the layered nano-fillers. The large agglomerated tactoids of about 3 μm thickness are seen in Figure 5-4a (unprocessed sample). On the other hand, in Figure 5-4b, nano-meter sized thickness layers were straggled in the observation area. Figure 5-4c shows disorder and delaminated silicate layer structure with the thickness of 3-7 nm and length of 50-200 nm (average thickness of 5.8 nm and length of 67 nm). This is a very interesting observation of the discrete silicate layers.

Figure 5-5 shows the one-dimensional scattering pattern obtained from FFT analysis. Here, the scattering intensity ($I(q)$) is shown as a function of the magnitude of the scattering vector (q). We found a broad shoulder around $q \sim 0.02$ nm^{-1} and small remnant peaks in the q range from 0.04 to 0.09 nm^{-1}. The broadness is due to the fact that the dispersed OMLF particles are rather disordered and short-range ordered. The decay of intensity in the q range from 0.02 to 0.1 nm^{-1}can be expected by a power law in the form $I(q) \cong q^{-1}$, suggesting the form factor is the randomly oriented rod. Apparently, this is consistent with the shape of the dispersed OMLF particles in the TEM image (Fig. 5-4c).

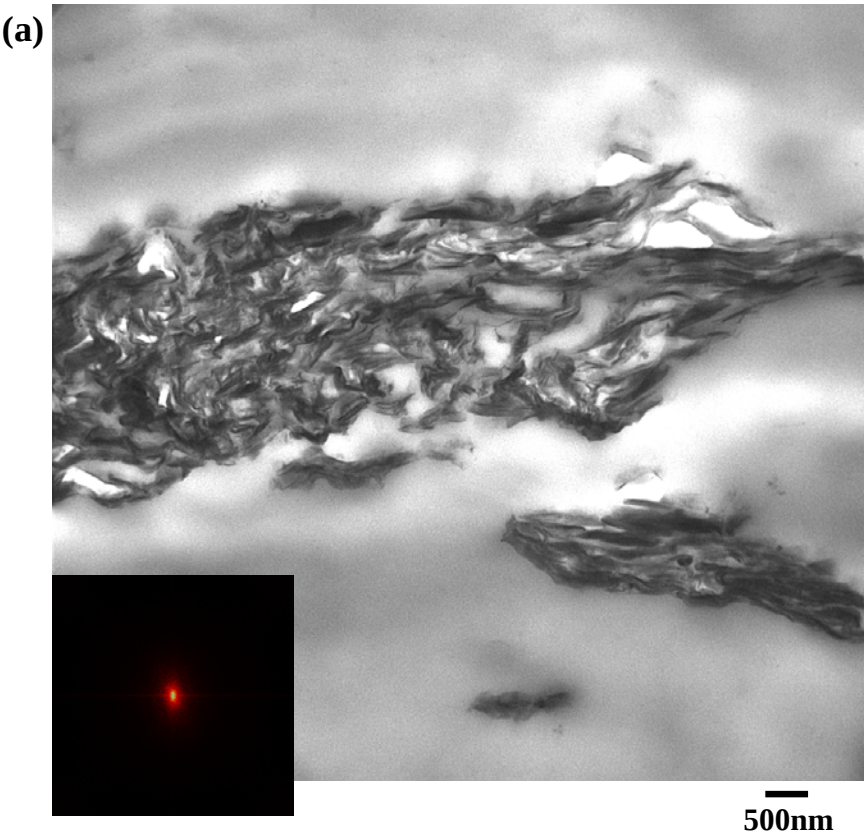

Figure 5-4. Bright filed TEM images of (a) unprocessed sample, (b) and (c) sample prepared by solid-state processing for 8 h. The dark entities are the cross section and/or face of intercalated-and-stacked silicate layers, and the bright areas are the matrix. The inset in (a) and (c) are a computed FFT spectrum of the micrograph.

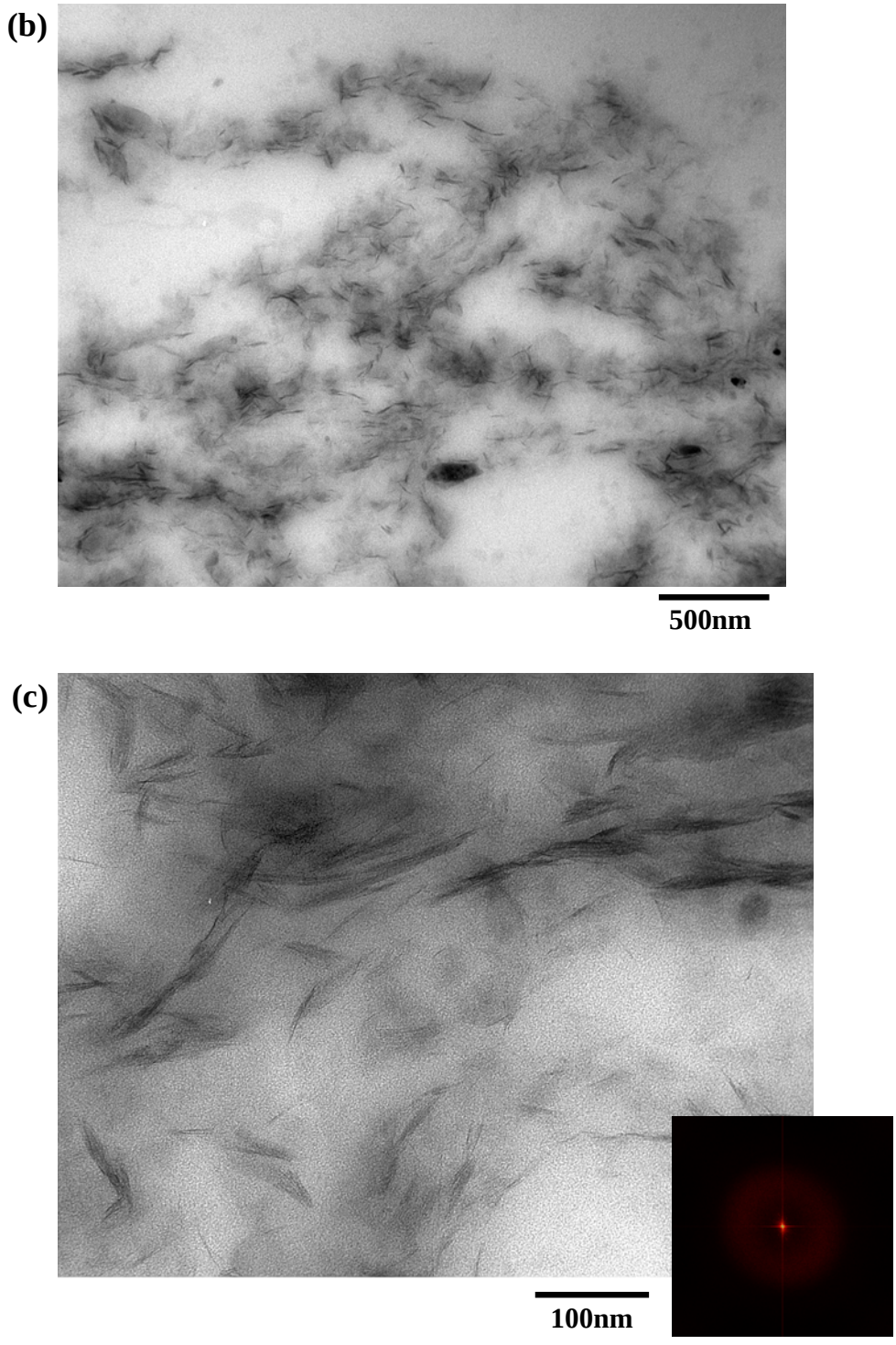

Figure 5-4. *(Continued)*

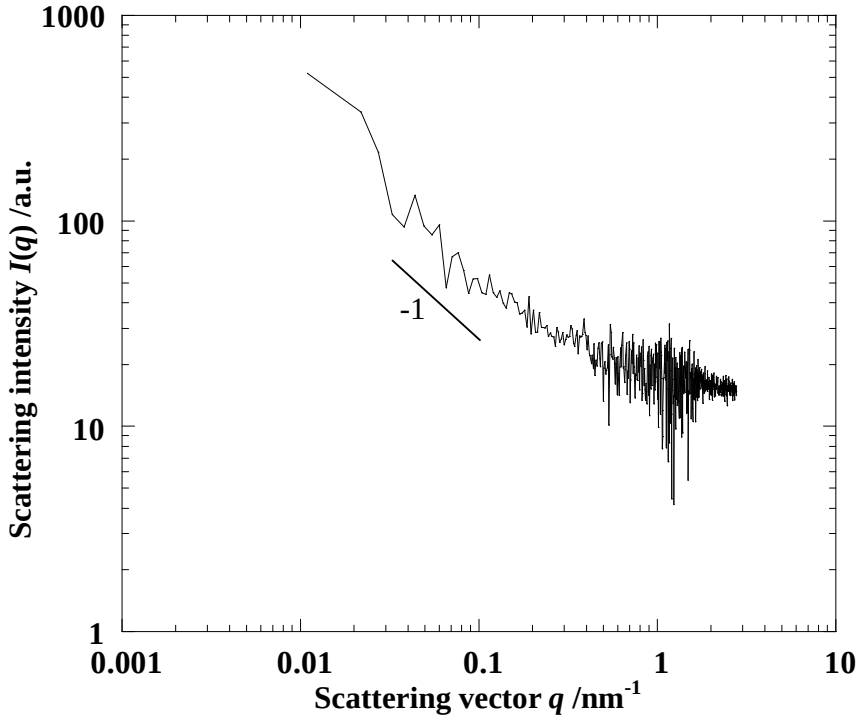

Figure 5-5. One-dimensional scattering pattern of processed PP/OMLF for 8 h obtained from FFT analysis. The solid line was drawn by the power low of $I(q) \cong q^{-1}$ at the q range of 0.02-0.2 nm^{-1}.

I estimated the form factors obtained from TEM images and FFT analysis combined with Debye-Bueche (DB) theory, i.e., average value of the particle length (L_{MMT}), thickness (t_{MMT}), of the dispersed particles and the correlation length (ξ_{MMT}) between the particles. The details of the evaluation were described in our previous paper [20]. The Debye-Bueche equation [21] is applicable in isotropic dense system [22]. The detail procedure for the Debye-Bueche plots was described in our previous paper [23]. To estimate the value of ξ_{MMT}, I employed the Debye-Bueche equation:

$$I(q)^{1/2} = \frac{(8\pi\langle\rho^2\rangle\xi^3)^{1/2}}{(1+\xi^2 q^2)} \qquad (5\text{-}1)$$

where ξ is the long-range structure correlation distance, q is the magnitude of scattering vector, $I(q)$ is the intensity of the scattered light at q and $\langle\rho^2\rangle$ is the mean-square fluctuation of the refractive index. [24].

Figure 5-6 shows the Debye-Bueche plot for FFT analysis. The plot is observed to be linear. From the slope and the intercept, we can estimate ξ (=slope/intercept)$^{1/2}$. Once the value of ξ (= 3.65 nm) is given, other morphological parameters are obtained by

$$\xi_{MMT} = \frac{\xi}{\phi_{MMT}} \qquad (5\text{-}2)$$

$$t_{MMT} = \frac{\xi}{(1-\phi_{MMT})} \qquad (5\text{-}3)$$

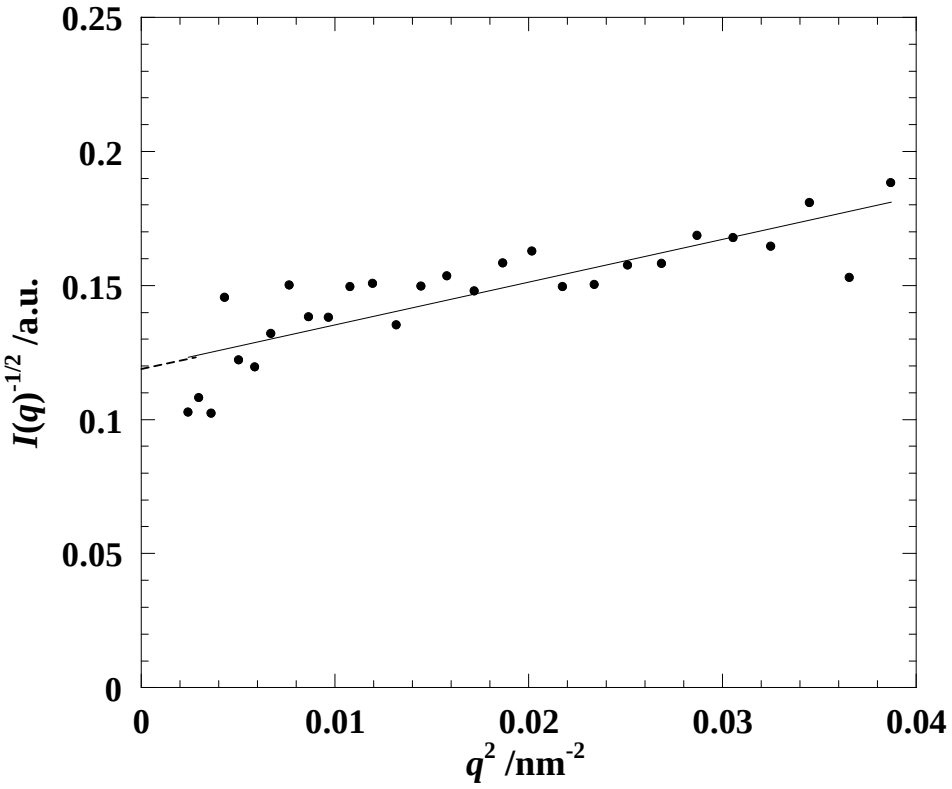

Figure 5-6. Debye-Bueche plot for FFT analysis. The solid line is calculated by linear regression. The dashed line indicates the intercept of the plot.

where ϕ_{MMT} is the volume fraction of the dispersed phase (MMT particles). The details of the evaluation were described in our previous paper [23]. The results are presented in Table 5-1.

Table 5-1. Form factors of two nano-composites obtained from TEM and FFT analyses

Parameters	TEM image	FFT with DB theory
L_{MMT} /nm	67±6	---
t_{MMT} / nm	5.8±0.5	3.7
ξ_{MMT} / nm	45±2	157

For the sample prepared by annealing without solid-state processing, L_{MMT} and t_{MMT} are in the range of (6-10) μm and (1-3) μm, respectively as revealed by TEM image (Fig. 5-4a). On the other hand, PP/OMLF prepared by solid-state processing exhibits a small value of L_{MMT} (67±6 nm) with almost double of stacking of the silicate layers (t_{MMT} =5.8±0.5 nm). ξ_{MMT} value of PP/OMLF with processing (45±2 nm) suggests that a more uniform dispersion of the silicate layers seems to be attained due to the solid-state processing. The absolute value of ξ_{MMT} shows much lower as compared with that of Debye-Bueche plot. The reason is not obvious at present. However, the value of t_{MMT} is virtually same as compared with that of Debye-Bueche plot. After solid-state processing, a stacked silicate layers contain two discrete silicate layers with finer dispersion. This is a unique observation of the discrete silicate layers. The intercalants into nano-galleries act as a lubricant at processing temperature. Since the melting temperature of the intercalant ($C_{16}TBP^+$) into the nano-galleries was –23.5 °C, we can observe the effect of layer delamination at 65 °C.

5-3-2 Solid-state processing with internal mixer

To investigate the effect of processing condition and potential for industrial application, I conducted solid-state processing with using internal mixer.

Figure 5-7 shows the results of TEM bright field images in which dark entities are the cross section of layered nano-fillers. For processing with a rotating speed of 50 rpm at 50 °C for 5 h, the dispersed morphology of the silicate layers exhibits same trend with applying pressure (corresponding to the shear stress of 0.32 MPa). The disordered and delaminated silicate layer structure is observed in TEM image. L_{MMT} and t_{MMT} are in the range of (372±38) nm and (33.2±3.8) nm, respectively. From these results, solid-state processing using internal mixer is extremely effective method to collapse the stacked structure in overcoming the pressure drop (Δp ~ 24 MPa [10]) within the nano-galleries.

Furthermore, I conducted solid-state processing using internal mixer with various torque condition to research the effect of applied torque on OMLF dispersion. Figure 5-8 shows POM photographs with applying torque 5 to 20 Nm. The agglomerated OMLF clearly shows solid-state processing with low torque conditions (Fig.5-8a, b). In contrast, no agglomerated structure is observed under high torque solid-state processing sample (Fig.5-8c, d). From these facts, solid-state processing have a torque threshold, in other words, shear stress threshold for the improvement of OMLF dispersion.

Moreover, to understand the kinetics of the solid-state processing, I attempt to apply a phenomenological formulation for the breakup of mineral particles (Rittinger's law):

$$dE = -b\left[\frac{1}{D^n}\right]dD \qquad (5\text{-}4)$$

where E is the energy for breakup, D is the mean diameter of particles and the parameter b and n are the breakup coefficients, which depend on the processing condition and materials [25]. If the

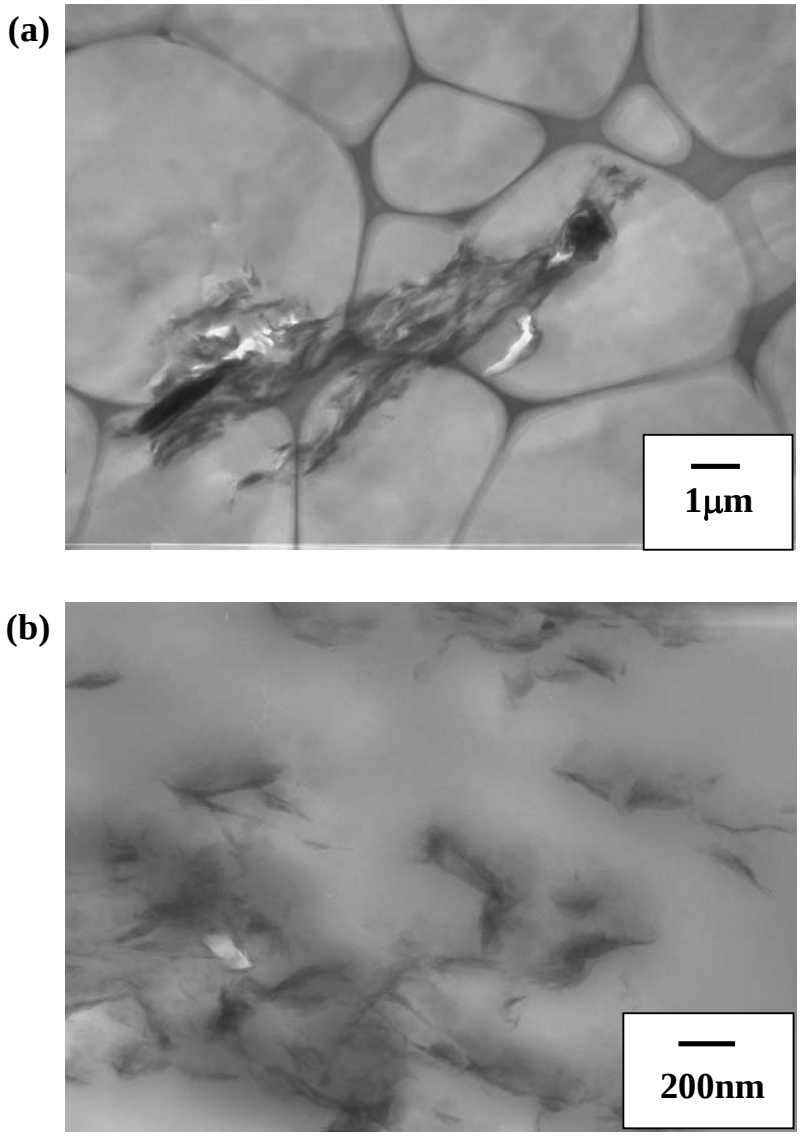

Figure 5-7. Bright field TEM images of (a) only melt compounded and (b) solid-state processing using internal mixer for 300min and melt compounded sample.

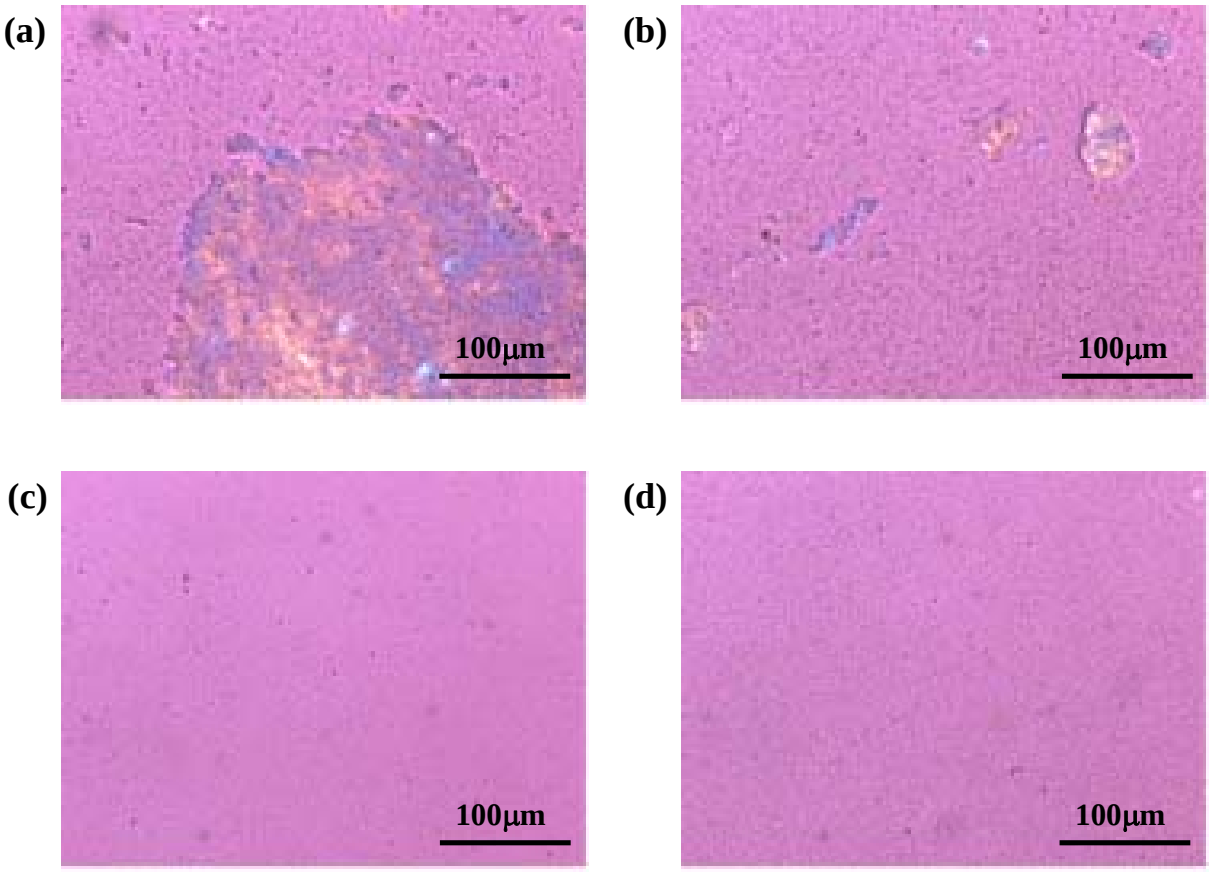

Figure 5-8. POM photographs of solid-state processing and melt compounded sample prepared with (a) 4.8N· m, (b) 8N· m, (c) 17N· m and (d) 20N· m average torque for 60min, respectively.

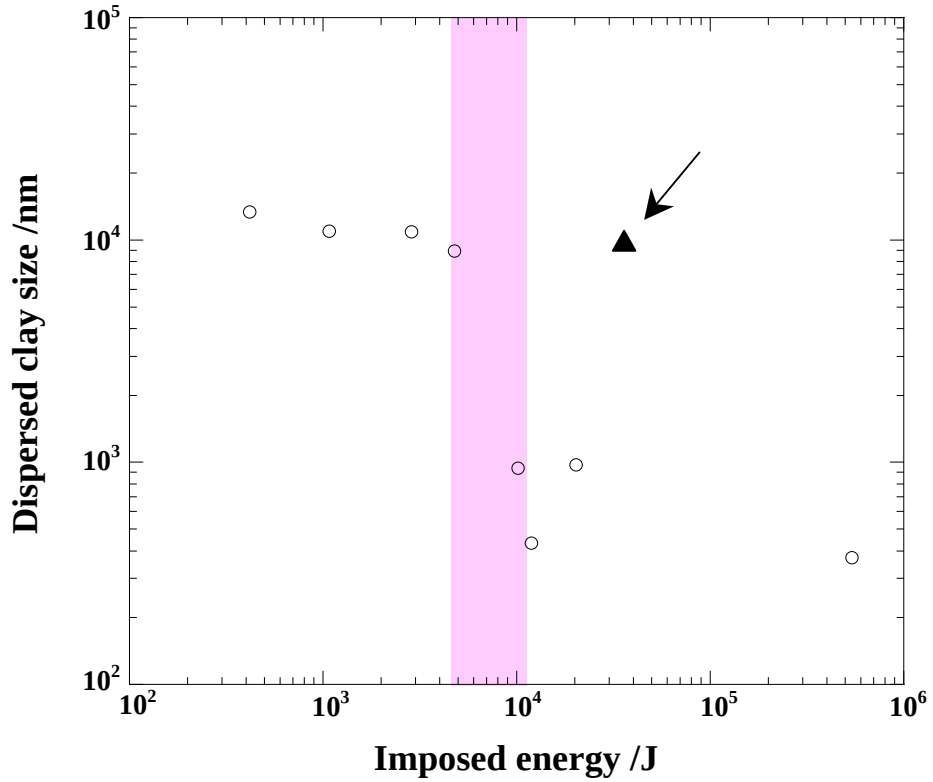

Figure 5-9. Dispersed clay size versus imposed energy during solid-state processing. Arrow indicates the condition for the torque of 2N· m for 300min.

mixing torque T is constant throughout the processing, the imposed energy E is proportional to residence time t, i.e., $E \propto T \cdot t$. Hence, eq. (1) can be rewritten as

$$T \cdot t \sim \frac{1}{D^{n-1}} \qquad (5\text{-}5)$$

Figure 5-9 shows the plot of imposed energy versus OMLF particle size. From Figure 5-9, it turns out that solid-state processing also exhibits an imposed energy threshold of around 10^4 J. In addition, for the case of long residence time with low torque conditions (marked with the arrow in Fig. 5-9), the particle size reduction was NOT improved as compared to the same imposed energy *via* high torque. From Figures 5-8 and 5-9, the finely dispersion of OMLFs could be satisfactorily attained under certain conditions of both shear stress (torque) and imposed energy over these thresholds.

5-4. Conclusions

I have described a novel and feasible method for the nano-scale control of the dispersed layered fillers via solid-state processing by using common experimental tools. This processing apply over the thresholds of shear stress and processing energy, then led to delaminate of the silicate layers and attained the discrete dispersion. This approach can be extended to prepare polymeric nano-composites with delamination of the nano-fillers in overcoming the pressure drop within the nano-galleries.

References

[1] Sinha Ray S, Okamoto M, *Prog. Polym. Sci.*, **2003**, 28, 1539-1641.

[2] Gardolinski, JEFC, Lagaly G, *Clay Miner.*, **2005**, 40, 547-556.

[3] Usuki A, Kawasumi M, Kojima Y, Okada A, Kurauchi T, Kamigaito O, *J. Mater. Res.*, **1993**, 8, 1179-1184.

[4] Katoh Y, Okamoto M, *Polymer*, **2009**, 50, 4718-4726.

[5] Yang K, Ozisik R, *Polymer*, **2006**, 47, 2849-2855.

[6] Bellair RJ, Manitiu M, Gulari E, Kannan RM, *J. Polym. Sci. Polym. Phys.*, **2010**, 48, 823-831.

[7] Lee EC, Mielewski DF, Baird R, *Polym. Eng. Sci.*, **2004**, 44, 1773-1782.

[8] Zhao L, Li J, Guo S, Du Q, *Polymer*, **2006**, 47, 2460-2469.

[9] Saito T, Okamoto M, Hiroi R, Yamamoto M, Shiroi T, *Macromole. Rappid Commun.*, **2006**, 27, 1472-1475.

[10] Saito T, Okamoto M, Hiroi R, Yamamoto M, Shiroi T, *Polymer*, **2007**, 48, 4143-4151.

[11] Shao W, Wang Q, Li K, *Polym. Eng. Sci.*, **2005**, 45, 451-457.

[12] Shao W, Wang Q, Ma H, *Polym. Int.*, **2005**, 54, 336-341.

[13] Shao W, Wang Q, Wang F, Chen Y, *J. Polym. Sci. Polym. Phys.*, **2006**, 44, 249-255.

[14] Wakabayashi K, Pierre C, Dikin DA, Ruoff RS, Ramanathan T, Brinson IC, Torkelson JM, *Macromolecules*, **2008**, 41, 1905-1908.

[15] Masuda J, Torkelson JM, *Macromolecules*, **2008**, 41, 5974-5977.

[16] Kim YH, Okamoto M, Kotaka T, *Macromolecules*, **2000**, 33, 8113-8116.

[17] Saito T, Okamoto M, Hiroi R, Yamamoto M, Shiroi T, *Macromol. Mater Eng.*, **2006**, 291, 1367-1374.

[18] Meille SV, Bruckner S, Porzio W, *Macromolecules*, **1990**, 23, 4114-4121.

[19] Yoshida O, Okamoto M, *Macromol. Rapid Commun.*, **2006**, 27, 751-757.

[20] Sinha Ray S, Yamada K, Okamoto M, Ogami A, Ueda K, *Chem. Mater.*, **2003**, 15, 1456-1465.

[21] Debye P, Bueche AM, *J. Appl. Phys.*, **1949**, 20, 518-525.

[22] Hsiao BS, Stein RS, Deutscher K, Winter HH, *J. Polym. Sci. Polym. Phys.*, **1990**, 28, 1571-1588.

[23] Okamoto M, Inoue T, *Polym. Eng. Sci.*, **1993**, 33, 175-182.

[24] Okamoto M, Inoue T, *Polymer*, **1995**, 36, 2739-2744.

[25] Bond FC, *Mining Eng.*, **1952**, 4, 484.

Chapter 6

Summary and Conclusions

In this thesis, the nonisothermal order-disorder phase transition in nano-confined space and the intercalation kinetics were clarified. A novel preparation method for polymer nano-composite was carried out. The summary of each chapter will be given as follows.

Chapter 2. Nonisothermal Order-Disorder Phase Transition of Alkylammonium Ions in Nano-confined Space

To understand the effect of confined space (interlayer space in montmorillonite (MMT)) on the nonisothermal ordering transition (chain packing) kinetics and disorder transition (chain melting) behavior including the conformational changes of the chain segment of the cationic surfactants, I have characterized MMT modified with dioctadecyl dimethylammonium ($DC_{18}DM$) ions (MMT-$DC_{18}DM$) using temperature-modulated differential scanning calorimeter (TMDSC), wide-angle X-ray diffraction (WAXD) and Fourier transform infrared spectroscopy (FTIR) technique. For MMT-$DC_{18}DM$, the chain conformational disorder-order phase transition took place during the cooling process. The transition peak was much broader and it appeared at lower temperature (T_c) when compared to the crystallized dioctadecyl dimethylammonium bromide ($DC_{18}DM$-Br), as a reference.

In MMT-$DC_{18}DM$, the formation of gauche conformers was enhanced and the chains were not as densely packed as in crystalline $DC_{18}DM$-Br. The normal crystallization took place in the bulk during the nonisothermal crystallization of $DC_{18}DM$-Br. The confined ions ($DC_{18}DMs$) in one or two dimensional order contributed to the nonisothermal chain packing for a higher cooling rate of 5.0-20.0 °C/min. The observed chain packing in confined space at

different T_c ranges (cooling rate > 5.0 °C/min) could be explained by much lower energy barrier.

Chapter 3. Intercalation of diphenyl sulfide into nano-galleries and preparation of poly(*p*-phenylenesulfide)-based nano-composites

For the reference system of poly(*p*-phenylenesulfide) (PPS)-based nano-composites, I investigated the intercalation behavior of diphenyl sulfide (DFS) molecules into nano-galleries based on organically modified layered fillers (OMLFs) consisting of different types of intercalants and nano-fillers with different surface charge density. The smaller initial interlayer opening led to the larger interlayer expansion, regardless of the miscibility between intercalant and DFS. I examined the preparation of PPS-based nano-composites with and/or without shear processing at 300 °C. The finer dispersion of OMLFs in the nano-composite was observed when using OMLF having small initial interlayer opening. The delamination of the stacked nano-fillers was governed by the initial interlayer opening, whereas the uniform dispersion of the nano-fillers was affected by the shear.

Chapter 4. Poly(*p*-phenylenesulfide)-based nano-composite formation: Delamination of organically modified layered filler via solid-state processing

Intercalation behavior for polymer chain into nano-gallery of organically modified layered filler (OMLF) through melt compounding process was discussed. The results suggest pressure drop controls the degree of intercalation. And to reduce pressure drop, solid-state processing for the preparation of poly(*p*-phenylenesulfide) (PPS)-based nano-composites having finely dispersed layered fillers was conducted. The mixture of PPS and OMLF (95:5 wt./wt.) was subjected to the processing using thermostatted hot-press at ambient temperature and 150 °C, below T_m of PPS (i.e., PPS is still at the solid-state), and applying pressures of 7, 14 and

33MPa for 30s. The mixture exhibited disorder and delaminated layer structure with the thickness of 40-80 nm into PPS matrix. On the contrary, nano-composite prepared by melt compounding at 300 °C for 3 min showed the large stacked silicate layers in the PPS matrix. The solid-state processing led to delaminate of the silicate layers and attained the discrete dispersion.

Chapter 5. Polypropylene-based nano-composite formation: Delamination of organically modified layered filler via solid-state processing

Solid-state processing for the preparation of polypropylene (PP)-based nano-composites having finely dispersed layered fillers was conducted. The mixture of PP and organically modified layered filler (OMLF) (95:5 wt./wt.) was subjected to the processing using alumina mortar heated 65 °C, below T_m of PP (i.e., PP is still at the solid-state), and ground for 8 h before melt compounding. On X-ray diffraction, the $d_{(001)}$ peak of OMLF was broaden and peak position shifted slightly. The mixture prepared by solid-state processing exhibited disorder and delaminated layer structure with the thickness of 3-7 nm into PP matrix through TEM observations. On the contrary, nano-composite prepared by melt compounding at 180 °C for 3 min (without solid-state processing) showed the large stacked silicate layers in the PP matrix. Furthermore, instead of using alumina mortar, I carried out solid-state processing using internal mixer. X-ray diffraction pattern and TEM observation exhibited similar results. The solid-state processing led to delaminate of the silicate layers and attained the discrete dispersion.

****

As described in the present thesis, the clarified phase transition of alkylammonium ions in nano-gallery of OMLF and intercalation behavior were great help for understanding the intercalation and/or dispersion phenomena during polymer melt processing.

Solid-state processing, based on above understanding, is able to prepare polymer nano-composite even though the polymer and OMLF combination that is not able to prepare polymer nano-composite through conventional polymer melt processing. The required processing condition for delamination of OMLF is applying shear stress and processing energy over these thresholds, and strong polarity of matrix polymer that was considered as necessary is not required for this novel processing.

The author believes the present study will make an important contribution to the producing polymer nano-composite and expanding the application.

List of publications

Scientific papers

(1) Saito T, Okamoto M, Hiroi R, Yamamoto M, Shiroi T, *Macromol. Rapid Commun.,* **2006**, 27, 1472-1475.

(2) Saito T, Okamoto M, Hiroi R, Yamamoto M, Shiroi T, *Macromol. Mater. Eng.,* **2006**, 291, 1367-1374.

(3) Saito T, Okamoto M, Hiroi R, Yamamoto M, Shiroi T, *Polymer*, **2007**, 48, 4143-4151.

(4) Kajino M, Saito T, Okamoto M, Sato H, Ozaki Y, *Appl. Clay Sci.*, **2010**, 48, 73-80.

(5) Saito T, Okamoto M, *Polymer*, **2010**, 51, 4238-4242.

Book chapter

Saito T, Okamoto M, "Polymeric Nano-Composites via Twin-Screw Extruder" in Resin melt compounding by twin-screw extruder –trouble occurrence factors and the countermeasure-, Gijyutu Jouhou Kyoukai, Tokyo, pp. 129-143 (2011)

Patent

Saito T, Okamoto M, "Thermoplastic Resin Composite and Its Preparation Method" Japanese Kokai Patent Application No. 2010-63235 (2010) Toyota Boshoku Co.

List of Presentations

(1) Saito T, Okamoto M, "*PPS-based Nanocomposites: Effect of nano-fillers on melt intercalation*" Proc. 17th Polymer Processing Technology Meeting Japan, 2005, Oct. 24, 25

(2) Saito T, Okamoto M, "*PPS-based Nanocomposites: Dispersion control of nano-fillers via solid-state processing*" Proc. 55th SPSJ Annual Meeting Japan, 2006, May 24-26

(3) Saito T, Okamoto M, "*PPS-based Nanocomposites: Dispersion control of nano-fillers via solid-state processing*" Proc. 55th SPSJ Symposium on Macromolecules Japan, 2006, Sep. 20-22

(4) Saito T, Okamoto M, "*PPS-based Nanocomposites: Dispersion control of nano-fillers via melt and solid-state processing*" Proc. 18th Polymer Processing Technology Meeting Japan, 2006, Oct. 23, 24

(5) Saito T, Okamoto M, "*Dispersion control of nano-fillers via solid-state processing*" Proc. 14th JSPP Symposium Japan, 2006, Nov. 22, 23

(6) Saito T, Okamoto M, "*PPS-based Nanocomposites: Dispersion control of nano-fillers via solid-state processing*" Proc. 4th Polymer Nanotechnology and Computational Polymer Science Meeting Japan, 2006, Dec. 7, 8

(7) T.Saito, M.Okamoto, "PPS-based Nanocomposites: Dispersion control of nano-fillers via solid-state processing" Proc. The Society of Rheology, Japan, 1st Tokai Region Master Student Presentation Meeting, 2007, Mar. 22

(8) T.Saito, M.Okamoto, "Polypropylene-based Nano-composite Formation: Delamination of Organically Modified Layered Filler via Solid-state Processing" Proc. of the Polymer Processing Society 26th Annual Meeting, Canada, 2010, July 4-8

(9) T.Saito, M.Okamoto, "Novel preparation method of PP/clay nanocomposites without using compatibilizer" Proc. 59th SPSJ Symposium on Macromolecules Japan, 2010, Sep. 15-17

(10) T.Saito, M.Okamoto, "Preparation of polypropylene-based nanocomposite via solid-state processing" Proc. 22nd Polymer Processing Meeting Japan, 2010, Oct. 25, 26

(11) T.Saito, M.Okamoto, "Polymeric nano-composite formation via solid-state processing" Proc. of the Polymer Processing Society 27th Annual Meeting, Morocco, 2011, May 10-14

(12) T.Saito, M.Okamoto, "PP-based nano-composite formation via solid-state processing" Proc. 60th SPSJ Annual Meeting Japan, 2011, May 25-27

Acknowledgments

The work of this thesis was performed at the Polymeric Nanocomposite Laboratory, Graduate school of Engineering, Toyota Technological Institute under the guidance of Professor Masami Okamoto. The author would like express special thanks to him for his continuous support and enthusiastic guidance through this work. His intellectual integrity, creativity, enthusiasm and dedication to science impressed me, but also guided me for my whole scientific career.

The author gratefully acknowledges Professor Tsutomu Takeichi for his valuable discussions and suggestions during the course of this thesis. He also would like to acknowledge Professor Shinichi Itsuno, Professor Akihiko Matsumoto and Professor Hideto Tsuji of Toyohashi University of Technology for serving on his dissertation committee.

He wishes to thank all members of Professor Masami Okamoto's Laboratory, Toyota Technological Institute for their cordial guidance, encouragement and friendship.

He thanks Toyota Boshoku Corporation especially all members of Research Laboratories for their kind collaboration and heartwarming friendship.

Finally, he wishes to express his exceptional thanks to his familly for their unwavering support and encouragement.

March, 2013

T. Saito

Tomotaka Saito